

# Advances in Power Transmission Science and Technology

Edited by  
Zeyong Yin, Chengyu Jiang, Datong Qin,  
Peixin Qiao and Geng Liu

# **Advances in Power Transmission Science and Technology**

Edited by  
Zeyong Yin  
Chengyu Jiang  
Datong Qin  
Peixin Qiao  
Geng Liu

# **Advances in Power Transmission Science and Technology**

Selected, peer reviewed papers of the  
International Conference on  
Power Transmission  
(ICPT 2011),  
October 25-29, 2011, Xi'an, China

*Edited by*

**Zeyong Yin, Chengyu Jiang, Datong Qin,  
Peixin Qiao and Geng Liu**



Copyright © 2011 Trans Tech Publications Ltd, Switzerland

All rights reserved. No part of the contents of this publication may be reproduced or transmitted in any form or by any means without the written permission of the publisher.

Trans Tech Publications Ltd  
Kreuzstrasse 10  
CH-8635 Durnten-Zurich  
Switzerland  
<http://www.ttp.net>

Volume 86 of  
Applied Mechanics and Materials  
ISSN 1660-9336

Full text available online at <http://www.scientific.net>

Distributed worldwide by  
Trans Tech Publications Ltd  
Kreuzstrasse 10  
CH-8635 Durnten-Zuerich  
Switzerland

Fax: +41 (44) 922 10 33  
e-mail: [sales@ttp.net](mailto:sales@ttp.net)

and in the Americas by  
Trans Tech Publications Inc.  
PO Box 699, May Street  
Enfield, NH 03748  
USA

Phone: +1 (603) 632-7377  
Fax: +1 (603) 632-5611  
e-mail: [sales-usa@ttp.net](mailto:sales-usa@ttp.net)

## Preface

The present volume includes selected papers from the International Conference on Power Transmissions 2011 (ICPT'2011). The conference is an international event which is hosted by Northwestern Polytechnical University and jointly organized by the State Key Laboratory of Mechanical Transmission, China Aviation Powerplant Research Institute, Zhengzhou Research Institute of Mechanical Engineering, and will be held in Xi'an, China during October 25-29, 2011.

This volume presents a selection of 202 papers from those submitted to the conference from universities and industries all over the world. All of the papers have been double-blind reviewed by picked experts. The papers selected for this volume depended on their quality and their relevancy to the conference. I hope this volume will provide the readers and researchers a broad overview of the recent advances in the field of power transmissions.

I wish to express my sincere appreciation and thanks to the Co-Chairs, all the members of the ICPT'2011 Conference Board, Organizing Committee and Scientific Committee, and all the referees, staffs, volunteers for their tremendous efforts. Without their hard work and excellent jobs, it was impossible to lead to the success of ICPT'2011 and this special issue.

I am grateful to over 80 referees from Chongqing University, Harbin Marine Boiler & Turbine Research Institute, China Aviation Powerplant Research Institute, Beijing University of Aeronautics and Astronautics, Dalian University of Technology, Nanjing University of Aeronautics and Astronautics, Shanghai University, Shandong University, Taiyuan University of Technology, University of Science and Technology Beijing, Xi'an Jiaotong University, Xi'an University of Technology, Northwestern Polytechnical University and Zhengzhou Research Institute of Mechanical Engineering for their strict reviews which guaranteed the quality of ICPT'2011 and this volume.

I am grateful to all the members of the Organizing Committee of ICPT'2011: Prof. Geng Liu, Prof. Liyan Wu, Prof. Sanmin Wang, Ms Hua Su, Ms Jingting Yuan, Ms Ru Yuan, Dr Zhaoxia He. Without their diligent work and countless contribution, it would be unthinkable that we may have the success of ICPT'2011 and this volume.

I also wish to thank the chairs and members of the Scientific Committee of ICPT'2011 for their contribution to the high-standard technical program.

Furthermore, I am deeply indebted to the volunteers of ICPT'2011 for their tremendous work to make the selected papers in this volume meet the high requirement for publication, and Trans Tech Publications for producing the volume.

Finally, I would like to thank all the authors for their contribution to this valuable special issue.

Prof. Zeyong Yin  
Chair of ICPT'2011  
Member of Chinese Academy of Engineering  
Aviation Industry Corporation of China

## **Conference Chairs**

### Chair:

Prof. Zeyong Yin, Member of CAE, Aviation Industry Corporation of China

### Co-Chairs:

Prof. Chengyu Jiang, Northwestern Polytechnical University, China

Prof. Datong Qin, The State Key Laboratory of Mechanical Transmission, China

Prof. Peixin Qiao, Zhengzhou Research Institute of Mechanical Engineering, China

### Secretary General:

Prof. Geng Liu, Northwestern Polytechnical University, China

## **Conference Sponsors**

Chinese Mechanical Engineering Society (CMES)

Chinese Society of Aeronautics and Astronautics (CSAA)

## **Conference Organizers**

Northwestern Polytechnical University, China

The State Key Laboratory of Mechanical Transmission, China

China Aviation Powerplant Research Institute, China

Zhengzhou Research Institute of Mechanical Engineering, China

## **Financial Support**

National Natural Science Foundation of China (NSFC)

## **Associated Organizations**

International Federation for the Promotion of Mechanism and Machine Science (IFTOMM)

Japan Society of Mechanical Engineers (JSME)

Verein Deutscher Ingenieure (VDI)

British Gear Association (BGA)

Shaanxi Association for Science and Technology (SNAST)

Shaanxi Mechanical Design Society (SNMDS)

# Table of Contents

## Preface und Committees

|  |     |
|--|-----|
| <b>Development of Helicopter Power Transmission System Technology</b><br>Z.Y. Yin, B.B. Fu, T.B. Xue, Y.H. Wang and J. Gao   | 1   |
| <b>Future Transmissions for Wind Turbines</b><br>B.R. Höhn   | 18  |
| <b>Dynamic Behavior of Helical Gears with Effects of Shaft and Bearing Flexibilities</b><br>K. Feng, S. Matsumura and H. Houjoh  | 26  |
| <b>Dynamic Modeling of Multi-Stage Planetary Gears Coupled with Bearings in Housing</b><br>Z.M. Xiao and D.T. Qin  | 30  |
| <b>A Static and Dynamic Model of Spiral Bevel Gears</b><br>J. Wang, J.T. Alves, M. Guingand, J.P. de Vaujany and P. Velex  | 35  |
| <b>Research on Meshing Characteristics for Face Gear with Arcuate Tooth</b><br>X.W. Cai, Z.D. Fang and J.Z. Su   | 39  |
| <b>A Challenge to Design of a New Harmonic Drive Device</b><br>S.T. Li   | 43  |
| <b>Study on Helical Tooth Profile Modification of Planetary Gear Transmission on the Basis of Gear Transmission Error</b><br>Y. Tang, S. Chang, Z.Q. Wang and K. Zhang | 47  |
| <b>Optimization Procedure for Complete Planetary Gearboxes with Torque, Weight, Costs and Dimensional Restrictions</b><br>U. Kissling and I. Bae                       | 51  |
| <b>Analysis System of Marine Planetary Gear Trains</b><br>G. Liu, S. Chang, L.Y. Wu and Y.S. Li  | 55  |
| <b>Application Probing of Advanced Helicopter Transmission System Technology</b><br>W.Q. Ding  | 59  |
| <b>Initial Pressure Influence on Pressure Flow Factor Used in Mixed-Lubrication Model</b><br>F.M. Meng and Y.P. Chen   | 65  |
| <b>Asymmetric Gears: Parameter Selection Approach</b><br>A. Kapelevich   | 70  |
| <b>Failures in the Development and Service of the Helicopter Transmission System</b><br>T.B. Xue and G.Q. Li   | 74  |
| <b>Modification Analysis of the New Axis-Fixed Cycloid Drive</b><br>M.Y. Liu, C.C. Zhu, C.N. Yan, X.Y. Xu and X.R. Zhang   | 82  |
| <b>Research on the Dynamic Response of a Combining Gear Drive System</b><br>Y.Q. Zheng, X.Z. Xue and S.M. Wang   | 86  |
| <b>Study on General Principle for Structure Fatigue Substantiation of Helicopter Transmission Systems</b><br>B. Hu   | 90  |
| <b>Thermal Effects Analysis on DCT Driven Plate in Vehicle Initial Condition</b><br>J.Y. Huang, Z.J. Liu, W. Sun and D.T. Qin  | 96  |
| <b>Simulation of Finite Element Analysis for Cutting Force of High-Speed Dry Gear Milling by Flying Cutter</b><br>Q. Guo, C. Lin and W. Quan                           | 100 |
| <b>Optimum Design of the 3Z-II Planet Drive Based on Matlab</b><br>Q.L. Huang, Y. Wang, M.L. Xu, J.G. Wang and Z.G. Luo  | 104 |
| <b>The Influence Analysis of Fatigue Limit for Mechanical Components Based on Standard Deviation of Full Scale Sub-Sample</b><br>B. Ouyang and W.Q. Ding               | 108 |
| <b>X – Zero Gear Drive with Minor Teeth Difference</b><br>Y.Q. Zhou, G. Zeng and C. Sun  | 112 |
| <b>Study on the Dynamic Excitation of the Star Gearing</b><br>L.D. Jiang, B.X. Liu, Z.R. Zhu and Y.L. Chen   | 116 |
| <b>The Design Concept Application on RMS for Tail Drive System of Civil Helicopter</b><br>W.Z. Liu, W.Q. Ding and Y.H. Wang  | 120 |

|   |     |
|---|-----|
| <b>Dynamic Modeling and Virtual Test of a New All Terrain Off-Road Vehicle</b><br>S.B. Lu, Y.N. Li and Y.L. Dong  | 125 |
| <b>Loaded Gear Contact Analyses for Pin Gear Reducers</b><br>S.T. Li  | 129 |
| <b>Primary Application of the ILS Technology in the Tail Rotor Drive System of the Certain-Type Helicopter</b><br>C. Duan, J. Gao, Y.H. Wang and Y. Lin   | 133 |
| <b>Study on Design and Simulation of the Vibration-Reduction of the Damp Structure for the Gearbox</b><br>X. Wang, J.B. Fu and X.M. Yin                   | 139 |
| <b>The Application of the Diagnoses Technique of Vibration on the Failure Analysis of Gear and Bearing in Gearbox</b><br>Y.S. Ai, Y.H. Wang and W.Z. Liu  | 143 |
| <b>Advanced Tooth Surface Modification for Spiral Bevel Gears</b><br>J.Z. Su, Z.D. Fang and X.W. Cai  | 148 |
| <b>Mold Machining Process and Applying Technologies of Spiral Bevel Gears</b><br>X.Y. Tie and H. Zhang  | 152 |
| <b>Lubrication Mode and Selection of the Helicopter Transmission System Roller Bearing</b><br>J.P. Qiu, M. Yin and L.S. Guo                               | 156 |
| <b>Analysis of Static Load Sharing in Star Gearing</b><br>L.X. Ying, L.D. Jiang, S.G. Yin and F.K. Kong   | 162 |
| <b>Active Gear Pair Vibration Control Based on Filtered-X RLS Algorithm</b><br>W. Sun, Y.N. Li, F. Zhang and G.Y. Li                                      | 166 |
| <b>Preload Design of Bearings in Helicopter Transmission System</b><br>M. Yin, J.P. Qiu and J. Gao  | 170 |
| <b>Dynamics Study of a Dynamic Balancing Linkage with Small Fluctuations in Load</b><br>T. Ren, W.T. Qu and W. Sun  | 176 |
| <b>Blind Separation Method for Gearbox Mixed Fault Signals</b><br>Y.B. Lei, Z.G. Chen and H.O. Liu  | 180 |
| <b>Analysis on Thermo-Mechanical Coupling Contact Stress of Cycloid Ball Planetary Drive</b><br>H.C. Xia, Z.M. Yang and Z.J. An                           | 184 |
| <b>Computational Tooth Root Stress Analysis of Crossed Beveloid Gears with Small Shaft Angle</b><br>C.S. Song, C.C. Zhu, T.C. Lim and R. Fan              | 188 |
| <b>Research on Relationship between Modulus and Tooth Number of Transmitting Gear and Vibration Noise</b><br>G.H. Dai, A.J. Zhao, H.F. Zhang and C.W. Gao | 192 |
| <b>Load-Excursion Failure Analysis of the Gearbox's Input Pinion</b><br>F.L. Ning   | 196 |
| <b>Optimal Design of Passive Magnetic Damper for Rotor Based on Sequential Quadratic Programming Method</b><br>C.Y. Zuo and J. Zhou                       | 201 |
| <b>Failure Analysis of Transmission Gear for Heavy Vehicles</b><br>T. Wang, F.Q. Zhao and J. Shen   | 206 |
| <b>Influence of Flyweight Profile on Regulating Characteristic of Rubber V-Belt CVT</b><br>H.F. Ding, C.C. Zhu and H.J. Liu                               | 210 |
| <b>A Study on Spiral Bevel Gear Fault Detection Using Artificial Neural Networks and Wavelet Transform</b><br>B.B. Fu and Z.D. Fang                       | 214 |
| <b>Virtual Modeling and Finite Element Analysis of Flexspline Based on Solidworks</b><br>R. Zhang and J.J. Yang   | 218 |
| <b>Research on Magnetic Transmission Design</b><br>H.Q. Wang, P.Q. Yu and D.J. Chen   | 222 |
| <b>Study on Strength Calculation and Bend Stress Test of Face Gear</b><br>H.M. Wu, X.Y. Yang and Y.B. Shen  | 227 |
| <b>The Longitudinal Vibration Analysis of the Drive Screw Under the Elastic Supports</b><br>H.D. Zhang and J.L. Sun                                       | 232 |

|   |     |
|---|-----|
| <b>New Calculation Method for the Load Capacity of Bevel And Hypoid Gears Based on Loaded Tooth Contact Analysis</b><br>B.R. Höhn, K. Stahl and C. Wirth                                  | 237 |
| <b>Research on the Load Sharing Technique and Experimental Validation of NGW Type Planetary Gear Train</b><br>H.F. Li, B.B. Fu and D. Fu  | 243 |
| <b>Dynamics Analysis of A Planetary Mechanism Soft Starter</b><br>X. Jiang, J.H. Bao, Y. Zhang and Y. Yu  | 247 |
| <b>Dynamic Properties Analysis of Compliant Foil Aerodynamic Bearings Based on Spring Model</b><br>S.X. Liu and X.Z. Ma   | 252 |
| <b>Dynamic Analysis of Combined Gear Drive</b><br>Y. Wang, H.X. Liu and S.M. Wang   | 256 |
| <b>Improve the Wear Resistant Life of the Sprag Clutch by Used the Chemical Vapor Deposition Technology</b><br>Y.Y. Jiang, Z.R. Yang and K.H. Shi   | 260 |
| <b>Dynamic Analysis and Multi-Object Optimization of the Forced Torsional Vibration for Vehicular Multi-Stage Planetary Gears</b><br>H. Liu, Z.C. Cai, C.L. Xiang and M.Z. Wang           | 263 |
| <b>The Design and FEM Analysis of End-Face Tooth of Coupling Flange</b><br>Q.X. Wang, W. Tang and N.J. Ye   | 268 |
| <b>Study on UV-LIGA Technology Fabrication of Micro Gear Transmission Device</b><br>L.Y. Zhang, C.L. Wang, Z.M. Liu, M. Lu, L.X. Meng, Y.G. Zhang and H.P. Zhang                          | 273 |
| <b>Quantitative Analysis of the Influence of Installation Errors on the Contact Pattern of Spiral Bevel Gears</b><br>G.L. Liu, R.T. Zhang and N. Zhao                                     | 278 |
| <b>The Application and Development of the High Speed Overrunning Clutch in the Transmission System of the Helicopter</b><br>Y.Y. Jiang, Z.R. Yang and J. Gao                              | 283 |
| <b>Single Versus Bi-Directional (Reversal) Gear Tooth Bending Stress and Life (S-N) Evaluation</b><br>J. Chen   | 287 |
| <b>Transmission Design for a Wind Powered Compressed Air Generation System</b><br>D. Shaw, J.Y. Cai and C.T. Liu  | 293 |
| <b>The Design and Experiment of Oval Bevel Gear</b><br>C. Lin, Y.J. Hou, Q.L. Zeng, H. Gong, L. Nie and H. Qiu  | 297 |
| <b>Research on Helicopter Main Gearbox Operating without Oil</b><br>M.J. Liao, X.S. Su, Z.R. Yang and B. Yao  | 301 |
| <b>Analysis of Load Sharing Behavior in Herringbone Gears Power Branching Transmission System</b><br>X.F. Yang, Z.D. Fang, B.B. Wang and J.F. Du  | 305 |
| <b>Improving Gearbox Design and Analysis for Offshore Wind Turbines</b><br>H. Long, J.Z. Wu and A. Firth  | 309 |
| <b>Investigation on Modulation Sidebands in a K-H-V Planetary Gear with Double-Enveloping Cycloid Drive Vibration</b><br>J.Y. Liu, S. Matsumura, B.K. Chen and H. Houjoh                  | 313 |
| <b>The Application and Investigation about Industry CT Scan Technology in the Measure and Design about Complex Box</b><br>L. Chen   | 319 |
| <b>Time Domain Computational Analysis for Shock Characteristics of Elastic Support Gearbox</b><br>G.H. Dai, C.W. Gao and Y.H. Liu   | 323 |
| <b>Effect of Tooth Surface Modification on the Load Sharing and Strength of Offset Face Gear Drive with Spur Involute Pinion</b><br>J.H. Wang, Y.B. Shen, Z.Y. Yin, J. Gao and Y.Y. Jiang | 327 |
| <b>Longitudinal Dynamic Modeling of the Snowmobile Considering Fuel Economy</b><br>X.S. Du, H.J. Liu, C.C. Zhu and H.F. Ding  | 333 |
| <b>Study on the Calculating Method of Bending Stress for Non-Circular Gear</b><br>J.Q. Li, Z.M. Liu, H.P. Zhang, L.X. Meng, L.Y. Zhang and Z.B. Wang                                      | 337 |

|  |     |
|--|-----|
| <b>Development Solution of Civil Helicopter Transmission Train Vibration Monitoring System</b><br>S.N. Zhang, W.Q. Ding and Y.H. Wang                                  | 342 |
| <b>The Effect of Superfinishing on the Contact Fatigue of Case Carburised Gears</b><br>J. Zhang and B.A. Shaw  | 348 |
| <b>Numerical Method of Determining the Curvature Interference Limit Curve for Modified Hourglass Worm Pairs</b><br>Y.P. Zhao and T.C. Wu                               | 352 |
| <b>Design, Analysis and Testing of a Mirco/Nano-Transmission Platform</b><br>C. Lin, S.S. Yu, K. Cheng and G.B. Tao  | 357 |
| <b>Optimal Design and Contact Analysis for Planetary Roller Screw</b><br>S.J. Ma, G. Liu, J.X. Zhou and R.T. Tong  | 361 |
| <b>The Application of Advanced Composite Material in Tail Driver Shaft of the Helicopter</b><br>K.F. Li and T.H. Xia   | 365 |
| <b>Research on Digital Design and Manufacture Technology of Rolling Swing Movable Teeth Transmission</b><br>Y.L. Yi and Z.J. An  | 370 |
| <b>A Lumped Parameter Model to Analyse the Dynamic Load Sharing in Planetary Gears with Planet Errors</b><br>X.Y. Gu and P. Velez                                      | 374 |
| <b>Sensitivity Analysis of Natural Frequency to Structural Parameters of Helical Gear Shaft for Wind Turbine Gearbox</b><br>J.G. Wang, Y. Wang, Y.T. An and Q.L. Huang | 380 |
| <b>Static/Dynamic Contact Finite Element Analysis for Tooth Profile Modification of Helical Gears</b><br>Y.J. Wu, J.J. Wang and Q.K. Han                               | 384 |
| <b>Helicopter Transmission System Technology Readiness Assessment</b><br>J.W. Liu, S. Wang and Y.H. Wang   | 389 |
| <b>Current Development Situation and Prospect of Circular-Arc Gear</b><br>H.M. Gao, Y. Liu, Y. Chen and S.J. Liu   | 394 |
| <b>A New Method of Constructing Tooth Surface for Logarithmic Spiral Bevel Gear</b><br>Q. Li, Z.L. Wei and H.B. Yan  | 399 |
| <b>Generation and TCA of Straight Bevel Gear Drive with Modified Geometry</b><br>J.S. Jiao and X.M. Cao  | 403 |
| <b>Effects of Technical Elements on Microstructure and Hardness of TiAlN/TiN Coatings</b><br>L. Lu, M.H. Ren and T. Jiang  | 407 |
| <b>Computer Simulation Analysis of Bending Stress for Face Gear with a New Type Fillet Tooth Surface</b><br>Y.B. Shen, J. Gao and W.Q. Ding                            | 411 |
| <b>Thermal Network Model for Temperature Prediction in Planetary Gear Trains</b><br>L.F. Chen, X.L. Wu, D.T. Qin and Z.J. Wen  | 415 |
| <b>The Design of RODS Software on the Basis of Transmission Machinery Robust Optimal Designing System</b><br>H.X. Zhang, X.C. Lu and L. Lu                             | 419 |
| <b>Study on Ultrasonic Lapping System of Spiral Bevel Gear</b><br>J.J. Yang, B.Y. Wei, X.Z. Deng and Z.D. Fang   | 424 |
| <b>Quantitative Evaluation of Aero Spiral Bevel Gear Meshing Quality</b><br>P. Jiang, G.L. Liu, R.T. Zhang and C.Q. Wang   | 428 |
| <b>Effect of Transmission Error on the Fluctuating Tension Force for Dual-Coiler Machine</b><br>Y.Q. Wang, F.Y. Wang and Y.X. Luo                                      | 434 |
| <b>Advanced Developments in Computerized Design and Manufacturing of Spiral Bevel and Hypoid Gear Drives</b><br>Q. Fan   | 439 |
| <b>Study on the Micro Thermal EHL Behavior of Wind Turbine Gearbox</b><br>B. Wu, W.K. Shi, L. Zhao and P. Fu   | 443 |
| <b>Experiment Study of Heat Transfer in Aeroengine Bearing Chambers</b><br>X.C. Yuan, H. Guo and L.Y. Wang   | 448 |
| <b>The Tooth Form Deviation Correction of CNC Spiral Bevel Gears Grinding Machine</b><br>W.Q. Zhang, X.D. Guo and M.D. Zhang   | 454 |

|   |     |
|---|-----|
| <b>Analysis of Thermoelastic Instability on Multi-Disc Clutch</b><br>W. Yang, G.D. Lu and H.S. Lv   | 458 |
| <b>Study of the Brush Seal Design and Test Technology</b><br>N. Li, G. Tang and L. He   | 463 |
| <b>Modeling and Simulation of Mechatronic System to Integrated Design of Supervision: Using a Bond Graph Approach</b><br>M.A. Mellal, S. Adjerid and D. Benazzouz                       | 467 |
| <b>Design and Manufacture of Helical Planetary Gear Reducer with Small Module and Big Helical Angle</b><br>J.M. Deng, H.P. Shen, L. He, W. Zhu, D.M. Tang, L. Ding, J. Li and W.Z. Zhou | 471 |
| <b>Study on Designing and Dressing of Worm for Grinding Process of Face Gear</b><br>X.Z. Li, R.P. Zhu, Z.M.Q. Li and F.J. Li  | 475 |
| <b>Bifurcation Analysis of Impact Model in Gear Transmission System</b><br>J.Y. Tang, Q.B. Wang, L.J. Wu and S.Y. Chen  | 479 |
| <b>Operational Modal Test for Wind Turbine Gearbox</b><br>Z.Q. Zheng, W.K. Shi and K.Y. Liu   | 483 |
| <b>Transmission System Health Management Technique</b><br>X.X. Cai, X.J. Guo and H.Y. Long  | 487 |
| <b>Strength Analysis of Logix Gear Based on UG</b><br>J.H. Wang, Y.C. Wang, F. Xie and X. Huang   | 492 |
| <b>Globoidal Indexing Cam's CAD/CAM Development on Pro/E</b><br>N.F. Xu, F. Xu and W. He  | 496 |
| <b>Anonymous Function Method and its Application in Screw Pump's Design and Processing</b><br>Y.X. Zhang, Q. Tang and X.Z. Ye   | 500 |
| <b>Rotor Dynamic Design of a Helicopter Tail Drive Shaft System</b><br>Y.H. Wang, W. Yuan and Y.N. Chen   | 504 |
| <b>A Model of Nonlinear Dynamic Modeling for Planetary Gear Transmission System with Backlash</b><br>F.J. Li, R.P. Zhu, H.Y. Bao and X.Z. Li  | 510 |
| <b>Dynamic Simulation Analysis of the Globoidal Indexing Cam Mechanism</b><br>F. Xu and W. He   | 514 |
| <b>Effects of Gear Manufacturing Error on the Dynamic Characteristics of Planetary Gear Transmission System of Wind Turbine</b><br>H.T. Chen, X.L. Wu, D.T. Qin, J. Yang and Z.G. Zhou  | 518 |
| <b>Effect of Shot Peened and Overload on Low Cycle Fatigue of Simulated Terminal Gear Specimen</b><br>Y.M. Zhao, G.C. Ge and X.X. Cai   | 523 |
| <b>Effects of Graphite Content on Performance of Powder Injection Molding Copper-Based Antifriction Materials</b><br>B. Qiao, L. Xiao, F. Shang, H.Q. Li and T.L. Guo                   | 527 |
| <b>Dynamic Contact Emulate Analysis of Logarithmic Spiral Bevel Gear with ANSYS/LS-DYNA</b><br>Q. Li, S.Q. Wu and H.B. Yan  | 531 |
| <b>Structure Design Research for Concrete Mixer Blade</b><br>H. Zhang, Q. Tang and Y.X. Zhang   | 535 |
| <b>Application of Contact Analysis in Strength Analysis of Helicopter Transmission System</b><br>W. Li  | 539 |
| <b>Adaptive Impulse Controller Design of Harmonic Drives System with Friction</b><br>G.J. Li  | 543 |
| <b>Research on Geometry Relationship of Pin-Rack Gearing</b><br>Z.H. Feng, M.K. Gou and S. Wu   | 547 |
| <b>Coupled Motion Control and Adjustment in Automatic Programming System of CNC Hobbing Machines</b><br>Q. Li, L.L. Yi, S.L. Wang and J. Zhou   | 552 |
| <b>Investigation and Application of the Helicopter Typical Flight States Identification</b><br>Z.H. Wan   | 556 |

|  |     |
|--|-----|
| <b>The Optimization Design for Rack Tooth Profile Curve of Straight Push-Rod Linear Reducer</b>                                |     |
| C.X. Zhou, Q.S. Huang and F. Guan  | 562 |
| <b>Mechanisms of Synchronous Belt Tooth Failure due to Fatigue Shear Fracture</b>  |     |
| J.H. Guo, H.Y. Jiang and D.S. Li   | 566 |
| <b>Precision Involute Gearboxes</b>  |     |
| B.R. Höhn, K. Stahl, H.P. Otto and H. Bauhoffer  | 570 |
| <b>Study on Face Gear's Bending Stress Based on Test and Finite Element Analysis Method</b>                                    |     |
| Z.H. Huang and B. Tang   | 574 |
| <b>Powertrain Control Logic Test for Plug-in Hybrid Electric Vehicle</b>   |     |
| M. Ye, Y.G. Liu and H. Shu   | 579 |
| <b>Effect of Atomic-Scale Roughness on Contact Behavior</b>  |     |
| F.L. Duan, H.B. Qiu, J.M. Yang and C.Y. Wu   | 584 |
| <b>The Technique of Centrifugal Load Loading on a Tail Rotor Shaft Fatigue Life Test</b>                                       |     |
| L.S. Lin   | 590 |
| <b>The Design of the Tooth Shape Silence Chain</b>   |     |
| G.X. Yang  | 594 |
| <b>Failure Analysis of Output Shaft in the Gearbox Transmission</b>  |     |
| W.J. Xu, Y.F. Chen, J. Wang and T. Wang  | 598 |
| <b>Influence Factors and Calculating Methods for Gear Windage Power Loss</b>   |     |
| Y.Z. Ge, X.M. Lei, Y.C. Zhang and P. Liu   | 602 |
| <b>Optimum Design of a 3-RRR Planar Parallel Manipulator with a Singularity-Free Workspace</b>                                 |     |
| M.W. Gao, X.M. Zhang and Z.W. Wu   | 606 |
| <b>Study on Dynamic Load Sharing Behavior of Two-Stage Planetary Gear Train Based on a Nonlinear Vibration Model</b>           |     |
| T.J. Li, R.P. Zhu and H.Y. Bao   | 611 |
| <b>Research on Milling-Turning Compound Processing of Spiral Bevel Gears Based on GibbsCAM</b>                                 |     |
| G.B. Tao, L.L. Yi, Z. Zheng and L.H. Hu  | 615 |
| <b>Design of Wind Turbine Gearbox Housing</b>  |     |
| Q.F. Cao, H.Y. Du, Y.C. Zhang and P. Liu   | 619 |
| <b>Numerical Analysis on Transmission Characteristics of Stephenson's Six-Bar Punching Mechanism with Servo Input</b>          |     |
| J.G. Hu, Y.S. Sun, Y.Q. Cheng and W.P. Ruan  | 623 |
| <b>Research on the Knowledge Fusion Technology Based Optimized Design of the Drive Axle Differential Gear</b>                  |     |
| K. Chen, C.W. Yao and G.F. Yin   | 629 |
| <b>Modular Design on Basic Parameters of Volume Reducer</b>  |     |
| T. Wang, J. Shen and F.Q. Zhao   | 633 |
| <b>An Accurate Modeling Method of the Plane Enveloping Hourglass Worm</b>  |     |
| X.A. Chen and L.M. Tang  | 637 |
| <b>Behavior Test on Wind Turbine Gearbox</b>   |     |
| L.Y. Tan and J.B. Liu  | 641 |
| <b>Rolling Contact Fatigue Life of Case-Hardened Steel Treated by Shot Peenings with Shot Diameters of 0.05 mm and 0.30 mm</b> |     |
| L. Wang, G.L. Liu, M. Seki, M. Fujii and Q. Li   | 645 |
| <b>Multiscale Analysis on Friction-Reducing Characteristics of Textured Surface in Nanoscale Sliding Contacts</b>              |     |
| R.T. Tong, G. Liu, L. Liu and S.J. Ma  | 649 |
| <b>Study on Dynamic Characteristics of Wind Turbine Planetary Gear System Coupled with Bearing at Varying Wind Speed</b>       |     |
| Z.G. Zhou, D.T. Qin, J. Yang and H.T. Chen   | 653 |
| <b>Design and Analysis for High-Speed Gear Coupling</b>  |     |
| X.M. Lei, Y.Z. Ge, Y.C. Zhang and P. Liu   | 658 |
| <b>Dynamic Optimization Design of a Warship's Gearbox Based on FEM</b>   |     |
| Y.H. Xue, X.H. Li, Z.G. Wang and J. Song   | 662 |

|  |     |
|--|-----|
| <b>Optimum Design of Motion Curve of Cam Mechanism with Lowest Maximum Acceleration</b><br>C.Q. Sun, A.H. Ren and G.X. Sun   | 666 |
| <b>Temperature Field and Residual Stress Analysis of the Gear on CO<sub>2</sub> Laser Welding Process</b><br>J. Luo, F. Li, K.L. Xue, D.J. Liu and H.W. Zhang                          | 670 |
| <b>Study of Load Distribution and Sharing Characteristics of Planetary Geartrain for Wind Turbines</b><br>J.G. Kim, G.H. Lee, Y.J. Park, Y.Y. Nam and T.H. Chong                       | 674 |
| <b>Study on Loads of Accelerated Contact Fatigue Testing and its Application</b><br>H. Zuo, Y.C. Zhang, P. Liu, W. Wang and S. Xiong   | 680 |
| <b>The Optimization and Simulation of New Type Non-Circular Gears in CVT</b><br>F.Y. Zheng, A.H. Ren, C.Q. Sun and G.X. Sun  | 684 |
| <b>Research of Simulation Technology in Low-Stress Machining on Tooth Surface of Spiral Bevel Gears Used in Aviation Industry</b><br>Y.Z. Wang, Y.Y. Chen, X. Han, L.F. Wu and H. Zeng | 688 |
| <b>Effect of Machining Precision Caused by NC Gear Hobbing Deformation</b><br>S.L. Wang, Y. Yang, J. Zhou, Q. Li, S. Yang and L. Kang  | 692 |
| <b>Research on Lead Modification of Cylindrical Gears with Consideration of System Deformation</b><br>S. Xiong, Y.C. Zhang, P. Liu, W. Wang and H. Zuo                                 | 696 |
| <b>Modeling and Analysis of Gear Driving System Based on the CATIA</b><br>W. Cao and R. Wang   | 700 |
| <b>The Research on General Modeling Methods of the Complicated Transmission Based on Hypergraph Theory</b><br>C.L. Xiang, Y.Y. Zhang, H. Liu and M. Cui                                | 704 |
| <b>A Simplified Approach Based Phase Angle for Tooth Contact Analysis of Planetary Gear Trains</b><br>K. Xu, G. Liu, X.Z. Deng, J.J. Yang and J.X. Su                                  | 709 |
| <b>Effect of Friction Coefficient on the Stiffness Excitation of Gear</b><br>Y.M. Hu, D.S. Xue and Y.J. Pi   | 713 |
| <b>Structural Design and Analysis of Thrust Collar in Main Wind Turbine Speed-Increasing Gearboxes</b><br>Q.Q. Xiang, M. Li, Y.C. Zhang and H.B. Zhou                                  | 717 |
| <b>Study of Bearing Modelling in the Helicopter Gearbox</b><br>L. Zamponi, E. Mermoz and J.M. Linares  | 721 |
| <b>Static Load Sharing in Power-Split Planetary Gear Trains</b><br>Y. Li, G. Liu and G.L. Liu  | 725 |
| <b>Solid Modeling Methods and Wire-Cutting Process Simulation of Non-Circular Gears</b><br>M. Zhang, D.Y. Kong, J.L. Zhao, Y.P. Liu and C.B. Hu  | 730 |
| <b>Gearbox Fault Diagnosis Using Vibration Signal with Wavelet De-Noising</b><br>Z.F. Dong, H. Cheng, H.J. Yang, W. Fu, J.W. Chen, Z.Y. Shi and D.L. Zhao                              | 735 |
| <b>Dynamic Analysis and Experimental Study of MW Wind Turbine Gearbox</b><br>H.J. Wang, X.S. Du and X.Y. Xu  | 739 |
| <b>Determination of Load-Sharing Displacement of Flexible Pin Roll in Planet Gear Train</b><br>Y.C. Zhang, L. Tan, P. Liu and H.B. Zhou  | 743 |
| <b>Research on Vibration Influence Chart of Planetary Gear Systems</b><br>L.H. Chang, G. Liu, L.Y. Wu and Z.H. Bu  | 747 |
| <b>Improvement of Positioning Error on a Ball Screw by Cooling System</b><br>Z.Z. Xu, Q. Zhang and S.K. Lyu  | 752 |
| <b>A Discrete Lumped-Parameter Dynamic Model for a Planetary Gear Set with Flexible Ring Gear</b><br>J. Zhang, Y.M. Song and J.Y. Xu   | 756 |
| <b>Modeling and Controlling of Anti-Slip Regulation Based on Limited-Slip Differential</b><br>J.J. Hu, P. Ge, Z.B. He and D.T. Qin   | 762 |
| <b>Advanced Methods of Gas Turbine Reducer Design and its Analyses</b><br>L. Xiao and R.M. Li  | 767 |
| <b>Deformation of Harmonic Drive in Transmission State Based on Contact Analysis with Shell Element Tooth</b><br>X.X. Chen, S.Z. Lin, J.Z. Xing and Y.S. Liu                           | 771 |

|  |     |
|--|-----|
| <b>Research on Torsional Dynamic Model and Rigidity Excitation of Cycloid Ball Planetary Transmission System</b><br>P. Zhang, Z.J. An and Z.M. Yang  | 775 |
| <b>Coordinated Torque Control for Mode-Switch between Motor and Engine Driving in Heavy Hybrid Electric Vehicle</b><br>Y. Yang, J.F. Huang, D.T. Qin and W.H. Yang                                       | 779 |
| <b>Analysis of Winding Dynamics of Film Web on Winder</b><br>G. Li and Y. Sun  | 784 |
| <b>Life Estimation of Tilt-Rotor Transmission Based on Dynamic Analysis</b><br>J.S. Guo, S.M. Wang and H.X. Liu  | 788 |
| <b>Fluid Dynamic Analysis and Experimental Study on Wet Friction Clutch</b><br>T.J. Lin, L. Pan and S.J. Zhang   | 792 |
| <b>Study on Visualization of Planetary Gear Based on Topological Theory</b><br>X.Y. Shi  | 797 |
| <b>Strategy Study on Comfort Optimization of Metro Train Traction</b><br>C.M. He, H. Li, G.S. Fei and S.J. Pang  | 801 |
| <b>Numerical Analysis of Concave-Slab Type Water Lubricated Rubber Alloy Bearings' Lubrication</b><br>J.X. Wang, Y.F. Han, G.W. Zhou, K. Xiao, Y. Qin and S. Wu  | 805 |
| <b>The Analysis of Gear Contact under Cyclical Load</b><br>L.P. Wang, Y.Q. Xu and Y. Yuan  | 809 |
| <b>Initial Behavior of Speed Increasing Helical Gears by Torque Fluctuation</b><br>C.I. Park   | 813 |
| <b>Static Simulation Analysis of Torsion Characteristics of Highly Flexible Coupling</b><br>K. Xiao, J.X. Wang, J.M. Li and Y.M. Zheng   | 817 |
| <b>Using Lubricating Oil Filter Debris Analysis to Monitor Abnormal Wear of Aero-Engine</b><br>Z.X. Zhu, J.Z. Zheng and D. Chen  | 821 |
| <b>Research on Gear Contact Fatigue Stress Test</b><br>T. Wang, H.M. Li, R.L. Zhang and Z.F. Wu  | 825 |
| <b>A Load Spectrum Method for Multi-Stage Planetary Transmission</b><br>C.F. Hu and Y.Q. Tan   | 829 |
| <b>The Design of Power Transmission of Electric Screw Press Directly Driven by Permanent Magnet Disc Synchronous Motor</b><br>J.T. Liang, S.D. Zhao, Y.L. Zhao and Z.Y. Sun                              | 833 |
| <b>Scanning Measurement and Evaluation of Gear Tooth Root and Bottom Profiles</b><br>S. Kurokawa, H. Kido, T. Taguchi, T. Okada, O. Ohnishi and T.K. Doi   | 838 |
| <b>A Method to Determine the Basic Value of Gear Root Stress Based on FEM</b><br>J. Zhang, H.C. Wu and H.J. Wang   | 842 |
| <b>Development and Application of Non-Contact Seal Assembly for High-Speed Shaft Ends</b><br>P. Liu, Q.P. Ou, H.B. Zhou and M. Li  | 846 |
| <b>Stress Analysis of the Skewed-Roller Slipping Clutch Based on Frictional Contact and Dynamic Equilibrium</b><br>M. Feng and G.R. Yan  | 850 |
| <b>Optimization of New Type Sintering Machine's Sprocket Wheel with Even-Number Teeth</b><br>M.H. Bai, L.B. An, S.B. Ren and L.J. Wang   | 854 |
| <b>Optimum Design of Toggle Transmission System in Double Toggle Mechanical Press Using Response Surface Methodology Combined with Experimental Design</b><br>J. Xie, S.D. Zhao, Z.H. Sha and J.T. Liang | 858 |
| <b>Original Research on Logarithmic Spiral Bevel Gear</b><br>H.B. Yan, Q. Li, Z.L. Wei and S.Q. Wu   | 863 |
| <b>Effects of Surface Roughness and Abnormal Surface Layer on Fatigue Strength</b><br>G. Deng, S. Suzuki and T. Nakanishi  | 867 |
| <b>Precise Modeling of Arc Cylinder-Gears with Tooth Root Fillet</b><br>Y.M. Cui, Z.D. Fang, J.Z. Su and Y.P. Liu  | 871 |
| <b>Study on 18Cr2Ni4WA Gear Contact Fatigue Experiment and Data Analysis</b><br>Z.F. Wu, T. Wang, R.L. Zhang and H.M. Li   | 875 |
| <b>Thermal Analysis of Axial Driving System for Numerically Controlled Machine Tool</b><br>B. Li, H.R. Cao and Z.L. Yang   | 879 |

---

|  |     |
|--|-----|
| <b>Reduction of Power Losses in Transmissions and Gearings</b><br>F.J. Joachim, N. Kurz and J. Börner                                      | 883 |
| <b>Manufacturing Method of Long-Cone-Distance Spiral Bevel Gears Based on CNC Machining Center</b><br>B.Z. Lei, B. Zhang and H. Zhang      | 889 |
| <b>Analysis of Gas Dynamics in a Rotating Disk Cavity</b><br>Y. Liu, Y.H. Zhang, G.D. Chen and R. Wan                                      | 893 |
| <b>Micropitting in Wind Turbine Gearboxes: Calculation of the Safety Factor and Optimization of the Gear Geometry</b><br>H. Dinner         | 898 |
| <b>Modal Analysis and Parameters Research of Internal Helical Gears Based on AWE</b><br>Y.J. Gong, X.Y. Wang, H. Zhao and K. Huang         | 904 |
| <b>Analysis on Deformation and Relieving of Spline in 1.5MW Wind Turbine Gearbox</b><br>M. Zhang, L.Y. Zhang, Y.H. Bao, F. Gao and C. Wang | 908 |

## Development of Helicopter Power Transmission System Technology

Yin Zeyong<sup>1, a</sup>, Fu Bibo<sup>2, b</sup>, Xue Tongbo<sup>2, c</sup>, Wang Yonghong<sup>2, c</sup>, Gao Jie<sup>2, c</sup>

<sup>1</sup> Aviation Industry Corporation of China, Beijing, China

<sup>2</sup> Aviation Powerplant Research Institute of China, Hunan, China

<sup>a</sup> Yinzy@cae.cn, <sup>b</sup> fubibo@163.com, <sup>c</sup> capi@608.163.net

**Keywords:** Helicopter power transmission system, transmission configuration, planetary gear train, split-torque gear train, face gear drive

**Abstract.** The helicopter power transmission system technology is the key technical area for improving the helicopter performance, reducing the noise/vibration level of helicopters and decreasing the cost of life cycle of helicopters. In this paper, the technical characteristics of the helicopter power transmission system are introduced first. Then, the development history and trend of the transmission configuration, the component and the design and analysis technique of the transmission system are described. The advanced material and process technology applied in the helicopter power transmission system are also described. Finally, the power transmission system technology used in the high speed helicopters is briefly presented.

### Introduction

The power transmission system, engine and rotor system are the three key rotation components of a helicopter. The function of the power transmission system is to distribute proportionally the engine power to the main rotor and the tail rotor, whose rotation speeds are much lower than that of the engine, to transmit the load from engine, main rotor and tail rotor to the airframe and to drive the helicopter accessories [1]. Generally, the power transmission system of the most widely used single rotor helicopter consists of the main gearbox (MGB), power drive shaft (PDS), tail drive shaft (TDS), intermediate gearbox (IGB) and tail gearbox (TGB), etc.(Fig.1 and Fig.2).

As well known, a helicopter power transmission system is dedicated to one specific helicopter. However, the advanced power transmission systems have such common features as compact structure, long drive train, large transmission power and high speed ratio. The development of the power transmission system involves the research which focuses on the advanced technologies such as the new design concept, advanced transmission structure, components and lubrication system design, advanced material and process technology, condition monitoring and failure diagnosis as well as the vibration and noise reduction. The development of transmission system technology is pushed by the needs for advanced products, and on the other hand its technology improvement will promote the product development.

The power transmission system has a significant impact on the performance, reliability and cost of a helicopter. As reported, the power transmission system's comprise almost 30% of the helicopter maintenance cost and 16% of the mechanical related malfunctions that often result in the loss of helicopter [2]. Its contribution to the weight of helicopters is about 10~15%,and to the procurement cost is about 12~20% as we summarized. Therefore the development of power transmission system technology aims at higher power density, longer life, higher reliability, better maintainability, higher survivability, lower noise and lower life cycle cost.

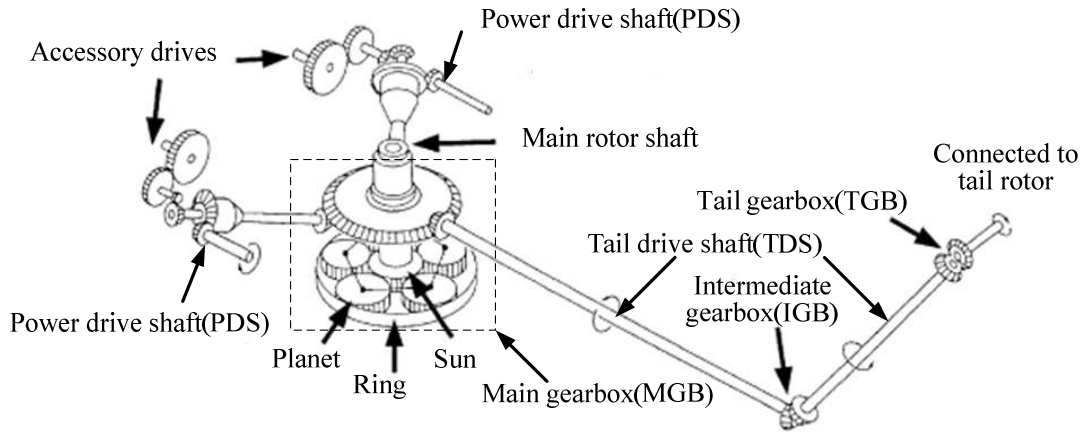


Fig.1 Sketch of drive train of power transmission system [3]

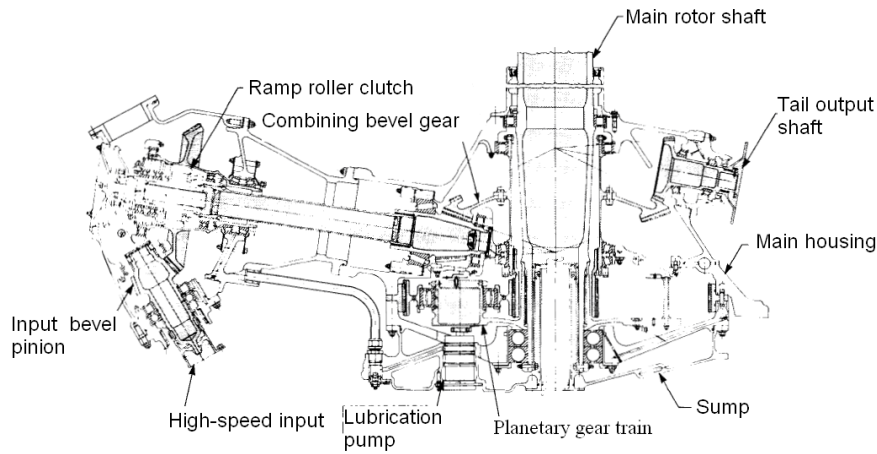


Fig.2 Section view of a typical MGB [4]

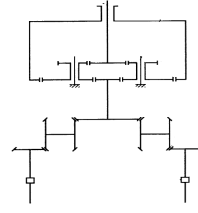
**Technical Characteristics of Power Transmission System**

**Development History of Power Transmission System.** Since 1950's, three generations of the power transmission system have been developed. For the third generation power transmission system, the ratio of weight to output torque of MGB is reduced to 0.060~0.063kg/kgf·m, the loss-of-lubrication operation capability reaches 45min and TBO (Time between Overhaul) 4000 flight hours. The fourth generation power transmission system is in development. The main technical parameters of the power transmission system generations as well as the helicopters which the power transmission systems are installed on are listed in Table 1, and some typical types of them are shown in Fig.3.

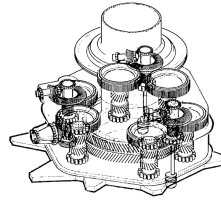
Table.1 Main technical parameters of power transmission systems

| Generation  | 1st                              | 2nd                                    | 3rd                              |  | 4th(Prototype)                     |
|---|----------------------------------|--|----------------------------------|--|------------------------------------|
| Into service                                      | 1950s                            | 1960s                                  | 1970s~1980s                      | 1990s~2000s                                  | 21 century                         |
| Helicopter model                                  | Mi-4<br>Bell 47<br>S-51<br>Ka-18 | Mi-6,Mi-8<br>UH-1C<br>Bell209<br>SA321 | A129<br>UH-60A<br>AH-64A<br>CH53 | Mi-28,K-50<br>UH-60L<br>AH-64D<br>Tiger,NH90 | Comanche<br>UH-60M<br>AH-64M       |
| MGB input speed(r/min)                            | <3000                            | <7000                                  | >20000                           | >20000<br>("Tiger"6000)                      | >20000                             |
| MGB total speed ratio                             | 13.47<br>(Mi-4)                  | 28.57<br>(Super Frelon)                | 81<br>(UH-60A)                   | 81<br>(UH-60L)                               | 81(UH-60M)<br>64.79<br>(Comanche)  |
| MGB TBO(h)  | <600                             | <1200                                  | 1500~3000                        | 3000~4000                                    | 4000~5000                          |
| MGB ratio of weight to output torque (kg/(kgf·m)) | ~0.075                           | ~0.070                                 | ~0.067                           | 0.060~0.063                                  | 0.056~0.058                        |
| MGB loss-of-lubrication operation capability      | No requirement                   | No requirement                         | 30min                            | 45min  | >45min<br>(Comanche reached 60min) |
| HUMS*   | None                             | None                                   | Partially                        | Partially                                    | Full                               |

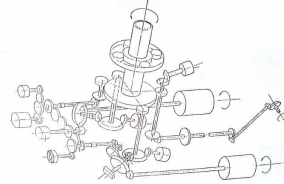
\* Note: HUMS: Health and usage monitoring system.



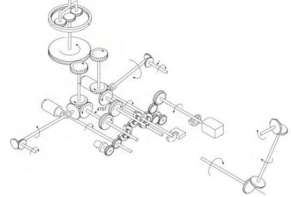
(a) K-50 helicopter and transmission system sketch



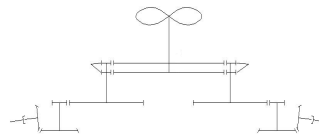
(b) CH53 helicopter and transmission system sketch



(c) "Tiger" helicopter and transmission system sketch



(d) Apache helicopter and transmission system sketch



(e) Comanche helicopter and transmission system sketch

Fig.3 Typical power transmission systems and corresponding helicopters

**Technical Characteristics of Up-to-date Power Transmission System.** The main technical characteristics of up-to-date power transmission system are as follows: high input rotation speed, high power density, long life, high reliability, good maintainability, high efficiency and high survivability.

(1) High input rotation speed

Most of the engines are designed without reduction gearbox at present, and their output rotation speeds (i.e. input rotation speed of MGB) are increased to 20000 r/min or more from the previous 6000 r/min or less, thus the technology for the high input speed MGB design and manufacturing is required.

(2) High power density

The power transmission system with high power density could obviously reduce a helicopter's net weight, increase its payload, and therefore improve the helicopter performance, thus corresponding transmission configuration and components, high strength material and more efficient lubrication system are needed.

(3) Long life, high reliability and good maintainability

In order to reduce the life cycle cost, a power transmission system should be of longer life, higher reliability and better maintainability. There is significant number of the critical and important parts in a power transmission system and their failure could result in catastrophic accident, therefore high reliability for the transmission system is requisite. It makes the design, manufacture, test, maintenance, diagnosis and inspection of the power transmission system more difficult.

(4) High efficiency

Due to the large difference of the rotation speeds between the main rotor (as well as tail rotor) and the engine output, the MGB of the power transmission system should consist of multiple complicated gear stages, thus the transmission efficiency of the gearbox is significantly affected. It is necessary to design the more efficient components of the transmission system. For advanced helicopter power transmission systems, the efficiency of a single stage drive of the MGB should be over 99% and about 97% for the whole MGB.

(5) High survivability

According to airworthiness regulations, taking into account the severe abnormal oil leakage, it is mandatory for the power transmission system to operate for a certain period without oil, which is the loss-of-lubrication operation capability. For advanced helicopter transmission systems, the loss-of-lubrication operation time could reach one hour. In addition, the crashworthiness requirements are defined in the airworthiness regulations. Furthermore, the ballistic tolerance is required for the military helicopter.

### **Development of Transmission Configuration, Installation Structure, Component technology and Design Analysis of Power Transmission System**

The developments of the power transmission system, engine and rotor system are affected and promoted each other. On one hand, high aerodynamic performance, more compact structure, light weight and high output rotation speed are the characteristics of advanced engine design (the output rotation speeds of turbo shaft engines reach 20000rpm/min and more at present). On the other hand, and to some degree, the lower speed rotor design could result in higher efficiency of the rotor. Thus the problem faced by a transmission designer is to design the power transmission system which has larger speed ratio and higher power density. A speed ratio up to 100 between the engine and the main rotor is expected [5].

#### ***Technical Development of Transmission Configuration and Installation Structure of Power Transmission System***

**Main transmission configuration.** Most of the MGB are the twin-engine power combining gearboxes, whose design method could also be used in other gearbox types. Therefore, here it is discussed in detail.

There are following four types of the transmission configuration of MGB main gear train generally (Fig.4):

- (1) Type A: cylindrical gear combining stage / bevel gear angle turn stage / planetary gear stage
- (2) Type B: bevel gear angle turn stage / cylindrical gear combining stage/ planetary gear stage
- (3) Type C: bevel gear angle turn stage/bevel gear angle turn and combining stage/ planetary gear stage
- (4) Type D: gear train of fixed-axis (simple fixed-axis gear train and split-torque gear train)

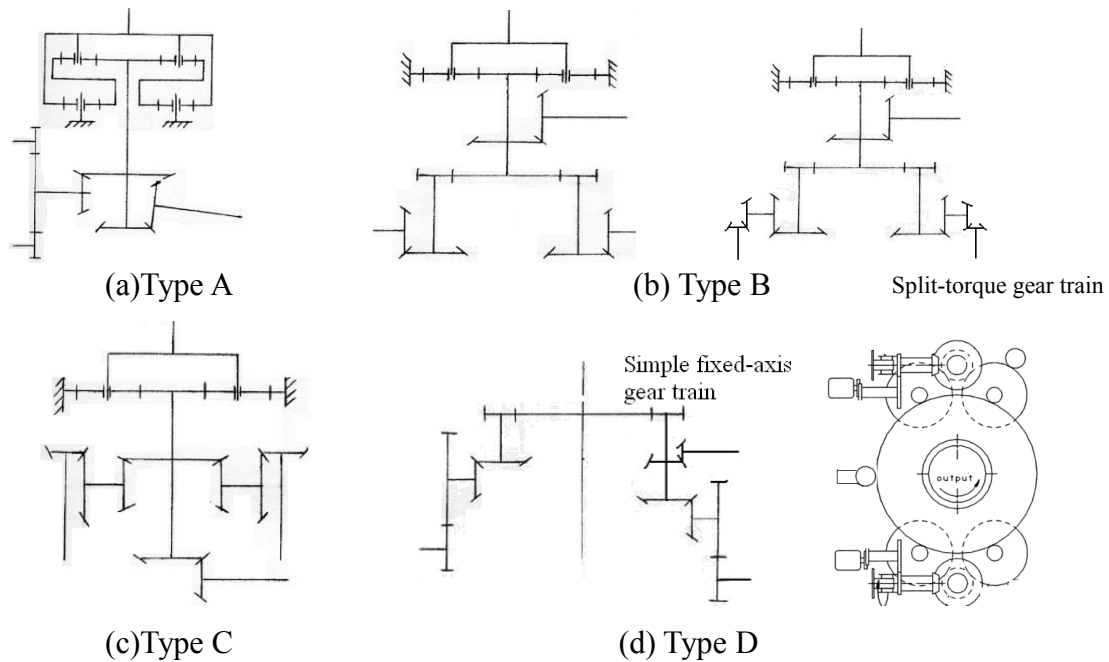


Fig.4 Drive train sketch of MGB

The MGB was often designed as Type A in the past because of plenty of existing engineering experiences, but the structure of some old MGB of this type seems complicated. In comparison with other types, the loads of its bevel gears may be larger and the MGB weight may be increased consequently.

Type B, when the first two stages are of bevel gears, could be used for the wide range of combining distance between two inputs of the gearbox but not suitable for the too small combining distance ones.

Type C could also be used for the wide range of combining distance. The structure of this configuration is compact and its diameter and height could be smaller. Its benefit on reducing the number of components and improving the reliability is very clear.

The structure of the MGB Type D is simple with fewer gears and bearings and suitable for the smaller height requirement. For the MGB transmitting large power, the split-torque gear train could be used, which is beneficial to the weight, improves the strength and fatigue life of the MGB and is more often used in the recently developed helicopters. For the MGB with large speed ratio a planetary gear train could be added as the last stage.

The IGB, TGB and TDS consisted of horizontal and pylon shafts are used in the medium and large size helicopters, whereas in small-sized helicopters only TGB and horizontal tail drive shafts are used. The IGB and TGB are of single stage spiral bevel gear drive.

**Development trend of transmission configuration.** The transmission configurations with conventional planetary gear train are still widely used (Fig.5) and the planetary gear train has the advantages of sharing torque and compact structure. However, as reported, the speed ratio of planetary gear train is restricted and could not exceed 4.7 [5, 6].

During the past decades, professors and engineers have been working on developing the high performance MGB transmission configurations such as those with bearingless planetary gear train (Fig. 6) and those with split-torque gear train (see Fig. 7) as well as improving the conventional planetary ones [1,6].

The configuration with bearingless planetary gear train offers advantages over the conventional planetary one. It could provide large speed ratio with high efficiency, sufficient stiffness and self-centering capability, give uniform load distribution between planet gears, and effectively prevent the planetary elements from casing deformation. Since it has no planet bearings, there is a weight saving, power losses and failure decreasing [1].

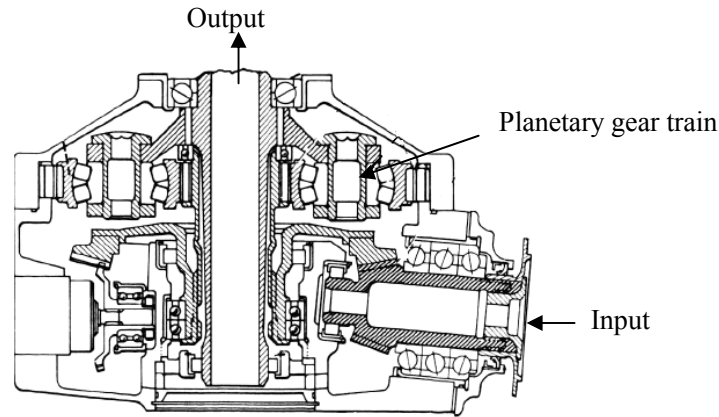


Fig.5 MGB transmission configuration with conventional planetary gear train

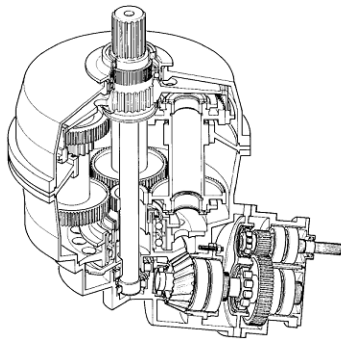


Fig.6 MGB with bearingless planetary gear train

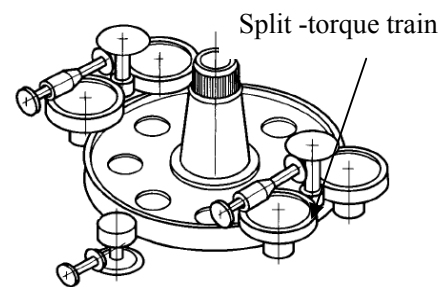


Fig.7 MGB with split-torque gear train

For the split-torque gear train, the engine power is split first and then combined. The configuration with the split-torque gear train also shows its advantage over the conventional planetary one in weight and reliability, especially for the large-sized helicopter.

The application of face gear is a progress of the power transmission system technology. Face gear is a new type of gear, which consists of an involute cylindrical pinion and a bevel gear, and has many advantages such as high load capacity, simple support structure and low sensitivity to assembling misalignment<sup>[7, 8]</sup> especially for the application in the split-torque gear train configuration.

A study provided the comparison between the MGB of a split-torque face gear train configuration (with transmission power of 1200kW and speed ratio of 66) and that of conventional 3 stage Type B configuration as shown in Table 2<sup>[5,6]</sup>.

Table 2 Comparison between the MGBs of split-torque gear train and conventional planetary gear train

| Characteristic                               | Split-torque | conventional planetary | difference |
|--|--------------|------------------------|------------|
| Total weight, (kg)                           | 193          | 330.6                  | - 40.1%    |
| Power losses, engine to rotor                | 2.2%         | 2.9%                   | - 24%      |
| Gears number in main drive train             | 8            | 12                     | - 33%      |
| Bearings number in main and tail drive train | 17           | 23                     | - 22%      |

Fig.8 shows a MGB with face gear train and the corresponding conventional one. Fig. 9 shows another example for the MGB with split-torque face gear train. The MGB in Fig.8 and 9 are composed of a face gear train and a planetary gear train.

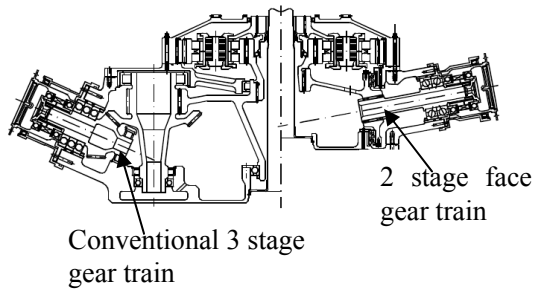


Fig.8 Face gear configuration and corresponding conventional one<sup>[7]</sup>

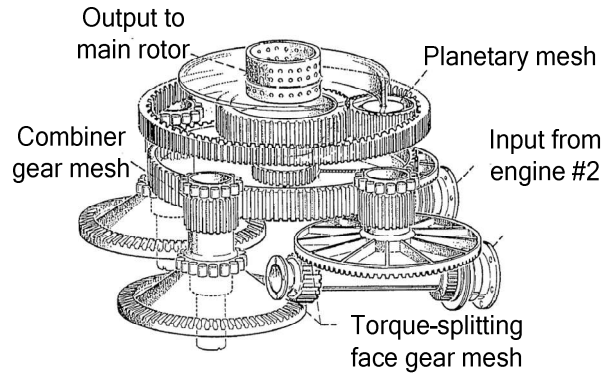


Fig.9 MGB with split-torque face gear train<sup>[9]</sup>

**Installation structure of MGB.** There are mainly 5 types of MGB installation structure, including rigid, elastomeric, nodalized beams structure etc. as following:

(1) Four struts installation (suspension installation)

For this type of installation structures, MGB is supported on the airframe with 4 struts connected with the 4 lugs of upper housing and the attachments at the bottom of MGB (Fig.10). The struts undertake lifting force, shear force and bending moment from main rotor, and the attachments at the bottom transmit the torque and shear force.

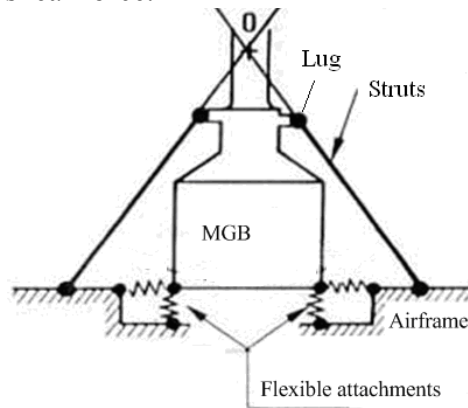


Fig.10 Installation structure of AS350 "Squirrel" MGB

(2) Eight struts installation

In this type of installation, MGB is supported with 8 struts, every two of which are connected together to form a supporting truss. The loads of the main rotor are transmitted to the airframe through the supporting truss (Fig.11).

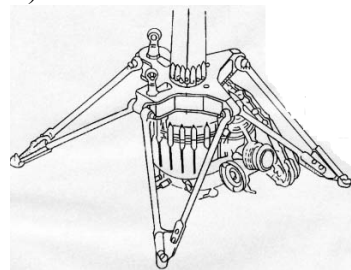


Fig.11 Installation structure of a MGB with eight struts

(3) Multiple struts installation

For this type, there are multiple supporting struts (more than 8, e.g. 12 pieces) to form a truss to support MGB as shown in Fig.12.

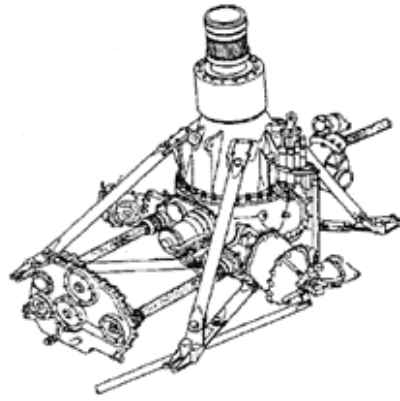


Fig. 12 Installation structure of EH101 MGB<sup>[10]</sup>

(4) MGB bottom installation

For this type, the MGB is directly bolted to the airframe with the attachments on its bottom as shown in Fig. 13.

(5) Nodalized beam installation

For this type, the MGB is installed on the airframe with nodalized beams. For example, on Bell 214 MGB, there are two attachments on the upper housing and three elastomeric supports on the lower housing, as shown in Fig. 14. The upper two attachments are installed with the nodalized beams which are connected with the airframe at their nodes. In this way the vibration transferred to the airframe is significantly reduced.

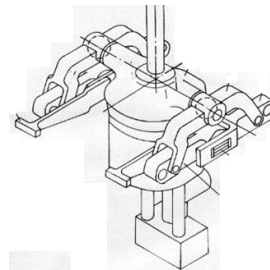
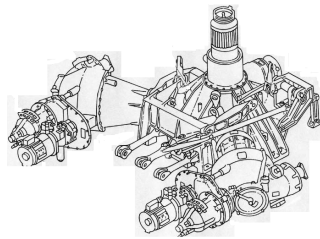


Fig. 13 “Black Hawk” MGB installation      Fig. 14 Bell 214 MGB installation

Four struts installation structure is usually applied in the MGB for which the main rotor shaft comprised a separate module with the upper housing, etc. (modular main rotor shaft). It has short path of load transmitting and passive or active damping devices could be adopted between MGB and airframe.

The redundancy and hence the crashworthiness of eight struts installation structure is larger than those of the 4 struts one. However, more space is needed to install it on the airframe and otherwise it is difficult to arrange MGB accessories. This structure is also widely applied at present.

Multiple struts installation structure is a hyperstatic structure with even larger redundancy and relatively small load on each strut. However, since all the load is transmitted by the MGB main housing, this may result in the MGB weight increase. It is more suitable for MGB of large-sized helicopters, especially the small height/diameter ratio ones.

MGB bottom installation structure also has larger redundancy and is relatively heavier than the 4 struts installation since the main casing of MGB is also subjected to all the loads from the main rotor.

The nodalized beam installation structure has an obvious effect on the vibration reduction and could be used for MGB with large height/diameter ratio and the MGB with the modular main rotor shaft.

### ***Development of Components***

**Gears.** In addition to the conventional involute gear, the gears with the non-involute profile and high contact ratio have been developed. The latter could run smoothly with higher loads capacity and lower noise level. The spiral bevel gear train with transverse contact ratio of more than 2 has also been developed<sup>[11]</sup>.

Compared to conventional "passive design", the "active design" for spiral bevel gear has been developed based on tooth contact analysis (TCA) and loaded tooth contact analysis (LTCA). In the past, because the tooth surface could not be precisely designed, only the static contact pattern could be examined during manufacturing, while the final satisfactory loaded contact pattern was acquired by repeatedly modifying machining parameters and shimming. Now, spiral bevel gear topography could be designed considering the structural deformation under the loads, and the best contact pattern under practical operation conditions could be obtained with less modification of the machining parameters and without shimming.

The best merit of face gear drive (Fig. 15)<sup>[12]</sup> is that the axial position error of the pinion has no influence on meshing performance, and the errors of other directions have little influence. Since the pinion is a spur gear without axial force applied on it, the supporting structure could be much simplified with reduction of weight. However, the tooth width determination, tooth strength calculation formula and tooth grinding method have become hotspots in the research of face gear drive because of the tooth undercutting at the inner radius, the tooth pointing at the outer radius and the inconstant top land width<sup>[13]</sup>.



Fig.15 Face gear drive

In the last decades in addition to the improvement of the conventional simple planetary gear train (Fig 16(a)), the study has been carried out on a variety of the other types of planetary gear train<sup>[14, 15]</sup> such as high contact ratio planetary (Fig 16(b)) and bearingless planetary gear train<sup>[1,9,14]</sup> (Fig.16(c)). The bearingless planetary gear train characterized with light weight, high reliability and coaxial output<sup>[1]</sup> is the most potential one for small and medium size power transmission systems in the future. However, there are still some technical issues like layout optimization and dynamic design to be solved.

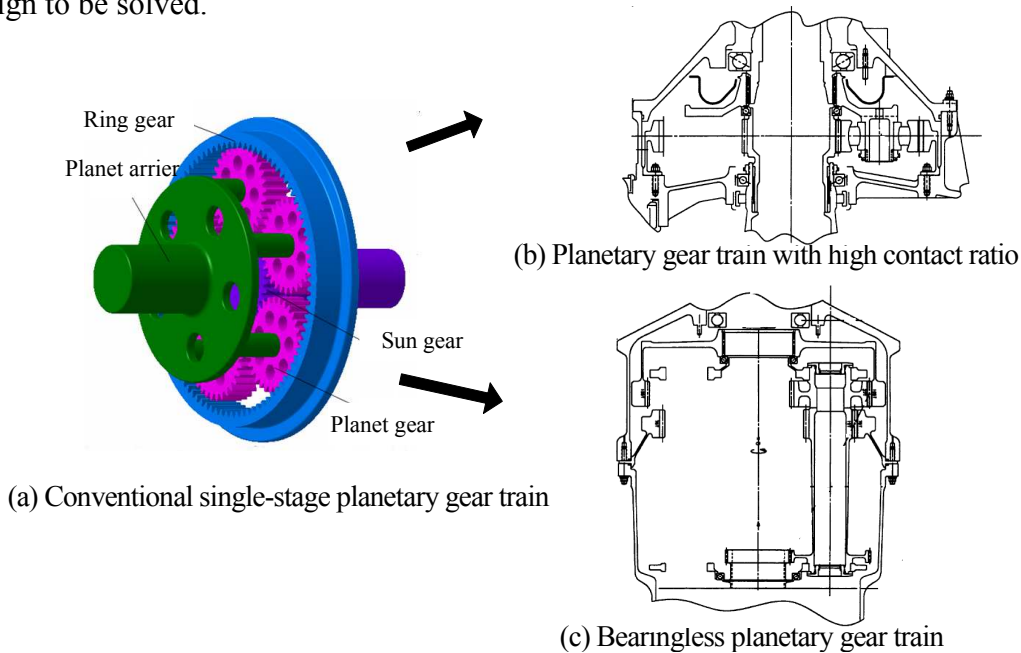


Fig.16 Configurations of planetary gear trains

**Shaft.** There are several types of rotor shafts. Such as the modular rotor shaft, MGB integrated rotor shaft and “rotational shaft and static mast”.

As explained above the modular rotor shaft is a separate unit shown in Fig.17 for SA330 "Puma" [15]. This structure is convenient for assembly and disassembly.

MGB integrated shaft (Fig 18) is usually used in the medium and large size helicopters such as that of SA321 "Super Frelon".

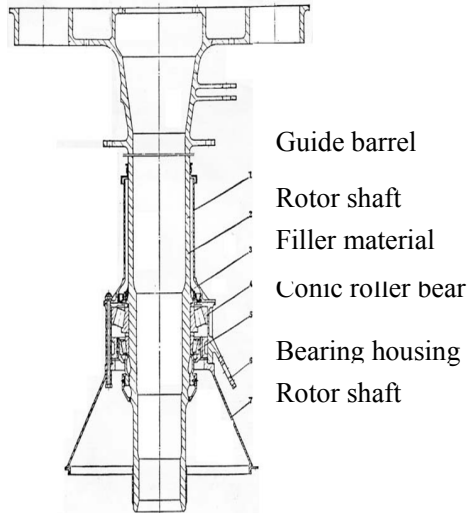


Fig.17 Modular shaft in SA330

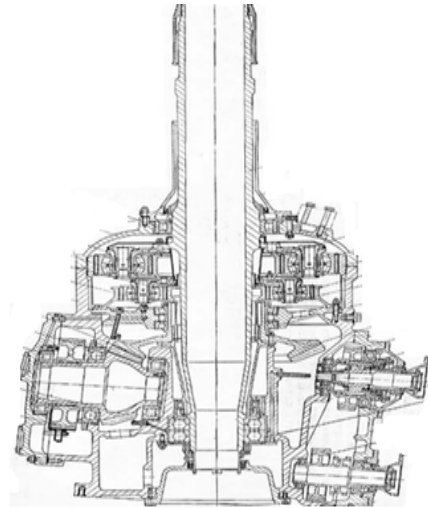


Fig. 18 MGB integrated shaft in SA321

For “the rotational shaft and static mast” configuration (Fig.19), the static mast is made to carry all the main rotor lift and horizontal force while the rotational shaft (torque shaft) only transmits the torque. The name “static mast” is derived from the fact that in the steady flight the horizontal rotor force acts as a static bending load on the mast instead of a cyclic load on the rotational shaft, which is beneficial for the fatigue life of the shaft [16]. Conic roller bearings or radial thrust ball bearings could be applied between the two components.

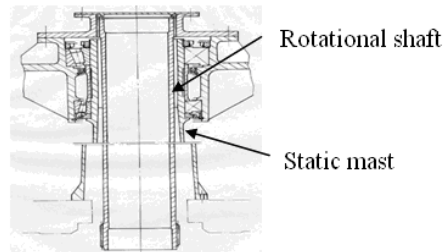


Fig.19 Example for rotational shaft and static mast

Using supercritical shafts (Fig.20) with light weight and simple structure has become a tendency in the tail drive shaft design. Magnetic suspension bearings and damping supporter would replace the conventional roller bearings and mechanical couplers [17]. Dynamic design for this kind of shafts is very important.

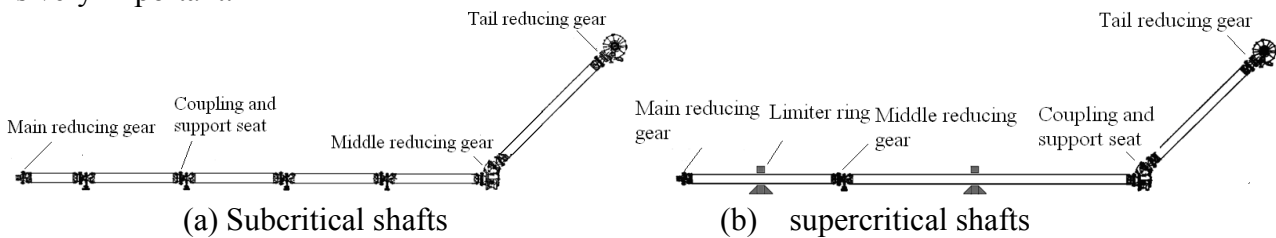


Fig.20 Subcritical and supercritical tail drive shafts

**Over-running clutch.** There are several types of over-running clutches, such as ramp roller (Fig 21(a)), sprag(Fig 21(b)) [6] and spring clutches(Fig 21(c)).

Ramp roller clutches have been applied in MGB of the speed up to 15000 r/min and the speed for sprag clutch is even more than that.

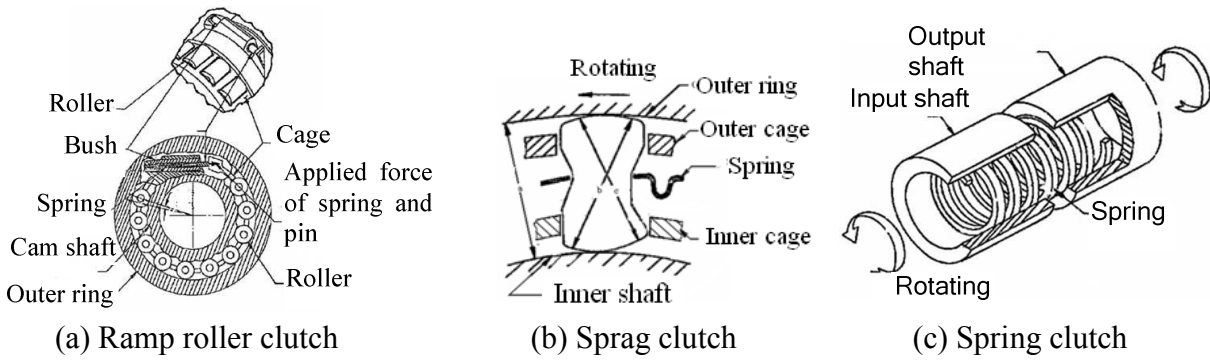


Fig.21 Sketches of over-running clutches

High speed spring clutch has become one of the features of new generation MGB, whose components are fewer than half of the sprag clutches'. High speed spring clutch with lighter weight and higher reliability could be used at the speed more than 20000r/min. However, due to the severe operation condition of its spring, the requirement for the spring is strict and the manufacturing is very difficult.

**Bearings.** There is a variety of the types of bearings used in power transmission system such as ball bearings, cylindrical roller bearings, conical roller bearings, spherical roller bearings (for planet gear), etc.

For high speed input stage of MGB, high speed conical roller bearings have been used and could be substituted for conventional ball bearings (see Fig. 22). It is reported that in an application with this kind of bearings, the radial stiffness of the bearings is increased by 4 times and the friction loss decreased by 20%<sup>[12,15]</sup>. However, the issues such as dynamics and loss-of-lubrication capacity at the high speed over 20000r/min, need to be considered more carefully.

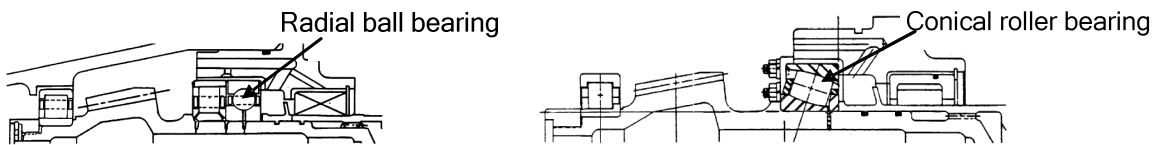


Fig. 22 Conical roller bearing taking the place of ball bearing

The angular contact porcelain ball bearings have been used, which could be substituted for the currently used ball/roller bearings. Its operating life is improved by 4~6 times compared with the steel ones<sup>[12,15]</sup>, and its loss-of-lubrication capacity is better than that of the steel ball bearings. The properties of porcelain rolling elements mainly depend on the composition of material, process of hot sintering and machining precision.

**Lubrication system.** MGB is lubricated by oil ejection as shown in Fig 23, while IGB and TGB by splash

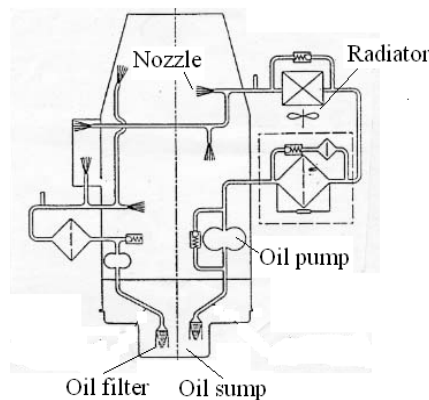


Fig.23 Sketch of oil system of MGB

Presently, multiple nozzle jets lubrication (Fig 24), grease lubrication, under-race injection (Fig 25) and centrifugal injection have been used.

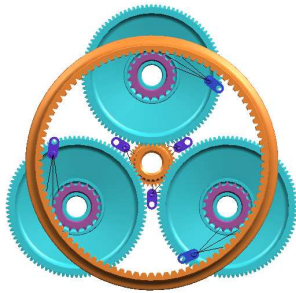


Fig.24 Multiple nozzle jet

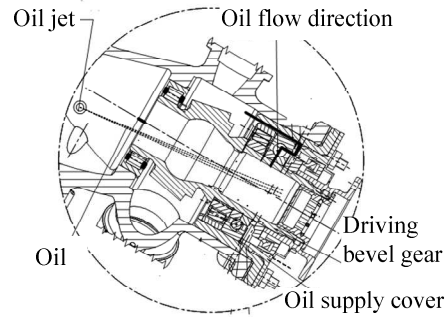


Fig.25 Sketch of under-race, injection

Oil filtration precision has been improved and reached  $10\mu\text{m}$  for some applications resulting in the improvement of the friction conditions of the rotating parts including gears and bearings.

**Development of Design and Analysis Technology**

**Integrated structural design.** In conventional design of power transmission system, gear, shaft and bearings are designed as separate parts, which are connected by splines, bolts and nuts (Fig.26). Now the integrated design technique for those parts has been developed (Fig 27 and Fig 28), decreasing connections and number of parts and improving reliability, which is one of the main technical characters for the third and forth generations of the power transmission system.

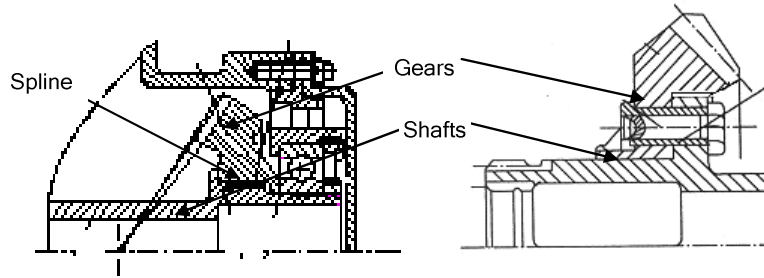


Fig. 26 Connection of gear and shaft by splines, bolts and nuts

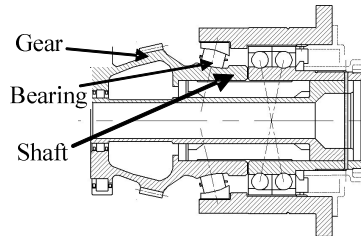


Fig.27 Integrated structure of bevel gear, bearing inner race and shaft

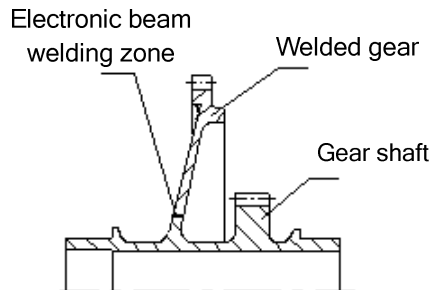


Fig.28 Welded double gears

The bearing with a flange is another example of the integrated structural design, which has been widely used in recent years (Fig.29).

The integrated design (Fig.30) of main rotor hub and rotor shaft, tail rotor hub and tail rotor shaft is also a successful application.

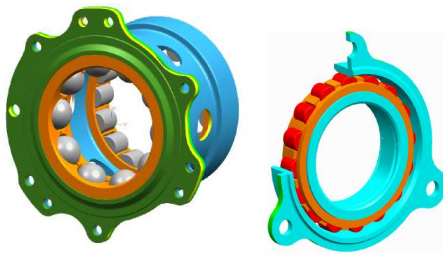


Fig.29 Bearing with flange

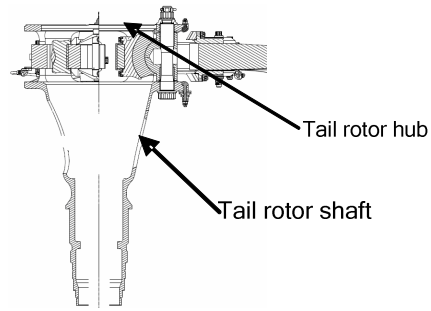


Fig. 30 Integrating of tail rotor shaft and hub

**Strength and life analysis.** In the previous design of the power transmission system, the “static” or “static + dynamics” strength analysis was used, but now “static + dynamics +fatigue” strength analysis has been adopted. The FEM based structure analysis technique (Fig.31) and the multidisciplinary design optimization have been developed, which are replacing the conventional method. The damage tolerance design technique based on the test substantiation has been established and applied in the power transmission system development.

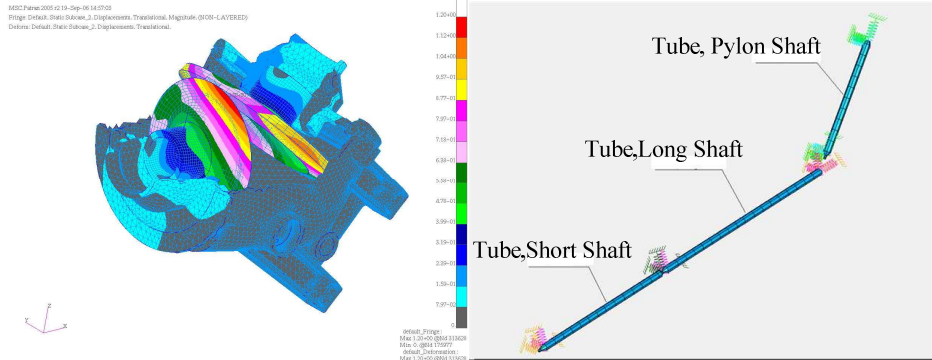


Fig.31 Finite element meshes for casing and shaft

The development history of the strength analysis methods and the corresponding required material property data are shown in Table 3.

Table 3 Strength analysis method and its required typical material property data

| Time          | Method of strength analysis                        | Typical material property data                          |
|---------------|--|---|
| Before 1960's | Static strength evaluation                         | $E, \mu, \rho, \delta, \varphi, \sigma_b, \sigma_Y$     |
| 1960's        | Safe life and vibration analysis                   | S-N curve   |
| 1970's        | Strain fatigue theory, limited life design         | $\epsilon - N$ Curve                                    |
| 1980's        | Fracture mechanics theory, damage tolerance design | Fracture property $K_{Ic}, d\alpha / dN, \Delta K_{th}$ |
| 1990's        | Reliability design, probability life design        | $-3\sigma$ data, flaw feature and distribution          |

As to the dynamics design technique, the power transmission system was separately analyzed in the past, and now the integrated analysis technique has been developed, taking into account the engines, the rotor of helicopter and the power transmission system as a whole. For example, the torsional vibration characteristic analyses considering the coupling of engine, rotor and power transmission system have already been carried out for several engineering applications.

**Vibration control and noise reduction.** In addition to the development of the components effectively reducing the MGB vibration such as the high contact ratio gears, intensive researches on the passive and active vibration control have been carried out in MGB and TDS installation design. The above mentioned nodal beam installation structure is an example for the vibration isolation (Fig.32) [18]. Besides, the active vibration control technique using electric and magnetic measures is also a hotspot of research.

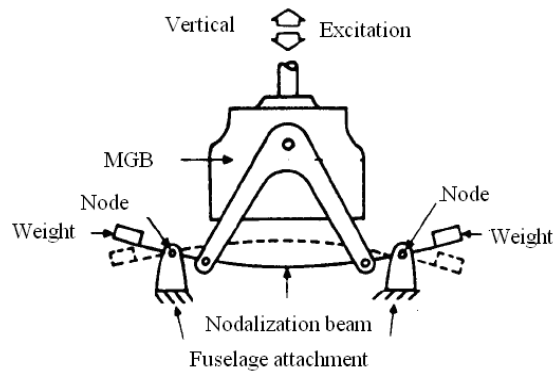


Fig. 32 Isolation by “Nodalized” beam

In addition, noise analysis technique of the transmission systems has also been investigated. The response characteristic of gearbox casings and gear shafts could be analyzed and their structure frequency could be adjusted by finite element method to reduce the vibration and noise level<sup>[19]</sup>.

**Condition monitoring and failure diagnosis.** Presently, most of helicopter power transmission systems mainly adopt the preventive maintenance strategy, i.e. periodic overhaul at workshop. The operation condition is monitored only by magnetic chips detecting and oil temperature indicating in flight. Nowadays, the condition monitoring and failure diagnosis system of power transmission system have been studied, emphasizing on the vibration behavior. The advanced technology of signal acquisition and process, such as signal wireless transmission, neural network and wavelet analysis, has been applied. And it will become possible to apply condition monitoring for the power transmission system in the foreseen future.

### Development of Material and Process Technology

**Gear, bearing and shaft material.** Gear steel used in the power transmission system has been developed with the high property characterized by high purity, ultra-high case hardness, high core toughness and high application temperature. The steel is developed in three generations. The first generation is the low alloy case hardened steel (e.g. AISI 9310) working at about 150°C. The second generation (e.g. M50NiL) could be used satisfactorily at 350°C [20]. The third generation steel could be used at even higher temperature. For instance, the hardness of CSS-42L, a stainless steel of the third generation used in the newly developed power transmission system, could reach HRC68 at room temperature, keep HRC62 at 430°C and retain HRC58 at 535°C. The tensile strength and the yield strength of steel CSS-42L reach much high level up to 1764MPa and 1200MPa respectively, while they are only 1230MPa and 1015MPa for AISI 9310.

**Casing material.** The use of the composite materials in the casings has been started, and for example, the MGB main casings of composite material have been used in RAH-66 Comanche and CH53 development type helicopters<sup>[14, 20]</sup>. However, the aluminum alloy (such as A357.0, 7075) and magnesium alloy (such as ZE41A, WE43) are still used dominantly. Composite material application in the casings will be a key feature of the next generation of power transmission system.

**Tail drive shafts material.** At present most of the tail drive shafts are made from conventional aluminum alloy (2024, 7475 and 7075) or titanium alloy (Ti6Al4V). However, it is reported that the composite materials such as carbon fiber composite materials have already been adopted [14,20]. The application of the composite materials in the tail drive shaft is also a key feature of the new generation transmission system.

**Process technology.** The gear steel melting technologies, e.g. air melting, vacuum degasification melting, vacuum induction melting(VIM), vacuum arc remelting (VAR) with consumable electrode, electroslag remelting and VIM+VAR, have been developed and applied successively. Of them, the high-purity VIM+ VAR has been commonly applied for the steels of the high-speed heavy-loaded gears and rotor shafts of the power transmission system.

The precise forging will replace the ordinary forging gradually. With the precise forging, an entire gear could be directly formed, thus the machining workload and cost are significantly reduced and the bending fatigue strength of the gears is increased as well.

The advanced case hardening technology of the bearings and gears, such as vacuum carburization, ionic nitriding and deep nitriding, are widely used improving the life and reducing the maintenance cost of power transmission system.

Deep-nitriding has its outstanding advantages, such as the deep hardening layer, high case hardness, stable metallographic structure of the layer at high temperature and small deformation during nitriding. The last one permits the grinding operation to be performed directly after the nitriding. Therefore the technology has been successfully applied in the power transmission system, especially for its integrated components consisted of gears, shafts and bearings.

### Power Transmission Technique of High Speed Helicopter

Along with the development of conventional helicopter, the high speed helicopter is being paid much more attention to by all of the world. There are two types of high speed helicopters, tilt-rotor aircraft and conventional helicopter with additional propellers.

The tiltrotor aircraft is a new concept aircraft, which takes off and lands vertically, and hovers like a helicopter. It draws people's attention due to its high flight speed of several times of that of the conventional helicopter. The V-22 tiltrotor aircraft went into service in 2009 (Fig. 33).

The power transmission system of tiltrotor aircraft is composed of proprotor gearbox, tilt-axis gearbox, midwing gearbox and shafting system(Fig.34). The proprotor gearbox and tilt-axis gearbox(Fig.35) are mounted in a rotatable nacelle of the tiltrotor aircraft together with the engine. The tilt-axis gearbox is of a spiral bevel gear drive. The spiral bevel pinion could pivot on the gear axis and rotates around the axis of itself.



Fig. 33 V-22 tilt-rotor helicopter

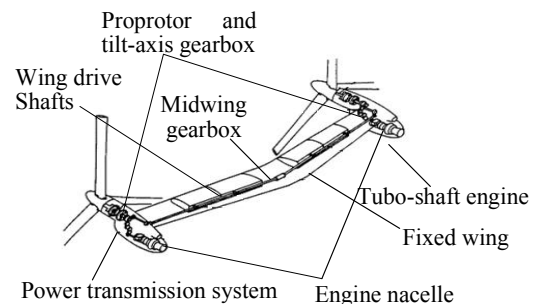


Fig. 34 The power transmission system of V-22

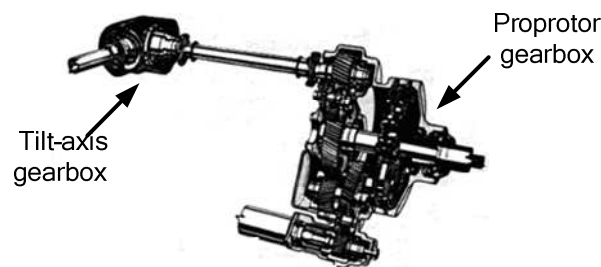


Fig.35 The proprotor and tilt-axis gearbox

The wing drive shafts of power transmission system of tilt-rotor aircraft are rather long. For example, another tilt-rotor aircraft BA609's is 13 meters long. In the event of an engine failure or one engine inoperative (OEI), the wing drive shafts transmit power to the gearboxes in the failed engine nacelle to drive the rotor and accessories. In comparison with the tail driving shaft of single-rotor helicopter, the power transmitted by the wing drive shafts is larger and its rotating speed is higher<sup>[21]</sup>. Therefore dynamic design for shafts is one of the key aspects for the power transmission system.

The high-speed helicopter X3 developed by Eurocopter uses two turboshaft engines to drive the main rotor and a pair of forward propellers on the sub-wings (Fig.36). To distribute proportionally engine power to the main rotor and propellers, a new power transmission configuration is needed for the high-speed helicopter. It is more difficult to meet the requirements of weight, life and reliability for the power transmission system due to larger dynamic loads with high speed and maneuverability.



Figure 36 X3 high-speed helicopter of European Helicopter

### Conclusion

The development of helicopter power transmission system shows that high comprehensive performance and low life cycle cost have become the key requirements in design to adapt to the progress of helicopters and engines technique. This results in the development of variety of the drive train, transmission configuration, structural design and analysis, as well as the application of new materials and process technology. Among these developments, the split-torque gear train and the new planetary gear train draw more and more concerns, since they have fewer parts, lighter weight and higher reliability as compared with the conventional design. What's more, the power transmission system used for high speed helicopter appears as a new-comer in the family of helicopter transmission systems. All of these attract us, the professionals, no matter professors or engineers we are in this field, to accelerate the development of the power transmission system technology together.

### Acknowledgments

The authors express their deep gratitude to the individuals and institutions for the historical information about the development of the helicopter power transmission system technology. The authors also express their gratitude to the colleagues who contributed to the preparation of this paper.

### Reference

- [1] John J.Coy,Robert C.Bill: Advanced transmission studies.44th Annual Forum of the American helicopter Society, June 16-18,1988.
- [2] H.Chin, K.Danai, D.G.Lewicki: Efficient fault diagnosis of helicopter gearboxes. Technical Report, F-5019.
- [3] David M.Blunt, Jonathan A. Keller: Mechanical Systems and Signal Processing, (2006), p. 2095
- [4] Andrew M. Mitchell. Testing of UH-60A helicopter transmission in NASA Lewis 2240-kW (3000-hp) facility. NASA Contractor report 2626, 986.
- [5] G. White: IMechE, Vol 196(1982), p.11.
- [6] G White. Design study of a split-torque helicopter transmission. IMechE,1998

- 
- [7] Robert R. Filler, Gregory F. Heath, Stephen C. Slaughter, David G. Lewicki. Torque Splitting by a Concentric Face Gear Transmission. the American Helicopter Society 58th Annual Forum, Montreal, Canada, June 11-13, 2002.
- [8] Faydor L. Litvin, Alfonso Fuentes, Claudio Zanzi, and Matteo Pontiggia: Face gear drive with spur involute pinion-geometry, generation by a worm, stress analysis. NASA / C R-2002-211362, 2002.
- [9] Robert C. Bill: Summary highlights of the advanced rotorcraft transmission(ART) program, AIAA92-3362,1992
- [10] A. Bianchi, S. Rossi: Modeling and finite element analysis of a complex helicopter transmission including housing, shafts, and gears. S611/005.
- [11] Joseph W. Lenski: Boeing helicopters advanced rotorcraft transmission(ART) program summary of component tests. AIAA/SAE/ASME/ASEE 28th Joint Propulsion conference and exhibit, 1992
- [12] Robert F. Handschuh, James J. Zakrajsek: Current research activities in drive system technology in support of the NASA rotorcraft program. The vertical lift aircraft design conference, January 18–20, 2006.
- [13] F.L. Litvin and A. Egelja: Handbook on face gear drives with a spur involute pinion”. NASA/CR-2000-2099909, ARL-CR-447.
- [14] Zachary S. Henry: Bell helicopter advanced rotorcraft transmission (ART) program. NASA contractor report 195479,1992
- [15] Jules G. Kish: Sikorsky aircraft advanced rotorcraft transmission(ART) program-final report. NASA Contractor report 191079,1992
- [16] D. C. Lombardo: Helicopter structures a review of load, fatigue design techniques and usage monitoring. AD-A267-115, 1993.
- [17] J. E. Brunken: A new concept in supercritical drive systems for advanced rotorcraft. The American helicopter society 56th annual forum, May 2-4 2000.
- [18] Raymond G. Kvaternik. Summary of recent NASA army contributions to rotorcraft vibrations and structural dynamics technology. NASA Langley research center, N88-16628.
- [19] T. L. Krantz, J. G. Kish: Advanced rotorcraft transmission (ART) program summary. AIAA/SAE/ASME/ASEE 28th Joint Propulsion Conference and Exhibit, AIAA-92-3365, July, 1992
- [20] J. C. Chaize, J. M. Berthier: New technologies, a factor of competitiveness for today’s helicopter, a must for tomorrows. 22th European rotorcraft forum and 13th European helicopter association symposium, 1996
- [21] Charles Duello: BA609 tilt rotor drive system. The American helicopter society 58th annual forum, June 11–13, 2002.

## Future Transmissions for Wind Turbines

Bernd-Robert Höhn

Gear Research Centre (FZG), Technical University of Munich, Germany

fzg@fzg.mw.tum.de

**Keywords:** Next generation for transmissions for Wind Turbines, optimization of efficiency and durability

**Abstract.** Most transmissions for wind turbines are set up by multiple consecutively arranged planetary gear sets and/or normal gear sets. Therefore these transmissions have a constant ratio. In order to feed the electricity produced by the wind turbines into the grid, an electric conversion to a constant frequency of 50 Hz is necessary. FZG developed a new concept for transmissions of wind turbines based on a planetary gear. By superposition of a small electric engine the transmission ratio is continuously variable. This makes an electric conversion unnecessary and thereby increases the efficiency of the wind turbine.

### Introduction

The use of wind for energy production has a long history. In Europe since more than 800 years the wind energy will be used for production of mechanical energy. The first use of wind power will be used directly for mills, saws and waterpumps. Beginning of the 18th century first experiments for generating electric power are known. But these experiments have not brought the brake-through for the wind power. In the beginning 8th decade of the 20th century a revival of wind power began. The world wide discussion about energy-waste and the forecast of ending of oil reserves in the world and the accompanying discussion about the CO<sub>2</sub>-emission and climate changes (increase of average temperature of the world) started the development of regenerative energy production more and more. The use the water power was one solution for generating electric power without increase of the CO<sub>2</sub>-emissions. Extreme big water energy-production started with the Yangste-dam in China and the Iquacu-dam in South America. In Germany the wind power becomes an acceptable part of electric energy production. In 2009 more than 7% of German electric energy consumption is produced with wind turbines. Main reason is caused by the politics which installed a new law that the grid owner has to buy the electric power from wind turbines to a high price above the market price. The consumer has to pay for it. Though an indirect subvention of wind power (and other regenerative energy production like photo voltaic) is installed in Germany. Subvention for photo voltaic has reached a value of more than 2 billion € per year!!! This subvention of regenerative energy leads to the very high installed wind power in Germany.

And how is the situation in wind turbine market worldwide? In Europe the increase of installing wind power has stopped through the financial crisis in 2009 and beginning 2010. The banks have stopped the financing especially for wind parks in the sea. Different is the situation in China and India. Their national industry has to fulfil the big demand for wind turbines.

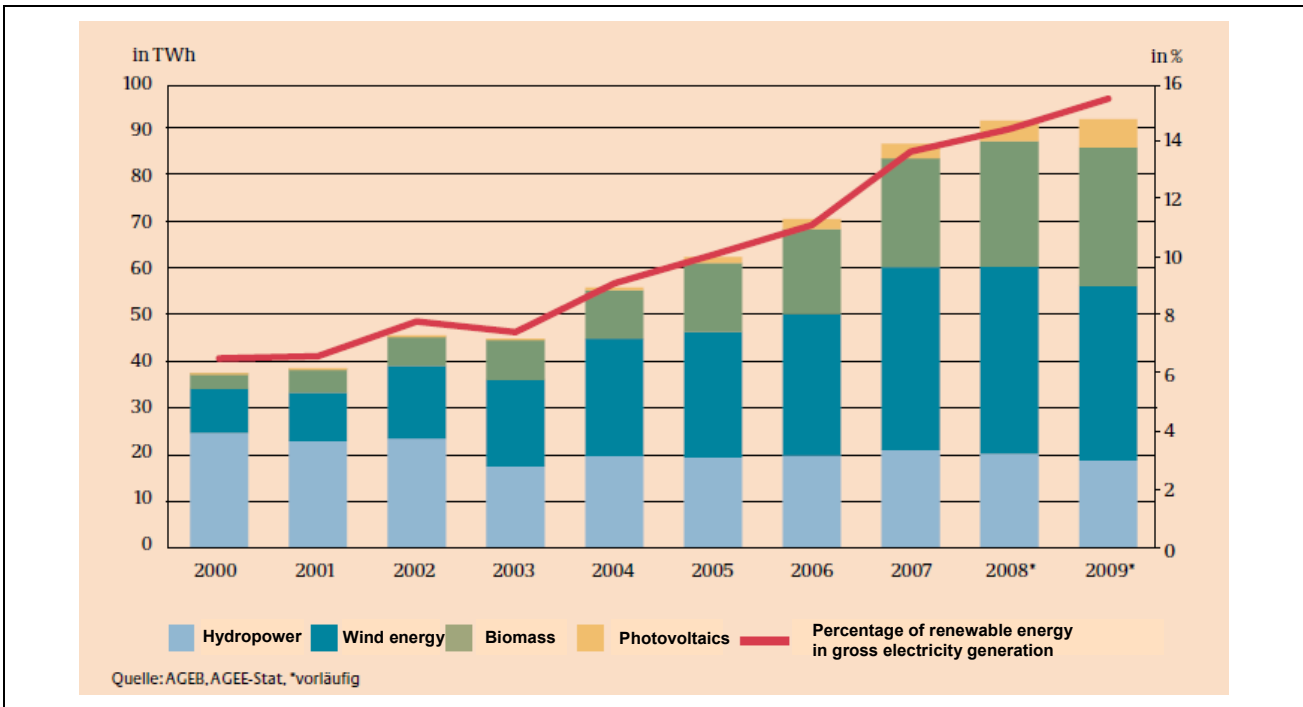


Fig. 1 Electric Energy out of regenerative energy sources [1]

**State of the Art**

The next figures show the state of art of wind turbines. Two technical solutions are in the market. With and without transmissions. In the market till 1MW the multipol low speed generators without transmissions have a market share up to 20%. As higher the power per unit (for offshore > 5 MW is planned) as lower is the speed of the rotor shaft and the need for transmissions is absolutely necessary regarding the weight of the gondola. As higher the speed of the generator as lower is the weight [2].



Fig. 3 Winergy



Fig. 2 Hansen

Though transmission ratio up to  $I = 100$  is normal for wind power > 2

MW. Fig. 2 shows the principle of Hansen for up to 5 MW. One planetary set after the rotor and two normal gear sets for increasing speed up to 100 times rotor speed. The generator shaft is parallel to the rotor shaft. Same principle you can see by Winergy Fig. 3. Rotor is connected to the carrier of the planetary gear set, the sun is connected to the output shaft and the ring gear is fixed to the housing. With this principle you have the highest

ratio in a planetary gear set. ZF will start with a similar design with Vestas in 2012.

Fig. 4 shows the design of Renk. They have designed a double planet with a higher ratio between ring gear (connected to the rotor = inputshaft) and sun. They offer this principle as Multibrid for a medium speed generator (about 200 min<sup>-1</sup>) with higher pole numbers and additional with another normal gear set for total ratios of about  $i=100$ .

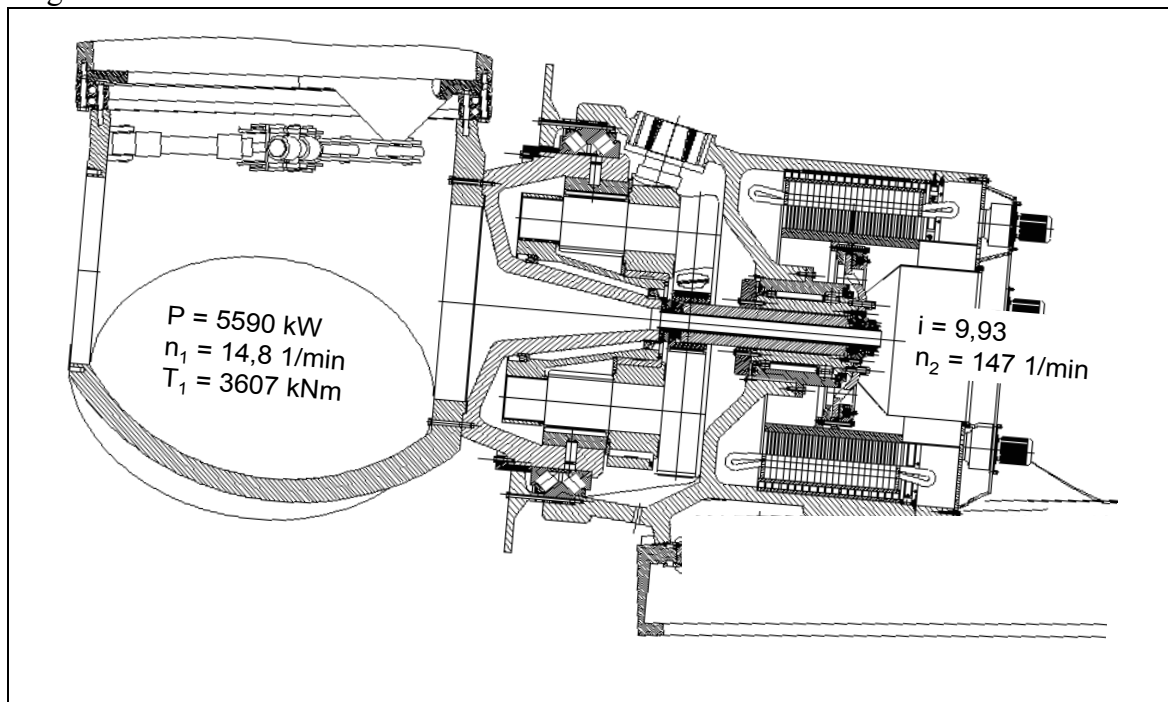


Fig. 4 Renk Multibrid

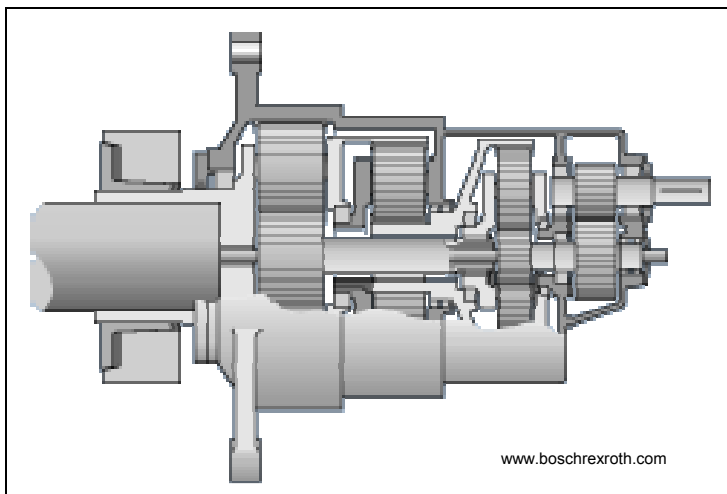


Fig. 5 Bosch Rexroth Redulus

Fig. 5 shows the principle from Bosch-Rexroth. They have a power split for the rotor power to two coupled planetary sets. The torque is divided to two planetary gear sets though the diameter of the ring gear are smaller for the same power compared to the principles of Hansen or Winergy. But the design is more complicated. More parts give more risks, a problem for guaranty wishes for a safe run for 20 years.

### Future Trends

**Voith windrive.** Caused by the actual financial and guaranty problems the European wind turbine firms are not intensively engaged in research and in developing the next generation of wind turbines. Only Voith as a newcomer introduces a new concept, the windrive in 2008. Fig. 6 shows the principle with a CVT, a hydrodynamic converter (Voith is the worldwide known specialist for such couplings and torque converter). This CVT combined with two planetary gear sets they offer a really new concept. The generator is a synchronous generator which acts with constant speed. Though the electric power is produced with a constant frequency of 50Hz and gives the power direct to the grid

without electric conversion as it is normal for all existing wind turbines with a fixed ratio. The rotor produces mechanical energy by different rotor speed between 12 and 16 min<sup>-1</sup>. If you have fixed ratio the generator turns between 1200 and 1600 min<sup>-1</sup> for a 2,5MW example. Fig. 7

shows a measured load spectrum of such a wind turbine. It is different from the aerodynamic potential curve for a given rotor. The dynamic potential for such a wind turbine shows Fig. 8. With a pitch-control the maximum power is only possible by a windspeed > 15m/s. With the Voith winddrive the generator turns with 1500 min<sup>-1</sup> for given rotor speed between 12 and 16 min<sup>-1</sup>. The disadvantage in gear box efficiency could be overtaken through the better total efficiency. For established systems the overall efficiency is.

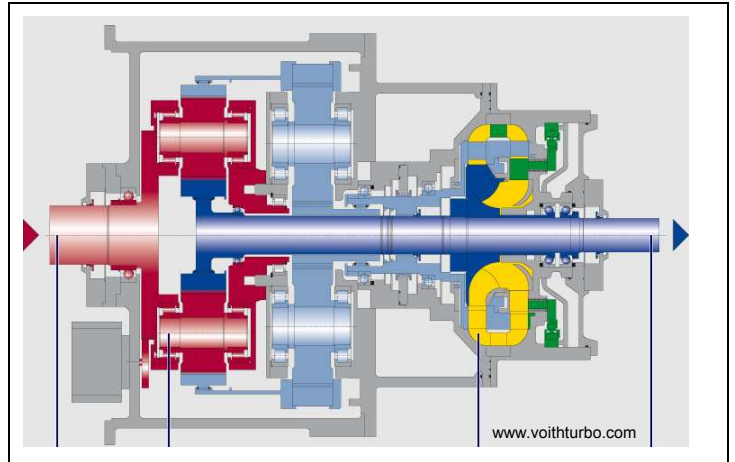


Fig. 6 Voith Windrive

$$\eta_{ges} = \eta_{transmission} \cdot \eta_{Gen} \cdot \eta_{el} \tag{1}$$

and for the Voith Windrive:

$$\eta_{Ges} = \eta_{transmission} \cdot \eta_{Gen} \tag{2}$$

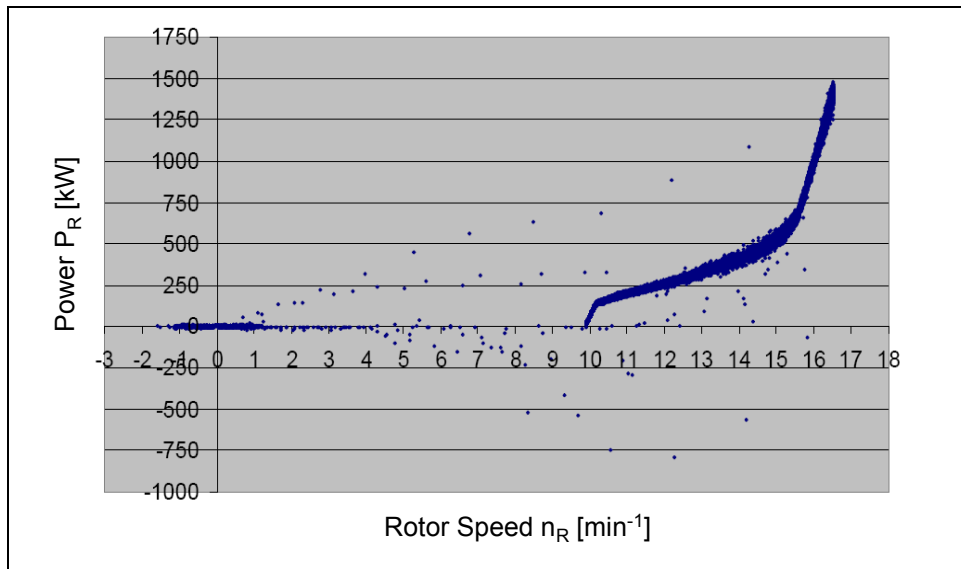


Fig. 7 Measured load spectrum

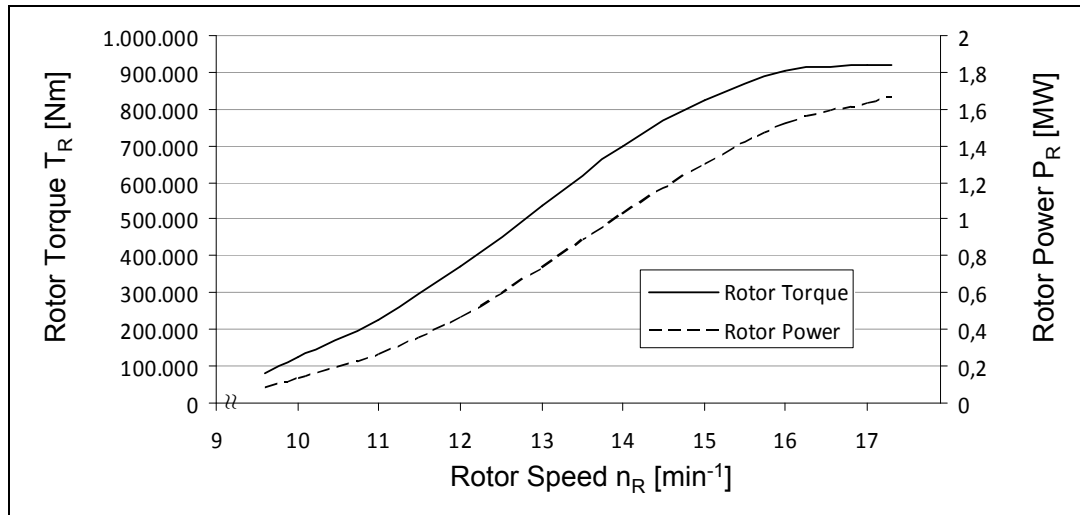


Fig. 8 Dynamic potential

Details of the efficiency for all components are kept very secret and confidential from the firms, therefore a detailed comparison is not possible. But let give an approximation and an example:

a) conventional system:

|                     |                                     |
|---------------------|-------------------------------------|
| Transmission        | $\eta_{\text{transmission}} = 0.96$ |
| Asynchron Generator | $\eta_{\text{Gen}} = 0.95$          |
| Electric conversion | $\eta_{\text{El}} = 0.94$           |
| With Eq. 1          | $\eta_{\text{Ges}} = 0.857$         |

b) Voith windrive:

|                       |                                     |
|-----------------------|-------------------------------------|
| Transmission          | $\eta_{\text{transmission}} = 0.93$ |
| Synchronous Generator | $\eta_{\text{Gen}} = 0.96$          |
| With Eq. 2            | $\eta_{\text{Ges}} = 0.893$         |

That means this system has a better efficiency and a better energy production factor which can be calculated in € or \$ or Rupie or Yen or.....

**FZG-Concept.** Engaged through the Voith idea and an old Siemens patent application of 1992 [3], FZG designed a new planetary gear set with a superposition of a small electric power to synchronous generator with constant speed for a rotor range speed between 12 and 16 min<sup>-1</sup> (Fig. 7). The targets for the future wind turbines are defined in Fig. 9. Fig. 10 shows the wind turbine drive train for such a constant generator speed. That means for such superposition a normal planetary gear set is used. If the electric engine runs as a motor you have a power addition in the planetary gear. Rotor power  $P_R$  and  $P_{EM}$  drive the generator  $P_G$  and the electric power for the motor  $M$  comes from the generator.

Only  $P_G - P_M$  goes to the grid. If the electric motor runs as a generator you have power split in the planetary gear box and both electric engines  $P_M$  and  $P_G$  give their power to the grid. The task for FZG was to find out, what power size of  $P_M$  is necessary for a wind turbine of  $P_G = 1,5$  MW (only as example, without problems scalable) and the given load spectrum, see Fig. 7. For characteristic curve A out of calculated power-wind-speed-diagram and in Fig. 8 for the given measured load spectrum for a wind turbine. For this calculation the Willis - equation and the derived formulas from Mueller [4] are used. Especially for the measured load spectrums you can see, that below of rotor speed  $n = 10$  min<sup>-1</sup> no electric power will be produced and for example  $n_{\text{Rot}} = 12$  min<sup>-1</sup> only 15 % of the maximum

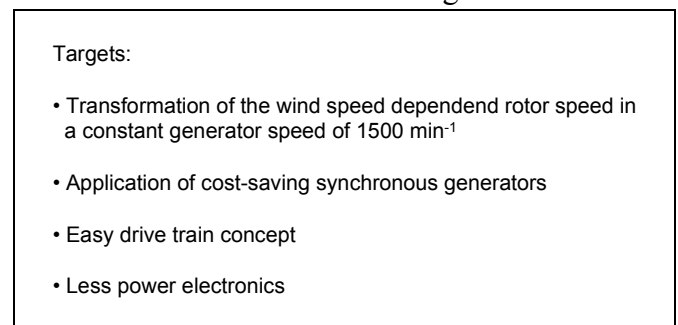


Fig. 9 Targets

(and given) power of the wind turbine (here 1,5 MW) will be produced. Fig. 11 shows the difference of the new concept and common basic concept once more. The result of these calculations done with Mueller formulas shown Fig. 12. The electric demand for motor power  $P_{EM}$  is for characteristic A  $P_E = 242$  KW and for characteristic B only  $P_{EM} 100 =$  KW. Fig. 13 show the power ratio between  $P_{EM}$  and  $P_{Rotor}$  You see that the power ratio is still increasing when rotor speed decreases. The absolute value is decreasing (see Fig. 12) which the rotor power decreases very much. If you use the motor  $P_E$  as generator (power split) and motor (power addition) the maximum power of that unit decreases to  $P_E = 84$  KW – Fig. 14. That means for the additional installed power of  $P_{EM}$  only 7 % of the maximum power of the rotor is necessary. This engine has to run as motor and generator and needs adequate power electronics. For such dimension - 84 KW against 1,5 MW by normal wind turbines - the power electronics is much cheaper. The synchronous generator delivers the electric power direct to the grid. How can be the design of such a concept. FZG made two examples.

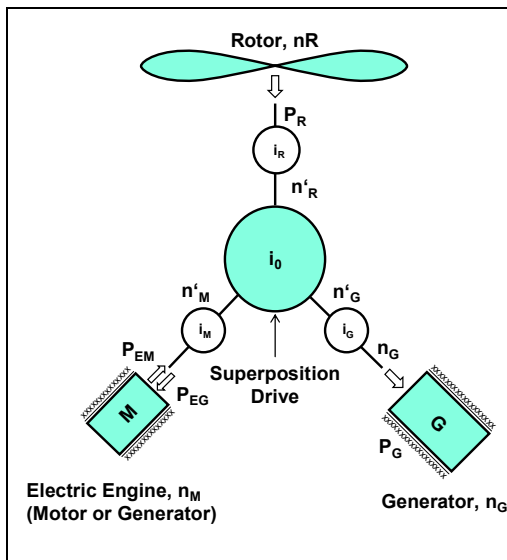


Fig. 10 Wind turbine drive train

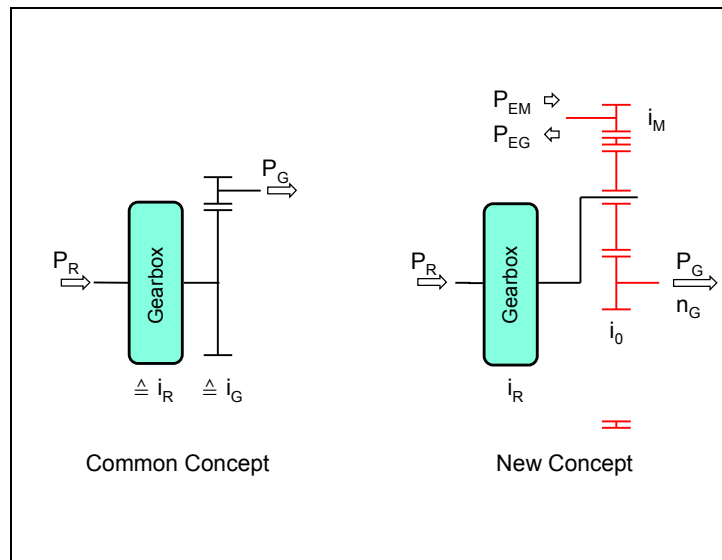


Fig. 11 Common and new concept

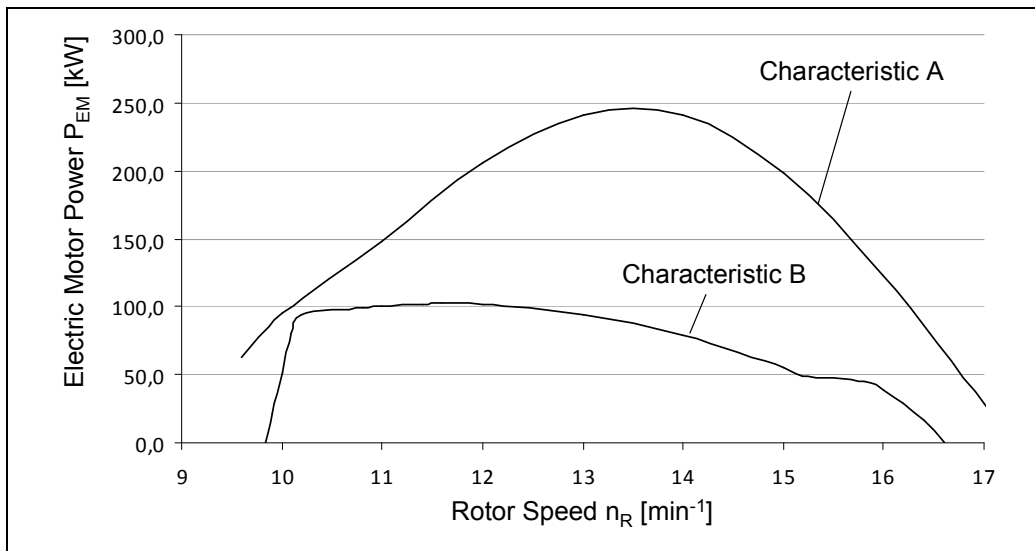


Fig. 12 Required electric power

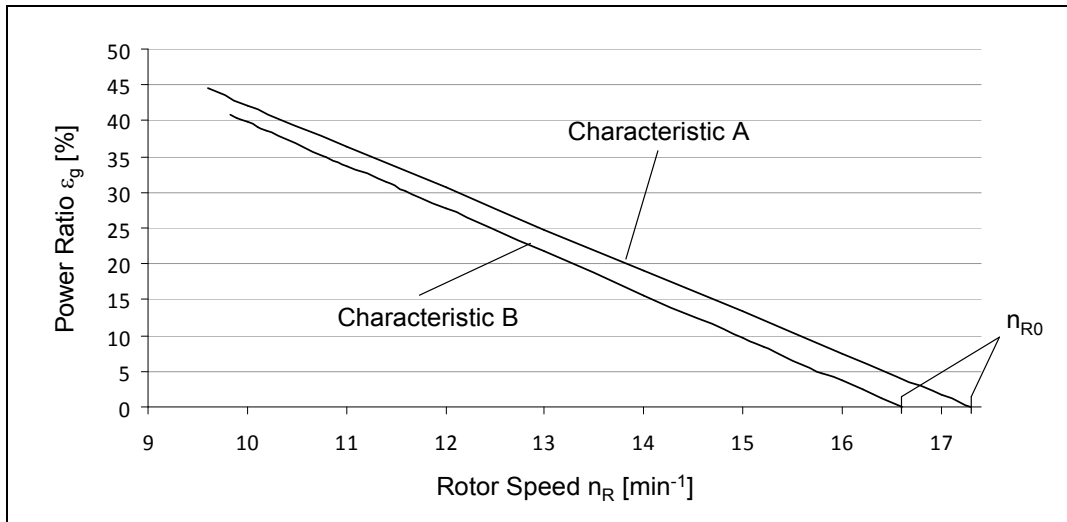


Fig. 13 Power ratio

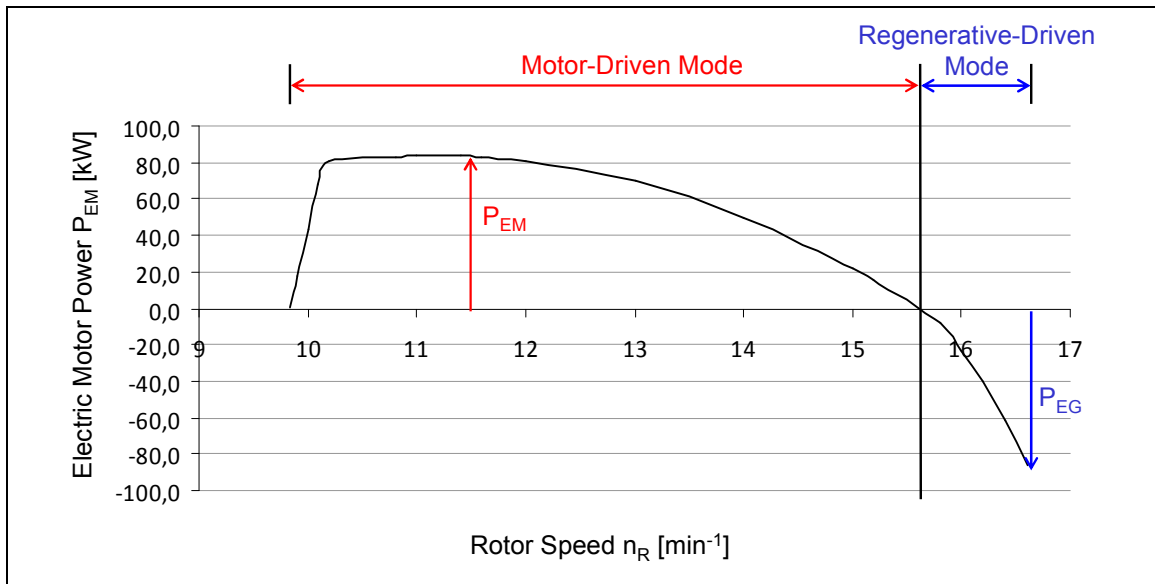


Fig. 14 Power of superposition motor

First we use a first planetary gear set for increasing speed like in the principle of Hansen, Winergy, Eikhoff or other, Fig. 15. The two normal gear stages are exchanged from a so called “plus-planetary gear set” [4] which has a high gear ratio, when you fix one ring gear. This fixed ring gear of the “plus-planetary set” is connected to the motor  $P_{EM}$  and works as motor for rotor speed lower than  $n_{Rot} = 15,5 \text{ min}^{-1}$  and as generator between  $n_{Rot} = 15,5 \text{ min}^{-1}$  till  $16,5 \text{ min}^{-1}$  (Fig. 14).

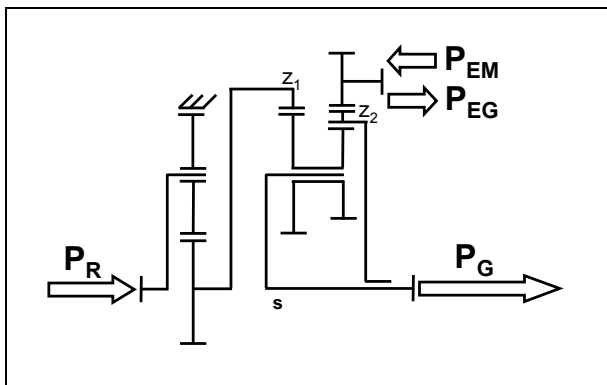


Fig. 15: Wind turbine drive train (1<sup>st</sup> example)

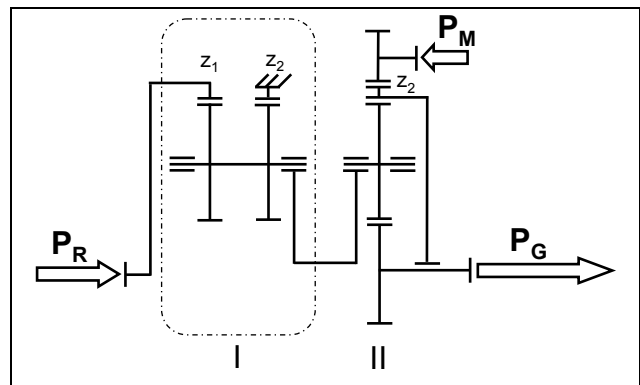


Fig. 16: Wind turbine drive train (2<sup>nd</sup> example)

Second example shows Fig. 16. Here the “plus-planetary gear” (no. I) is used as a first step with speed increase of about  $i = 25$  and a normal “minus-planetary set” (no. II) is used for superposition of  $P_{EM}$ . The advantage is the lower torque in the ring gear of II (Fig. 16) the disadvantage is the lower efficiency of the “plus-planetary gear set” used by high tooth power in the “plus-planetary gear set”. These disadvantages can be reduced dramatically to the low loss tooth geometry which is developed from FZG with several research projects since 2003. Fig. 17 shows the comparison with normal tooth geometry. The plus gear box has an efficiency of  $\eta = 0,89$  for the speed increaser of  $i = 25$  and with low loss geometry from FZG  $\eta = 0,96$ . This value is necessary that the total efficiency will become higher than normal design (see Eq. 2). If you calculate the total efficiency like the example (see Eq. 1 and Eq. 2), you will get

|   |
|---|
| <p>Efficiency Factor for Standard Tooth Geometry [1], [2]:</p> $\eta_{12} = 0.9975 \cdot 0.9981 = 0.9956$ $\eta_{15} = (i_{12}/\eta_{12} - 1)/(i_{12} - 1) =$ $(0.962 / 0.9956 - 1)/(0.962 - 1) = 0.8881$ <p>Efficiency Factor for low-loss-Tooth Geometry:</p> $\eta_{12\_opt} = 0.9993 \cdot 0.9991 = 0.9984$ $\eta_{15} = (i_{12}/\eta_{12} - 1)/(i_{12} - 1) =$ $(0.962 / 0.9984 - 1)/(0.962 - 1) = 0.9594$ |
|---|

Fig. 17: Comparison of load depended losses

|                     |                                     |
|---------------------|-------------------------------------|
| $\eta_G = 0.95$     | plus + minus planetary gear set     |
|                     | of Fig. 16 inclusive bearing losses |
| $\eta_{Syn} = 0.96$ |                                     |
| $\eta_{ges} = 0.91$ | much better than                    |
|                     | $\eta_{ges\ normal} = 0.866$        |

## Summary

The FZG-concept shows the possibility with an electric superposition for a rotor speed of about  $12 - 16 \text{ min}^{-1}$  a constant generator speed of  $1500 \text{ min}^{-1}$ . The superposition power is only 7 % of the rotor power. A cheap power electronic can be used. The overall efficiency of such a concept can be higher than normal conventional wind turbine with a transmission with a fixed ratio. The FZG will become the partner for future wind turbine concepts for concept design and total calculation for gears and bearings.

## References

- [1] *Energie in Deutschland*, www.bmwi.de, August 2010
- [2] T. Weiss, B. Pinnekamp: *Concept for a Multi Megawatt Wind Turbine – Gear and Field Experience*, AGMA Fall Technical Meeting 2008
- [3] G. Hehenberger: *Energiegewinnungsanlagen und Verfahren zum Betreiben dieser*, WO 2010/063052 A2
- [4] H.W. Müller: *Die Umlaufgetriebe*, Springer Verlag, ISBN 3-540-63227-1, 1998

## Dynamic Behavior of Helical Gears with Effects of Shaft and Bearing Flexibilities

Kai FENG<sup>1, a</sup>, Shigeki MATSUMURA<sup>1, b</sup> and Haruo HOUJOH<sup>1, c</sup>

<sup>1</sup>Precision and Intelligence Laboratory, Tokyo Institute of Technology 4259-R2-34, Nagatsuta-cho, Midori-ku, Yokohama, 226-8503, Japan

<sup>a</sup> feng.k.ab@m.titech.ac.jp, <sup>b</sup> smatsumu@pi.titech.ac.jp, <sup>c</sup> hhoujoh@pi.titech.ac.jp

**Keywords:** Helical gear, dynamic response, shaft and bearing deformation

**Abstract.** This study presents a numerical model of helical gears to consider the effects of shaft and bearing flexibility. A primary feature of this study is that the time-varying mesh stiffness is not just determined by the geometry of gear pair but also updated for each iteration according to the change of center distance. The effects of shaft and bearing flexibilities are discussed by comparing the dynamic response of gear pairs supported with a rigid and a flexible bearing-shaft system. The results show that the pressure angle and contact ratio are significantly changed due to the center-distance variation of gears and the gear pair with a flexible bearing-shaft system has much larger vibration. Finally, experimental tests are conducted to validate the proposed model. The predicted results show good agreement with the experimental data.

### Introduction

Helical gears, which provide stronger, smoother running gear trains than spur gears, are widely used for high speed, high power mechanical systems, such as car automobiles, machine tools and airplanes. To date, the reduction of gear vibration and noise are still the paramount concern in the design of transmission system, especially for the applications with high speeds and high torques. In most of previous researches, the pressure angle and the contact ratio were considered to be constant in calculations. However, in fact, the pressure angle and contact ratio are directly associated with operating conditions and the flexibility of shafts and bearings. They are normally time-varying values due to the deformation of shaft and bearings. Research works of Kahraman [1] and Kim et al. [2] discussed the effects of the shaft and bearing flexibilities. The pressure angle and the contact ratio both depend on the translational motion of gears. And they showed the bearing deformation has a significant effect on the vibration of the gear set.

The primary objective of this study is to investigate the effects of distance change between the centers of gear pairs, which are caused by the deformations of shafts and bearings. A model with six degrees of freedom (DOF) is used to predict the dynamic behavior of a helical gear pair with the pressure angle and the contact ratio updated at each iteration. Experimental data from a test rig is used to validate the calculation procedure. Factors, which may change the center distance between the gear and the pinion, such as torque and bearing stiffness, are discussed to show the effects of the variation of center distance on gear dynamic behavior.

### Description of the Model

**Modeling of Time-varying Mesh Stiffness.** Webber [3] developed a mathematical model to calculate the bending deflection of teeth by considering gear teeth as a non-uniform cantilever beam, which has been proved by many other researchers with experimental data [4]. Similar strategy will be adopted in this study to simulate the tooth flexibility. A gear is treated as a flexible disk and a series of beams with a variable cross-section which are fixed on the disk. Therefore, the tooth deflection due to gear mesh can be decomposed into three components: beading and shear deformation of teeth, flexible disk rotation and contact deformation between the mating flanks. As shown in Fig. 1, each part is represented as an equivalent spring. Note that only  $k_{12}$  and  $k_{23}$  are changed with the variation of the pressure angle.

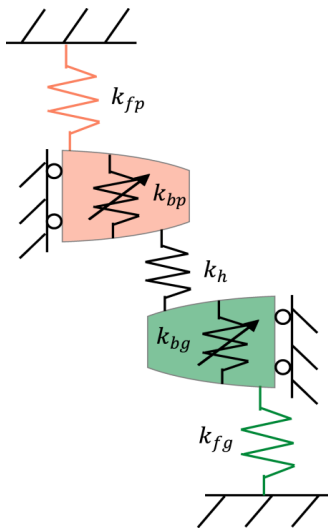


Fig. 1 Calculation of gear mesh stiffness

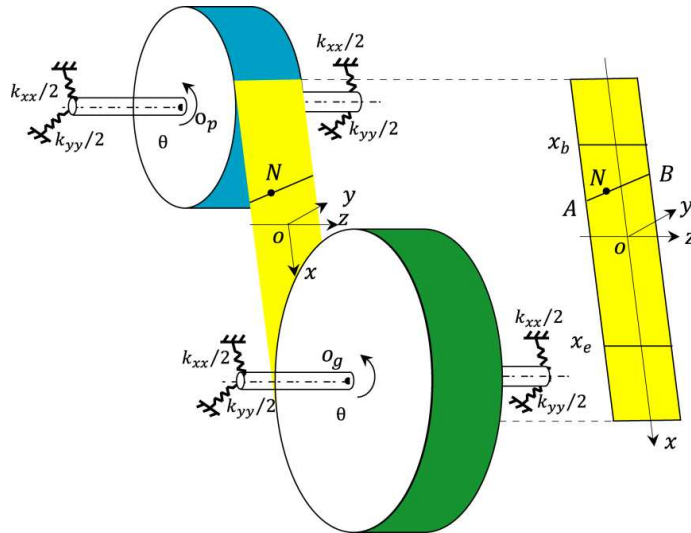


Fig. 2 Six DOF helical gear dynamic model

**Mathematical Model of a Helical Gear Pair.** A mathematical model of geared rotor-bearing systems with six degree-of-freedom (DOF), including rotational motions and translation motions, is considered in this study. A 6 DOF model, which needs less computational efforts, has been reported to be sufficiently accurate compared to full 12 DOF model [5]. The coordinate system is constructed as depicted in Fig. 2. The horizontal and vertical axes are defined along the directions of line-of-action (LOA) and off-line-of-action (OLOA) respectively. The rotational vibrations of gear pairs are described using rotational coordinates,  $\theta_p, \theta_g$ .

Helical gears are similar to spur gears except that the teeth are shifted an angle to the axis. Therefore, helical gears can be considered a refinement over spur gears. In this study, a helical gear is treated as a combination of a pack of narrow spur gears which have the same geometry factor as the helical gear in the normal plane. The meshing forces of helical gears are calculated with an integral of mesh forces each slice along gear width, which are determined by the mesh stiffness and deflections of the corresponding spur gear. Hence, the total mesh forces and the moment of one tooth (contact line AB) are obtained by integrating the forces of each spur gear.

**Effects of Center Distance.** Due to the variation of center distance between the driving gear and the driven gear, both the pressure angle and contact ratio of the helical gear pairs will change as the gears rotate. This study extended the model presented in ref. [5] to include the variation of the pressure angle and contact ratio due to the motions of shaft centers.

**Rotor-bearing System.** Besides the gear mesh which is considered as a spring with periodically varying stiffness, all other flexible components are modeled as linear springs, as shown in Fig.2. Equivalent stiffness and damping coefficients are used to simulate the flexibility of the shafts and bearings. The mesh forces are periodically varying due to the change in the number of teeth in contact as the gears rotate.

**Problem Formulation**

**Misalignment Errors.** In practical operation of a gear system, the occurrence probability of misalignment errors is very high, which may consist of three components, a shaft distance error and two shaft angle errors in or perpendicular to the surface of shaft centerlines. Since this study focuses on the variation of center distance of gear set, only two parameters are considered the error of shaft distance, denoted as  $\epsilon$ , and the error of shaft angle in shaft center surface, denoted as  $\theta$ .

**Tooth Profile Modification.** Lengthwise crowning and profile crowning (convex profile) with parabolic variations are one of the main methods used for tooth modifications. This study aims to investigate the effect of this two profile modification on gear dynamics when the change of shaft center is considered.

**Validation with Experimental Data**

To validate the proposed model, dynamic behavior of the helical gear pairs is measured using the experimental apparatus as shown in Fig. 3. The gear system consists of a pinion shaft and a helical gear pair mounted on flexible shaft which supported by a gearbox via four rolling element bearings. An eddy current dynamometer is connected to the output shaft as a load. To measure the vibration of the gear, two accelerometers were mounted to the driven gear at two sides of the shaft.

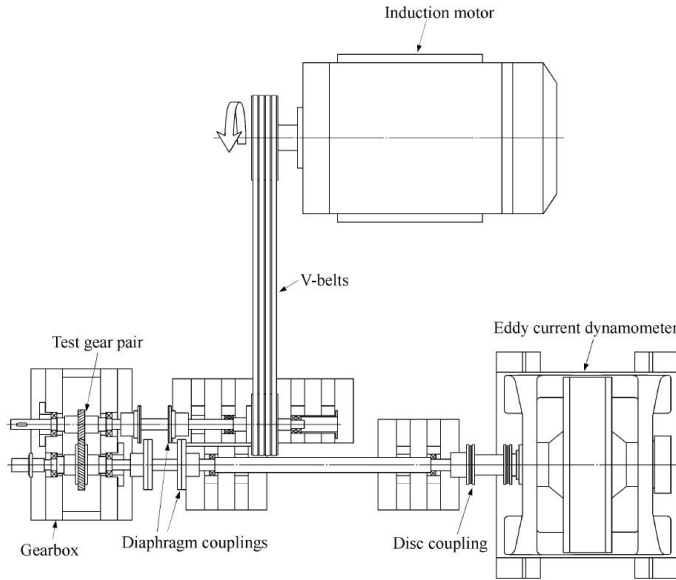
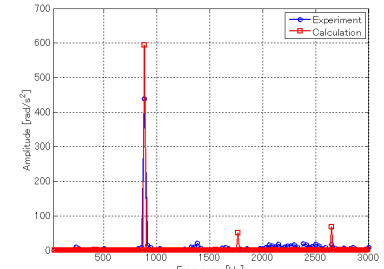
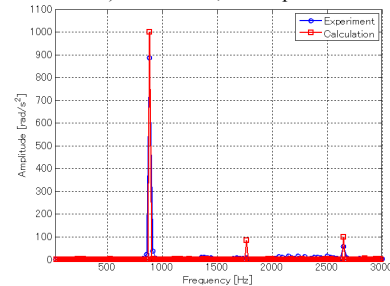


Fig. 3 Schematic representation of the text rig



a) 172 Nm, 1000 rpm



b) 245 Nm, 1000 rpm

Fig. 4 Experimental validation

The predicted rotational vibration of the driven gear in frequency domain are compared with experimental data, as shown in Fig. 4. As we can be observed, both the experimental and analytical results show that magnitudes of the first two mesh harmonics are most dominate. In some extent, the results from the proposed model give good agreement with the experimental results, although they are noted a litter larger. The distinction might be caused by the gearbox, which was not considered in this analysis model.

**Calculation Results and Discussions**

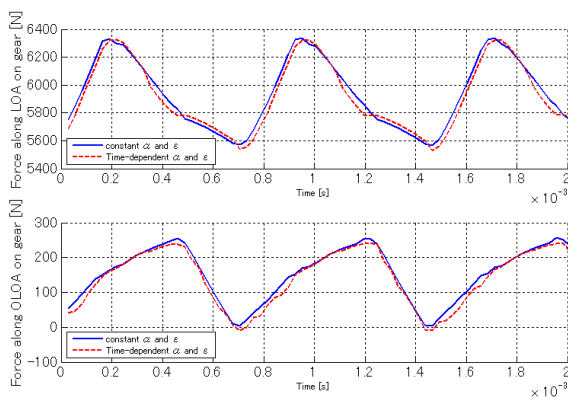


Fig. 5 Mesh forces along LOA and OLOA directions

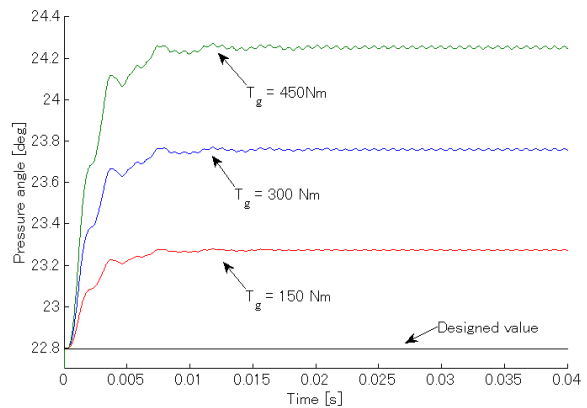


Fig. 6 Pressure angle for different torques

The mesh forces along LOA and OLOA directions of a gear set with constant and time-dependent pressure angle and contact ratio are plotted in Fig. 5. It is important to note that the mesh forces along both two directions have a small decrease if the variations of pressure angle and contact ratio are considered. The reason is that the pressure angle, which because larger if the rise of the center distance is accounted, will decrease the mesh stiffness of the gear pair. Figure 6 shows the time response of the transverse pressure angle for different load torques of the gear pair. It is observed that

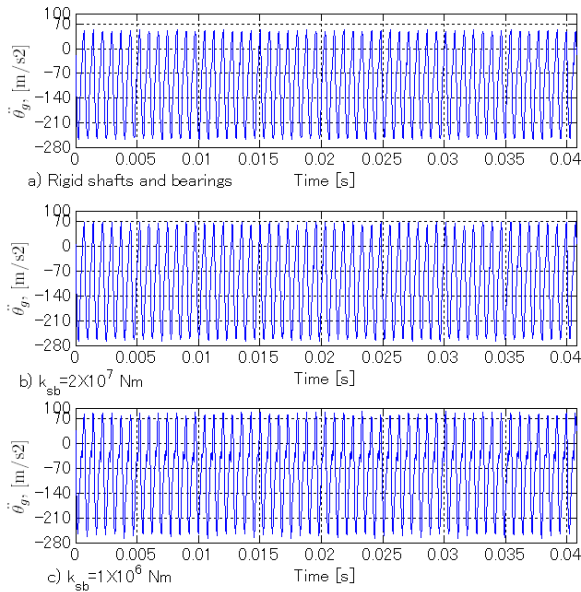


Fig. 7 Dynamic responses with flexible and rigid shafts

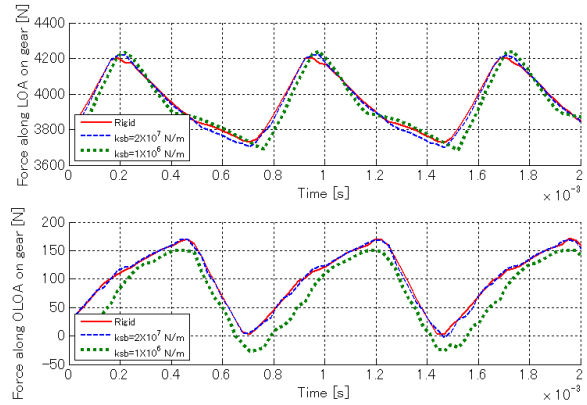


Fig. 8 Mesh forces with flexible and rigid shafts

the pressure angle increases with the rise in load torque. And after the gear reaches the stable state, the fluctuating margin of pressure angle is larger with a higher torque.

To investigate the influence of shaft-bearing stiffness, dynamic responses of gears pairs supported by rigid and flexible shafts and bearings are compared in Fig. 7. And the corresponding mesh forces in LOA and OLOA directions are plotted in Fig. 8. It is clear that flexible bearing-shaft system results in a larger rotational vibration and the vibration magnitude increases as the shaft-bearing stiffness decreases from  $2 \times 10^6$  N/m to  $2 \times 10^7$  N/m. As shown in Fig. 8, if the shaft-bearing stiffness decreases, the mesh force along LOA direction will have larger fluctuating margin and the mesh force along OLOA direction will have a significant decrease in magnitude. That is because that the mesh stiffness of the gear pair becomes smaller due to a larger center distance of the gear pair supported by softer shaft-bearing system. Therefore, the mesh force in OLOA direction decreases. However, the mesh force in LOA direction is determined by the torque and larger shaft deformation results in a larger vibration.

## Conclusion

Since the shafts and the bearings are compliant, this study focuses on the variations of the pressure angle and the contact ratio due to the change of center distance between the gear pair. We presented a 6 DOF model of helical gears to calculate the time-varying mesh stiffness by treating a helical gear as a combination of a pack of narrow spur gears. Experimental tests were conducted to validate the proposed model. The predictions show that the consideration of a time-dependent pressure angle and contact ratio is essential, since the dynamic response of a gear pair is significantly influenced by the variation of pressure angle and contact ratio.

## References

- [1] A. Kahraman: Transaction of the ASME Vol. 124(1) (1993), p. 68
- [2] W. Kim, H.H. Yoo and J.T. Chung: Journal of Sound and Vibration Vol. 329 (2010), p. 4409
- [3] C. Webber: Sponsored research (Germany), British Dept. of Scientific and Industrial Research, Report No.3.
- [4] R.G. Munro, D. Palmer and L. Morrish: Proc. Instn. Mech. Engrs., 215, C (2001), p. 793
- [5] S. He, R. Gunda and R. Singh: ASME J. of Mech. Design Vol. 129(2007), p.48

## Dynamic Modeling of Multi-Stage Planetary Gears Coupled with Bearings in Housing

Zhengming Xiao<sup>1, 2, a</sup>, Datong Qin<sup>1, b</sup>

<sup>1</sup>The State Key Laboratory of Mechanical Transmission, Chongqing University, Chongqing, 400044, China

<sup>2</sup>College of Electromechanical Engineering, Kunming University of Science and Technology, Kunming, Yunnan, 650093, China

<sup>a</sup>suzem@sina.com, <sup>b</sup>dtqin@cqu.edu.cn

**Keywords:** Shield tunnelling machine; Multi-stage planetary gears; Coupling dynamics; Natural characteristic

**Abstract.** This work develops an analytical model of multi-stages planetary gear transmission (PGT) coupled with bearings in housing based on analyzing the displacement relationships of gearing system. The model adopts three planar degree-of-freedom for each of the central components, and the rotational degree-of-freedom for the planets of each stage. Considering the gyroscopic effects, the modified transverse-torsional model is established in the rotating Cartesian coordinates by lumped-parameter method, which is more accurate and may match with the physical model better than the purely torsional model. According to the design parameters of the 3-stage planetary gears of main reducer of shield tunnelling machine, the natural frequencies and vibration modes are investigated by using this transverse-torsional model.

### Introduction

Shield tunnelling machine (STM) is the key equipment in the tunnelling project. The driving system of Earth Pressure Balance STM includes eight main reducers with three-stage PGT, which are used to drive the cutter head. To satisfy the requirements of large torque, low noise and high reliability, the dynamics of the PTG is a critical issue. The coupled vibration of multi-stage PGT will accelerate the damage of the gearbox. To get the correct results of the coupled vibration research as well as for dynamic design and structure optimization of the gearbox of the STM, the building of accurate model of multi-stage PGT is important.

Planetary gears are widely used in many applications due to advantages compared with parallel shaft arrangements such as high power density, diminished bearing loads and large ratio in a small volume [1]. Despite these distinguishing advantages, the noise and vibration of planetary gears remain key concerns in their applications. Most of the published dynamic models of the planetary gear train were limited to single-stage planetary gear sets [2, 3, 4, 5, 6, 7], but multi-stage planetary gears often have more serious noise and vibration problems [8, 9]. Generally, in the literatures deal with multi-stage planetary gears, the pure torsional model is used because of their complex structure [10]. The dynamic response of gear train is the main source to excite the gearbox housing through bearings, therefore, this study aims at modeling the analytical model of three-stage planetary gears coupled with the bearings in housing, and then, analyzing the natural characteristic according to the structural property and geometry parameters of main reducer in STM.

### Displacement Relationship of Components

The analysis deals with planar vibration of single stage planetary gears. Each of the sun, ring, carrier and N planets, are treated as rigid bodies. Component bearing are modeled by linear springs. Gear mesh interactions are represented by springs acting along the line of action. There are two classical lumped-parameter models for spur planetary gears, the purely torsional model and

transverse-torsional model. The purely torsional model includes  $N+3$  DOF just considering the rotational degree of freedom of each component. In the transverse-torsional model, each component has three degree of freedom: two translations and one rotation.

For the multi-stage planetary gears (three-stage for the SMT reducer), if the model use three degree of freedom to express each component, it is very difficult to analyze the dynamic properties because of the so many degree of freedom. At the some time, the purely torsional model can't agree with the physical model very well, it may be too simple to investigate coupling vibration of multi-stage planetary gearbox. So, here we choose to use the modified transverse-torsional model for the three-stage planetary gears, and the analytical model of planetary gears is shown in the Fig. 1. The model admits three planar degree-of-freedom for each of the central components, and the rotational degree-of-freedom for the planets of each stage. The model include the gyroscopic effects induced by carrier rotation, where the sun and carrier translations  $x_i, y_i$  ( $i=s,c$ ) are measured with respect to a rotating coordinates fixed to the carrier.

Figure 2 shows a sun-planet-ring mesh in the fixed coordinates  $oij$  and rotating coordinates  $o\zeta\eta$ . The positions of sun and carrier can be described by vector form as  $\mathbf{r}_s = x_s\mathbf{i} + y_s\mathbf{j}$  and  $\mathbf{r}_c = x_c\mathbf{i} + y_c\mathbf{j}$ . According to using coordinate revolution transformation, the accelerations of the central components are  $\ddot{\mathbf{r}}_s = (\ddot{x}_s - 2\omega_c\dot{y}_s - \omega_c^2x_s)\mathbf{i} + (\ddot{y}_s + 2\omega_c\dot{x}_s - \omega_c^2y_s)\mathbf{j}$  and  $\ddot{\mathbf{r}}_c = (\ddot{x}_c - 2\omega_c\dot{y}_c - \omega_c^2x_c)\mathbf{i} + (\ddot{y}_c + 2\omega_c\dot{x}_c - \omega_c^2y_c)\mathbf{j}$ .

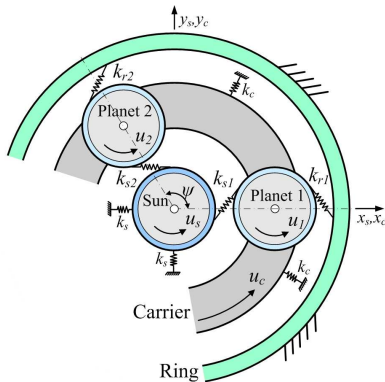


Fig.1 Lumped parameter model of PGT

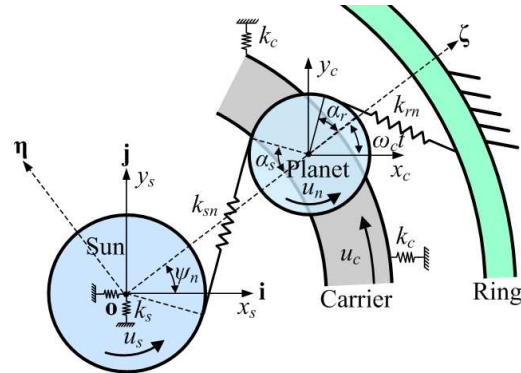


Fig.2 A sun-planet-ring mesh

**Modeling and Equations of Motion**

For multi-stage PGT, the dynamic model can be developed based on the single-stage PGT lumped parameter model and considering the coupling relationships. The STM main reducer is composed of three-stage planetary gears as shown in Fig. 3. The coupled stages are modeled as rigid joint, and the coupling relationships of all components as shown in Fig.4. The following assumptions are made in developing the dynamic model of the three-stage PGT [2, 3].

- 1) The gear wheels and the nut carrier are assumed to be rigid bodies.
- 2) The gear tooth flexibilities are modeled as linear gear mesh springs.
- 3) Frictional forces arising from tooth sliding motions are considered to be negligible.
- 4) Damping and clearance non-linearity are not considered.

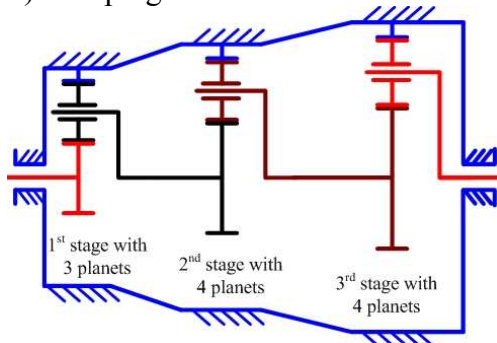


Fig. 3 Layout for three-stage PGT

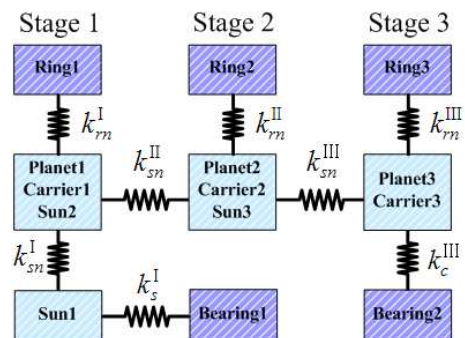


Fig. 4 Coupling relationship of all components

According to the Newtonian mechanics principle, for three-stage PGT with fixed ring gears (Number of planets: 3, 4, 4), equations of motion are given as:

$$\begin{aligned}
& m_s^I (\ddot{x}_s^I - 2\omega_c^I \dot{y}_s^I - (\omega_c^I)^2 x_s^I) - \sum k_{sn}^I \delta_{sn}^I \sin \psi_{sn}^I + k_s^I x_s^I = 0 \\
& m_s^I (\ddot{y}_s^I + 2\omega_c^I \dot{x}_s^I - (\omega_c^I)^2 y_s^I) + \sum k_{sn}^I \delta_{sn}^I \cos \psi_{sn}^I + k_s^I y_s^I = 0 \\
& (I_s^I / (r_s^I)^2) \ddot{u}_s^I + \sum k_{sn}^I \delta_{sn}^I = 0 \\
& (I_p^I / (r_p^I)^2) \ddot{u}_n^I + k_{sn}^I \delta_{sn}^I - k_{rn}^I \delta_{rn}^I = 0 \quad (n=1, 2, 3) \\
& (m_c^I + \sum m_p^I + m_s^I) (\ddot{x}_c^I - 2\omega_c^I \dot{y}_c^I - (\omega_c^I)^2 x_c^I) + \sum k_{sn}^I \delta_{sn}^I \sin \psi_{sn}^I + \sum k_{rn}^I \delta_{rn}^I \sin \psi_{rn}^I - \sum k_{sn}^I \delta_{sn}^I \sin \psi_{sn}^I = 0 \\
& (m_c^I + \sum m_p^I + m_s^I) (\ddot{y}_c^I + 2\omega_c^I \dot{x}_c^I - (\omega_c^I)^2 y_c^I) - \sum k_{sn}^I \delta_{sn}^I \cos \psi_{sn}^I - \sum k_{rn}^I \delta_{rn}^I \cos \psi_{rn}^I + \sum k_{sn}^I \delta_{sn}^I \cos \psi_{sn}^I = 0 \\
& (I_c^I / (r_c^I)^2 + \sum m_p^I + I_s^I / (r_s^I)^2) \ddot{u}_c^I - \sum (k_{sn}^I \delta_{sn}^I \cos \alpha_s^I + k_{rn}^I \delta_{rn}^I \cos \alpha_r^I) + \sum k_{sn}^I \delta_{sn}^I (r_s^I / r_c^I) = 0 \\
& (I_p^I / (r_p^I)^2) \ddot{u}_n^I + k_{sn}^I \delta_{sn}^I - k_{rn}^I \delta_{rn}^I = 0 \quad (n=1, 2, 3, 4) \\
& (m_c^I + \sum m_p^I + m_s^I) (\ddot{x}_c^I - 2\omega_c^I \dot{y}_c^I - (\omega_c^I)^2 x_c^I) + \sum k_{sn}^I \delta_{sn}^I \sin \psi_{sn}^I + \sum k_{rn}^I \delta_{rn}^I \sin \psi_{rn}^I - \sum k_{sn}^I \delta_{sn}^I \sin \psi_{sn}^I = 0 \\
& (m_c^I + \sum m_p^I + m_s^I) (\ddot{y}_c^I + 2\omega_c^I \dot{x}_c^I - (\omega_c^I)^2 y_c^I) - \sum k_{sn}^I \delta_{sn}^I \cos \psi_{sn}^I - \sum k_{rn}^I \delta_{rn}^I \cos \psi_{rn}^I + \sum k_{sn}^I \delta_{sn}^I \cos \psi_{sn}^I = 0 \quad (1) \\
& (I_c^I / (r_c^I)^2 + \sum m_p^I + I_s^I / (r_s^I)^2) \ddot{u}_c^I - \sum (k_{sn}^I \delta_{sn}^I \cos \alpha_s^I + k_{rn}^I \delta_{rn}^I \cos \alpha_r^I) + \sum k_{sn}^I \delta_{sn}^I (r_s^I / r_c^I) = 0 \\
& (I_p^I / (r_p^I)^2) \ddot{u}_n^I + k_{sn}^I \delta_{sn}^I - k_{rn}^I \delta_{rn}^I = 0 \quad (n=1, 2, 3, 4) \\
& (m_c^I + \sum m_p^I) (\ddot{x}_c^I - 2\omega_c^I \dot{y}_c^I - (\omega_c^I)^2 x_c^I) + \sum k_{sn}^I \delta_{sn}^I \sin \psi_{sn}^I + \sum k_{rn}^I \delta_{rn}^I \sin \psi_{rn}^I + k_c^I x_c^I = 0 \\
& (m_c^I + \sum m_p^I) (\ddot{y}_c^I + 2\omega_c^I \dot{x}_c^I - (\omega_c^I)^2 y_c^I) - \sum k_{sn}^I \delta_{sn}^I \cos \psi_{sn}^I - \sum k_{rn}^I \delta_{rn}^I \cos \psi_{rn}^I + k_c^I y_c^I = 0 \\
& (I_c^I / (r_c^I)^2 + \sum m_p^I) \ddot{u}_c^I - \sum (k_{sn}^I \delta_{sn}^I \cos \alpha_s^I + k_{rn}^I \delta_{rn}^I \cos \alpha_r^I) = 0 \\
& \delta_{sn} = (x_c - x_s) \sin \psi_{sn} + (y_s - y_c) \cos \psi_{sn} + u_s - u_c \cos \alpha_s + u_n; \quad \delta_{rn} = x_c \sin \psi_{rn} - y_c \cos \psi_{rn} - u_c \cos \alpha_r - u_n; \\
& x_s^I = x_c^I, x_s^I = x_c^I; y_s^I = y_c^I, y_s^I = y_c^I; u_s^I = r_s^I u_c^I / r_c^I, u_s^I = r_s^I u_c^I / r_c^I; \quad \psi_{sn} = \psi_n - \alpha_s; \psi_{rn} = \psi_n + \alpha_r
\end{aligned}$$

Where the superscript I, II and III denote the Stage 1, Stage 2, Stage 3;  $I_i$  for  $i=s, p, c$  ( $s, p$  and  $c$  represent the sun, planet and carrier) are the moments of inertia,  $r_i$  are base circle radii of the gears or radius of the carrier, and  $m_p$  is the mass of a planet;  $u_j$  for  $j=s, c, 1, \dots, N$  ( $N$  indicates the number of planets) are rotational deflections of bodies along the lines of action;  $x_k, y_k$  ( $k=s, c$ ) are sun and carrier translations;  $\alpha_s, \alpha_r$  are the sun-planet and ring-planet pressure angles;  $k_{sn}, k_{rn}$  are the  $n$ th sun-planet and ring-planet mesh stiffnesses.  $k_s, k_c$  are the bearing stiffnesses of sun and carrier.  $\delta_{sn}, \delta_{rn}$  are the  $n$ th sun-planet and ring-planet relative displacement.  $\psi_n$  is the  $n$ th planet phase angle.

### Natural Frequencies and Vibration Modes

In the three-stage PGT reducer, the sun gears are the input and the nut carriers thrusting the spindle are the output of each PGT unit. The ring gears are fixed, and the transverse motions of planets are not considered, therefore, the transverse-torsional dynamic model of the three-stage PGT includes 23 DOF. It is not difficult to see that the differential equations of motion for system can be assembled in matrix form as

$$\mathbf{M}\ddot{\mathbf{q}} + \mathbf{G}_\omega \dot{\mathbf{q}} + (\mathbf{K}_b + \mathbf{K}_m - \mathbf{K}_\omega) \mathbf{q} = \mathbf{0} \quad (2)$$

Where  $\mathbf{M}$ ,  $\mathbf{K}_b$ ,  $\mathbf{K}_m$  and  $\mathbf{q}$  are the positive definite mass matrix, diagonal bearing stiffness matrix, symmetric mesh stiffness matrix and generalized coordinate vector, respectively.  $\mathbf{G}_\omega$  is gyroscopic matrix led by the Coriolis accelerations.  $\mathbf{K}_\omega$  is diagonal centripetal stiffness matrix led by the centripetal accelerations. When the carrier speed is not large, the  $\mathbf{G}_\omega$  and  $\mathbf{K}_\omega$  are too small than others parameters matrix, which can be neglected. To determine the natural frequencies and vibration modes the time-invariant system is considered. All mesh stiffnesses are considered to be constant and equal to their average stiffness over one mesh cycle, and the bearing stiffnesses also use average stiffnesses to represent. The eigenvalue problem of (2) for the linear time-invariant case using average mesh stiffness is

$$(\bar{\mathbf{K}}_b + \bar{\mathbf{K}}_m)\boldsymbol{\varphi}_i = \omega_i^2 \mathbf{M}\boldsymbol{\varphi}_i \tag{3}$$

Where  $\bar{\mathbf{K}}_b$  is mean bearing stiffness matrix,  $\bar{\mathbf{K}}_m$  is mean mesh stiffness matrix,  $\omega_i$  are the natural frequencies,  $\boldsymbol{\varphi}_i$  are the associated vibration shape vector. The parameters of the three-stage PGT are listed in Table 1. By solving the free vibration eigenvalue problem, the natural frequencies are computed as shown in Table 2, and the associated mode shapes also can be obtained.

Table 1 Parameters of the three-stage planetary train

| Parameter           | First stage         |                     |                   | Second stage        |                      |                    | Third stage        |                       |                     |
|---------------------|---------------------|---------------------|-------------------|---------------------|----------------------|--------------------|--------------------|-----------------------|---------------------|
|                     | Sun <sup>I</sup>    | Planet <sup>I</sup> | Ring <sup>I</sup> | Sun <sup>II</sup>   | Planet <sup>II</sup> | Ring <sup>II</sup> | Sun <sup>III</sup> | Planet <sup>III</sup> | Ring <sup>III</sup> |
| Number of teeth     | 25                  | 20                  | 65                | 21                  | 27                   | 69                 | 24                 | 24                    | 72                  |
| Module(mm)          | 4                   |                     |                   | 5                   |                      |                    | 6                  |                       |                     |
| Pressure angle(deg) | 21.7                |                     |                   | 21.3                |                      |                    | 21.1               |                       |                     |
| Mesh stiff.(N/m)    | 3.8×10 <sup>8</sup> |                     |                   | 5.4×10 <sup>8</sup> |                      |                    | 7×10 <sup>8</sup>  |                       |                     |
| Bearing stiff.(N/m) | 1×10 <sup>9</sup>   |                     |                   |                     |                      |                    | 1×10 <sup>9</sup>  |                       |                     |

Table 2 Natural frequencies of gear train ( $f$ / Hz)

| Vibration modes | Natural frequencies   |
|-----------------|---|
| Rigid-body mode | $f_1=0$   |
| Planet mode     | $f_{10}=f_{11}=f_{12}=2288, f_{17}=f_{18}=f_{19}=3653, f_{21}=f_{22}=4522$  |
| Over all mode   | $f_2=f_3=503, f_4=f_5=884, f_6=937, f_7=f_8=1213, f_9=1467, f_{13}=2352, f_{14}=2622, f_{15}=2642, f_{16}=2677, f_{20}=3653, f_{23}=5424$ |

For three-stage planetary gears with fixed rings, all modes can be classified into one of the three categories: (a) a rigid-body mode; (b) over all modes; (c) three group of planet modes (degenerate modes) [2, 3, 4] with multiplicity N-1(N indicates the number of planets ).

**Rigid-body mode:** So long as the input and output members are not constrained, the stiffness matrix is semi-definite resulting in a “rigid body” mode at zero frequency. At this mode, all gears and carriers rotate as rigid bodies without any deflection according with the transmission ratio, and any body has no translational motion.

**Planet modes:** At these modes, the central components have no motion; the planets of one stage are the only components that deflect, and the vector sum of the deflections of planets is zero. These are called planets modes. For the planet mode at 4522Hz, the vibration only exists in the first-stage. Similarly, that only exists in the second-stage at 3653Hz, and in the third-stage at 2288Hz.

**Over all modes:** It is characterized by existence of single-stage or multi-stage coupling vibrations. In the vibration modes with 503 Hz、884 Hz and 1213Hz, each central component has two translation and no rotation; All planets have pure rotations. These modes can be called translational modes. The modes at 1467Hz, 2352Hz and 5424Hz, where all the members in contribution only on the rotational motion; and at 5424Hz, there only the first stage have rational motion. These modes can be called rotational modes. The modes at others frequencies have complicated coupling motion among each components of all stages in different direction. Fig. 4, 5 shows the translational mode with 503 Hz and rotational mode with 1467Hz. In the mode shapes figures, where the equilibrium positions of the PGT are shown as dashed and the displaced positions are shown as real lines.

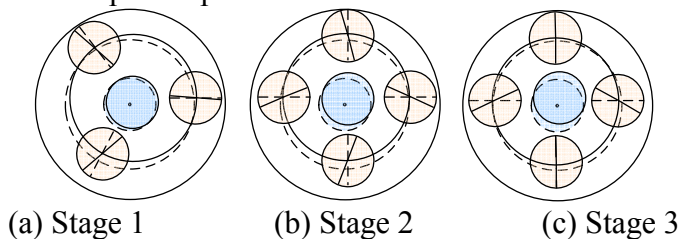
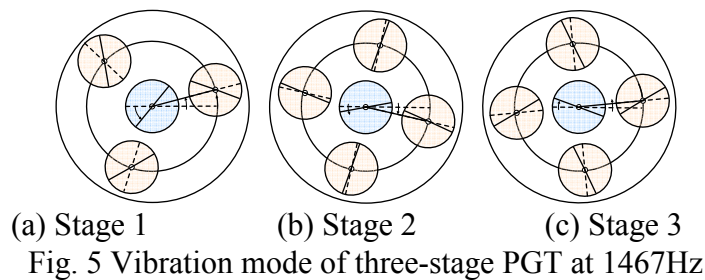


Fig. 4 Vibration mode of three-stage PGT at 503Hz



## Conclusions

The modified transverse-torsional model for the three-stage planetary gears coupled with bearings was developed by lumped parameter method. The natural frequencies and vibration modes are calculated by using this model with the mean value of the gear mesh stiffness and bearing stiffness. All vibration modes can be classified into three types: rigid-body mode, planet modes and over all modes. Rigid-body mode with zero frequency has non-deforming motion. planet modes with degenerate natural frequencies have rotational motions of the planets in one stage only and no motion of any central components. Over all modes can be subdivided into translational modes, rotational modes and complicated coupling modes.

For the main reducer of shield tunnelling machine, the mesh frequency of high-speed stage is 345Hz at the high speed operating condition with 1145rpm. The first order natural frequency of the gears train is 503Hz; therefore, the multi-stage planetary gears have highly structured properties relative to the mesh frequency. It is rare for the gears train of main reducer being excited to lead sympathetic vibration under the operating condition. This modified model can be used to investigate the vibration transfer between gears train and housing through bearings. This work lays a foundation for lubricating dynamic property and coupling vibration of the multi-stage planetary gearbox.

## Acknowledgement

This project is supported by National High Technology Research and Development Program of China (863 Program, Grant No. 2007AA041802).

## References

- [1] J. D. Smith: *Gears and Their Vibration* (Marcel-Dekker, New York 1983).
- [2] A. Kahraman: *Journal of Mechanical Design* Vol. 116 (1994), p. 714-
- [3] J. Lin and R. G. Parker: *Journal of Vibration and Acoustics* Vol. 121 (1999), p. 316
- [4] J. Lin and R. G. Parker: *Journal of Sound and Vibration* Vol. 249 (2002), p. 129
- [5] V. K. Ambarisha and R. G. Parker: *Journal of Sound and Vibration* Vol. 302 (2007), p. 577
- [6] M. Inapolat, A. Kahraman: *Journal of Sound and Vibration* Vol. 323 (2009), p. 677
- [7] Y. Song, W. Xu, C. Zhang, et.al: *Chinese Journal of Machine Engineering* Vol. 42(2006), p. 16, in Chinese.
- [8] A. Kahraman: *Mech. Mach. Theory* Vol. 36 (2001), p. 953
- [9] A. Al-shyyab, K. Alwidyan, A. Jawarneh, et al: *Proc. IMechE, Part K: J.Multi-body Dynamics* Vol. 223 (2009), p. 1
- [10] Z. Xiao, D. Qin, et.al: *China Mechanical Engineering* Vol. 21 (2010), p. 2176, in Chinese.

## **A Static and Dynamic Model of Spiral Bevel Gears**

Jing Wang, Joël Teixeira Alves, Michèle Guingand,  
Jean-Pierre de Vaujany, Philippe Velez

Université de Lyon, CNRS, INSA Lyon, LaMCoS UMR5259, F-69621, France

18-20 rue des Sciences, 69621 Villeurbanne cedex

michele.guingand@insa-lyon.fr

**Keywords:** spiral bevel gears, dynamic model, load distribution.

**Abstract.** Two three-dimensional lumped parameter dynamic models of spiral bevel gears are presented and compared. The first approach is classic and relies on a single averaged mesh stiffness element connecting the gears whereas a time-varying non-linear distribution of discrete stiffness elements over the potential contact area is used in the second model.

### **Introduction**

Gear dynamic behaviour has long been recognised as a major concern because it can strongly impact transmission reliability and the noise level and quality [1]. The maximum dynamic forces on tooth contacts can be substantially higher than those predicted for quasi-static conditions thus leading to a reduction of the gear set durability. In this context, it is crucial to be able to predict the possible overloads on the teeth and the corresponding critical speeds. A large number of dynamic models have been presented in the literature but most of them deal with spur and helical gears [2] while those aimed at simulating hypoid or spiral bevel gears are comparatively sparse [3-5].

In this paper, two dynamic models are presented which make it possible to estimate instantaneous displacements and mesh loads over a wide range of speeds. An original approach is proposed which relies on distributed mesh stiffness elements as opposed to the classic model with one single mesh stiffness connecting the two pinions of a pair. The major advantage of the distributed stiffness modelling is that instantaneous (or dynamic) contact force and pressure distributions can be estimated. However, for both models, the input data needed in terms of quasi-static stiffness and no-load transmission error are generated by the same numerical software ASLAN developed at LaMCoS – INSA Lyon.

### **Static Model**

The quasi-static calculations comprise: a) the pinion geometry definition based on the simulation of the cutting process followed by the analysis of no-load kinematics and b) calculations under load. The two steps of the process are detailed below.

**Definition of the Pinion Geometry.** The proposed methodology allows the geometrical definition of pinions cut by face-milling (Gleason), in the case of standard geometry [6]. For the sake of simplicity, only a limited number of machine motions are taken into account. The motion of generation is reduced to two motions in the machine framework: one rotation of the cradle and one rotation of the cut pinion which are linked by a constant ratio. Both tooth flanks are simultaneously cut. Mounting, position errors such as axial errors, offset and angular errors can be introduced when the pinion and the gear are assembled and their geometries are put in correspondence.

**Analysis under Load.** The load sharing between the teeth in mesh is solved by combining the classic compatibility conditions in terms of displacements and the static mesh force balance which ultimately leads to contact pressure distributions, mesh stiffness and transmission errors under load. The displacement fields account for the global structural deflections of the two pinions (tooth bending, base rotation, etc.) and the local contact displacements via a matrix of influence coefficients. The structural deflections are derived from Finite Element Models [7] and the contact effects are characterised by using the theory of Boussinesq and Cerruti [8].

At every point on the potential contact area, the normal contact problem is solved by using the following conditions:

$$\begin{cases} U_{1i} + U_{2i} + e_{i_i} - \alpha = y_i = 0 \\ p_i \geq 0 \end{cases} \text{ in the contact area} \quad (1)$$

$$\begin{cases} U_{1i} + U_{2i} + e_{i_i} - \alpha = y_i \geq 0 \\ p_i = 0 \end{cases} \text{ outside the contact area} \quad (2)$$

where  $U_{1i}$  and  $U_{2i}$  are the normal displacements at point  $i$  for solids 1 and 2 respectively,  $e_{i_i}$  is the initial normal separation at point  $i$ ,  $\alpha$  is the global normal approach (from which transmission error can be derived) and  $p_i$  is the pressure at point  $i$ . The distance under load at point  $i$  between the two solids in contact is denoted  $y_i$ .

Having divided the contact area into a number  $N$  of rectangular surfaces centred at point  $i$  and area  $S_i$ , the static equilibrium is formulated as:

$$\sum_{i=1}^N p_i R_i S_i = \text{Torque} \quad (3)$$

where  $R_i$  is the lever arm associated with the surface controlled by point  $i$  and *Torque* is the external torque on the pinion.

## Dynamic Models

**Modelling Principles.** Three-dimensional models have been set up which rely on 2-node finite elements with six degrees of freedom (DOF) per node (axial, bending and torsion displacements). The pinion and gear are assimilated to two rigid cones connected by a Wrinckler's elastic foundation [9] (distributions of independent stiffness elements). Using the properties of infinitesimal displacement screws, the deflection at any potential point of contact is expressed in terms of the pinion-gear DOFs and the initial normal separation when the gears are unloaded [2]. The positions and the value of the stiffness elements are updated as the gears are rotating and the tooth profiles are moving. At every time-step, the mesh forces and moments on the pinion and the gear are calculated leading to a time-varying non-linear stiffness matrix and forcing term. The shafts are modelled by Timoshenko's beam elements with secondary shear effects and the bearings are simulated as lumped stiffness elements derived from Palmgrem's formulation. Finally, a constant input torque and input speed are imposed by the motor on the pinion shaft from which the resisting torque and output speed are deduced.

**Equations of Motion.** Considering a single mesh stiffness function (referred to as model 1), the mesh strain energy is determined by assuming that the time-varying mesh stiffness acts, in the normal direction, at the centroid of the contact interface between the pinion and the gear:

$$U_E = \frac{1}{2} \cdot k_j \cdot d(B_m)^2 = \frac{1}{2} \cdot k_j \cdot (V^T \cdot q_E)^2 \quad V = \begin{cases} \vec{n}_1 \\ \vec{n}_1 \wedge \overrightarrow{O_1 B_m} \\ \vec{n}_2 \\ \vec{n}_2 \wedge \overrightarrow{O_2 B_m} \end{cases} \quad (4)$$

$$= \frac{1}{2} \cdot q_E^T [k_j \cdot V \cdot V^T] q_E = \frac{1}{2} \cdot q_E^T \cdot [K_E] \cdot q_E$$

where  $j$  represents the mesh position,  $B_m$  is the time-varying centroid of the contact interface,  $\vec{n}_1 = -\vec{n}_2$  are unit normal vectors at the contacts (supposed to be the same at all points).

A distribution of stiffness elements in introduced in Model 2 so that mesh strain energy becomes:

$$\begin{aligned}
 U_E &= \sum_{i \in (A)} U_{Ei} = \frac{1}{2} \sum_{i \in (A)} k_i \cdot q_E^T \cdot V_i \cdot V_i^T \cdot q_E - \sum_{i \in (A)} k_i \cdot V_i^T \cdot q_E \cdot e_i + \frac{1}{2} \sum_{i \in (A)} k_i \cdot e_i^2 \\
 &= \frac{1}{2} q_E^T \cdot \underbrace{\left( \sum_{i \in (A)} k_i \cdot V_i \cdot V_i^T \right)}_{K_E} \cdot q_E - \underbrace{\left( \sum_{i \in (A)} k_i \cdot V_i^T \cdot e_i \right)}_{F_2} \cdot q_E + \frac{1}{2} \sum_{i \in (A)} k_i \cdot e_i^2
 \end{aligned}
 \tag{5}$$

where A represent the instantaneous contact area, i is the index of a potential contact point.

It is to be noted that an additional forcing term  $F_1$  caused by tooth initial separations appears in the equations. In what follows, dissipations of all sorts are modelled via a global constant viscous damping matrix [C]. Rayleigh’s damping is considered so that [C] is a linear combination of the mass and averaged stiffness matrices. After assembly of all the elemental matrices, the equations of motion are determined from Lagrange’s equations and they are solved by using a time-step integration scheme combined with a unilateral normal contact algorithm.

$$[M]\ddot{q} + [C]\dot{q} + [K(t, q)]q = [F_0] - [F_1] - [F_2]
 \tag{6}$$

**Simulation Results**

**Dynamic Forces and Dynamic Factors.** Considering Model 1, one example of mesh force versus time evolution is represented in Fig. 1 for a pinion rotational speed of 17 200 rpm. The numerical transients who appear during the first mesh periods are due to the choice of initial conditions (static solution with averaged mesh stiffness matrix) which, depending on the speed regime, may be rather different from the actual displacements and speeds. However, it can be noticed that steady state conditions are reached very quickly.

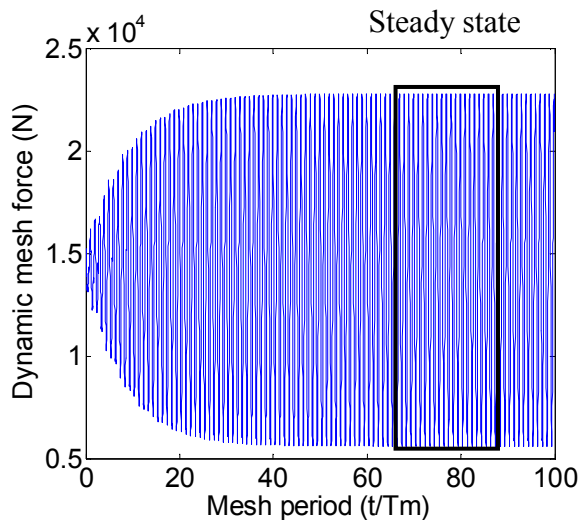


Fig.1 : Dynamic responses of model 1.

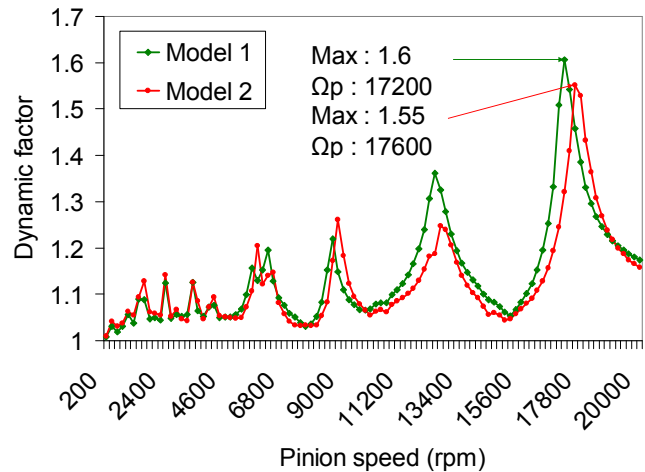


Fig.2 : Dynamic factor versus pinion speed for two models.

The previous results have been extended over a range of rotational speeds by calculating the dynamic factor defined as  $DF = \max(F_d/F_s)$ , with  $F_d$ ,  $F_s$  the dynamic and static mesh forces respectively. Models 1 and 2 have been used and the corresponding response curves are plotted in Fig. 2. The two curves are in good agreement and exhibit both a major tooth critical speed around 17 000 -18 000 rpm depending on the model along with several secondary critical speeds excited by the higher mesh frequency harmonics. However, it can be observed that the two different approaches are not exactly equivalent in terms of amplifications and critical speeds thus illustrating the drawbacks of the classic models with one equivalent time-varying mesh stiffness element. Significant dynamic effects are observed regardless of the model (DF between 1.5 and 1.6) highlighting the role of vibrations on gear durability.

**Pressure Distributions.** Using Model 2, the force distributions on tooth flanks can be estimated. Fig. 3 shows an example of comparison between the quasi-static results delivered by ASLAN and those given by the dynamic model at low speed (1 rpm here). The pressure patterns are in close agreement and show that the maximum pressure is obtained in the central part of the tooth flank.

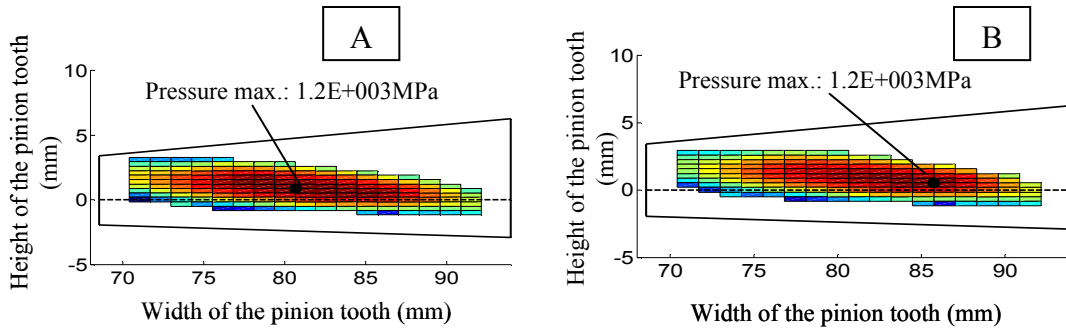


Fig. 3 : Quasi-static pressure distributions obtained by ASLAN (A) and the dynamic model 2 (B).

## Conclusions

Two multi-DOF dynamic models of spiral bevel gears have been presented and compared which both rely on an accurate description of tooth geometry and mounting conditions. The models differ in that they rely on different mesh stiffness simulations. Model 1 is in the vein of the classic models usually found in the literature whereas Model 2 includes a more local description of the actual contact conditions. Whatever the model used, the dynamic response curves exhibit similar trends: i) significant mesh force amplifications at the major tooth critical speed and ii) secondary resonances generated by the higher order harmonics of the mesh stiffness functions.

## References

- [1] V. K. Tamminana, A. Kahraman and S. Vijayakar, *J. Mech. Des* Vol.129, 011011 (2007).
- [2] M. Ajmi, P. Velex, *Mech. Mach. Theory* Vol.40 (2005), p. 173
- [3] M. Li, H. Y. Hu, *J. Sound Vib* Vol. 259 (2003), p. 605
- [4] Q. Gao, M. Tanabe and K. Nishihara, *J. Sound Vib* Vol. 319 (2009), p. 463
- [5] J. Wang, T. C. Lim and M. F. Li, *J. Sound Vib* Vol. 308 (2007), p. 302
- [6] International Organization for Standardization, 2006, *Bevel and Hypoid Gear Geometry ISO 23509(2006)*
- [7] J. Teixeira Alves, M. Guingand and J. P. de Vaujany, *Mech. Mach. Theory* Vol. 45 (2010), p. 349
- [8] J. Boussinesq: *Application des Potentiels à L'étude de L'équilibre et du Mouvement des Solides Élastiques* (Albert Blanchard, Paris 1959).
- [9] Information on [http://hal.archives-ouvertes.fr/hal-00121935\\_v1/](http://hal.archives-ouvertes.fr/hal-00121935_v1/).

## Research on Meshing Characteristics for Face Gear with Arcuate Tooth

Xiangwei Cai<sup>1,a</sup>, Zongde Fang<sup>1,b</sup> and Jinzhan Su<sup>1,c</sup>

<sup>1</sup>School of Mechanical Engineering, Northwest Polytechnical University, Xi'an 710072, China

<sup>a</sup>caixiangwei@163.com, <sup>b</sup>fauto@nwpu.edu.cn, <sup>c</sup>sujinzhan@mail.nwpu.edu.cn

**Keywords:** face gear with arcuate tooth; flank modification; tooth contact analysis; transmission errors

**Abstract.** The generating of face gear with arcuate tooth has been proposed in this paper, and the meshing characteristics are investigated. Based on the concept of imaginary gear cutter, tooth surface equation has been derived, flank modification has also been considered. The transmission errors and bearing contacts of the face gear drive with arcuate tooth under different assembly conditions are investigated by applying the tooth contact analysis. The numerical results reveal that the bearing contacts are not sensitive to the errors of misalignments, and a more favorable type parabolic function of transmission errors with better symmetry and reduced amplitude may be obtained according to the modification of the face gear.

### Introduction

A new type of face gear drive with arcuate tooth that has better meshing performance than the helical and spur involute face gear drives is studied in this paper[1,2]. The contents of the paper cover:

- (1) Concept of generation of face gears with arcuate tooth by imaginary gear cutter.
- (2) Simulation of meshing and contact for determination of transmission errors and shift of bearing contact.

### A Mathematical Model of Face Gear with Arcuate Tooth

Fig.1 illustrates the generating mechanism for face gears with arcuate tooth. During the generation process, the cutter head rotate about its axis and conical surface is formed which can be regarded as a tooth of imaginary gear cutter. Besides, the cutter head perform circular motion and the manufacture of face gear can be simulated by considering the meshing of a gear blank with a imaginary gear cutter. This generating process will produce one space and the gear blank is indexed to one tooth and the generating cycle is repeated until all the teeth and spaces are produced.

Fig.2 depicts the normal section of the gear cutter  $\Sigma_s$  that generates the face gear space. The profile is modified to be a parabolic style in order to improve the meshing characteristics of the face gear drive instead of the straight edged one. Parameters  $a_m$ ,  $R_f$  and  $\alpha_n$  are the design parameters. The parabolic line of the normal section can be represented in coordinate system  $S_i(X_i, Y_i, Z_i)$  and  $S_a(X_a, Y_a, Z_a)$  by

$$\mathbf{R}_i = [u_i \quad -a_i u_i^2 \quad 0 \quad 1]^T \quad (1)$$

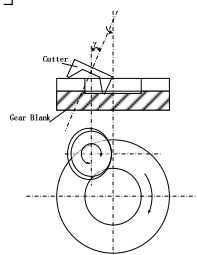


Fig.1. Generating mechanism for face gears with arcuate teeth

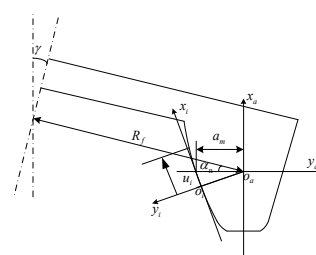


Fig.2. Normal section of gear cutter

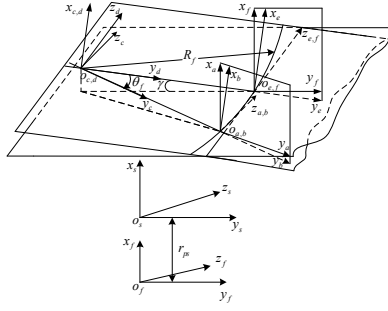
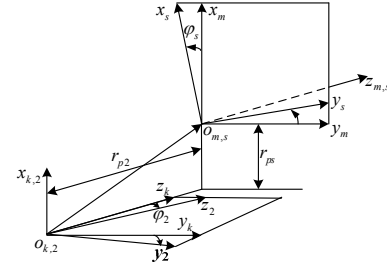
Fig.3. Relations between coordinate system  $S_a$  and  $S_s$ 

Fig.4. Generation of face gear by imaginary gear cutter

$$\mathbf{R}_a = \mathbf{M}_{ai} \mathbf{R}_i \quad (2)$$

Where  $a_i$  is coefficient of the parabolic normal section, and  $u_i$  is one of the surface parameters of  $\Sigma_s$ .

The tooth surface of imaginary gear cutter is formed by a rotary cutting surface of cutter head with a titled angle. Fig.3 shows the formation of the gear cutter surface and the relations between coordinate system  $S_a$  and  $S_s$ . Auxiliary Coordinate systems  $S_c$  and  $S_d$  denote the rotation of the cutter spindle, and  $S_b$  and  $S_e$  represent the transformation of the titled angle.

Gear cutter surface  $\Sigma_s$  is represented in coordinate system  $S_s$  by the matrix equation

$$\mathbf{R}_s(u_i, \theta_f) = \mathbf{M}_{sf} \mathbf{M}_{fe} \mathbf{M}_{ed} \mathbf{M}_{dc} \mathbf{M}_{cb} \mathbf{M}_{ba} \mathbf{R}_a \quad (3)$$

Where  $\theta_f$  is also the surface parameter of  $\Sigma_s$ .

The tooth surface  $\Sigma_2$  of the face gear is generated as the envelope to the family of tooth surface  $\Sigma_s$  of the imaginary gear cutter. We apply for derivations the fixed coordinate systems  $S_m$  and  $S_k$  and movable coordinate systems  $S_s$  and  $S_2$  (Fig.4). The cutter and the face gear perform related rotations about the  $x_m$  and  $x_k$  axes. Here,

$$\frac{\varphi_s}{\varphi_2} = \frac{N_2}{N_s} \quad (4)$$

Where  $N_s$  and  $N_2$  are the numbers of teeth of the gear cutter and the face gear, respectively.

Surface  $\Sigma_2$  is determined by the following equations:

$$\mathbf{r}_2(u_i, \theta_f, \varphi_s) = \mathbf{M}_{2s}(\varphi_s) \mathbf{r}_s(u_i, \theta_f) \quad (5)$$

$$\left( \frac{\partial \mathbf{r}_2}{\partial u_i} \times \frac{\partial \mathbf{r}_2}{\partial \theta_f} \right) \cdot \frac{\partial \mathbf{r}_2}{\partial \varphi_s} = f_{s2}(u_i, \theta_f, \varphi_s) = 0 \quad (6)$$

Vector function  $\mathbf{r}_2(u_i, \theta_f, \varphi_s)$  represents in coordinate system  $S_2$  the family of the gear cutter surfaces  $\Sigma_s$ . Equation  $f_{s2} = 0$  is the equation of meshing. Eqs. (5) and (6) considered simultaneously represent the tooth surface  $\Sigma_2$  by three related parameters.

### Simulation of Gear Meshing and Tooth Contact Analysis(TCA)

The meshing between the concave side of the pinion and the convex side of the gear is analyzed in the face gear drive. Coordinate system  $S_f$  is the fixed one and is rigidly connected to the frame of the face gear drive (Fig.5). Coordinate systems  $S_1$  and  $S_2$  are rigidly connected to the pinion and face gear, respectively. Auxiliary coordinate systems  $S_p$ ,  $S_q$  and  $S_e$  are applied for simulation of errors of alignment  $\Delta\gamma$  of the shaft angle,  $\Delta q$  of the axial displacement and  $\Delta E$  of the offset of the face gear. The tangency of surfaces  $\Sigma_1$  and  $\Sigma_2$  is considered in  $S_f$  as the following equations[3]:

$$\begin{cases} \mathbf{r}_f^{(1)}(u_p, \theta_p, \varphi_p, \phi_1) = \mathbf{r}_f^{(2)}(u_g, \theta_g, \varphi_g, \phi_2) \\ \mathbf{n}_f^{(1)}(u_p, \theta_p, \varphi_p, \phi_1) = \mathbf{n}_f^{(2)}(u_g, \theta_g, \varphi_g, \phi_2) \end{cases} \quad (7)$$

Eqs.(7) yield a system of seven non-linear equations in eight unknowns considering the two meshing equations of the face gear and the pinion respectively, since  $|n_f^{(1)}| = |n_f^{(2)}|$ . One of the unknowns, say  $\phi_1$  is chosen as the input parameter, and the solution of equations mentioned above is a computerized iterative process based on the Newton-Raphson method[4].

### Numerical Examples for Gear Meshing Simulation

The main design parameters of the face gear drive are listed in Table 1. A three-dimensional gear tooth profile of the gear drive can be plotted by applying the developed gear mathematical model and computer graphics as depicted in Fig.6. Comparison of meshing and contact for face gear drive with modified profile of the face gear to the one with no modification is depicted in Fig.7. Fig.8. Shows the shift of the paths of contact caused by errors of alignment  $\Delta E$ ,  $\Delta q$  and  $\Delta \gamma$ , respectively.

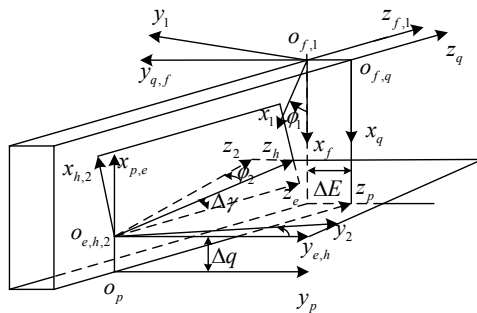


Fig.5 Coordinate systems applied for simulation of meshing

Table 1. The parameters of design

| Parameters                        |      |
|-----------------------------------|------|
| Pinion tooth number $N_1$         | 42   |
| Face gear tooth number $N_2$      | 180  |
| Gear cutter tooth number $N_s$    | 45   |
| Normal module $m_n$ /(mm)         | 3.0  |
| Pressure angle $\alpha_n$ (°)     | 22   |
| Titled angle $\gamma$ (°)         | 8    |
| Cutter head radius $R_{p'}$ /(mm) | 120  |
| Parabola coefficient $a_1$        | 0.01 |

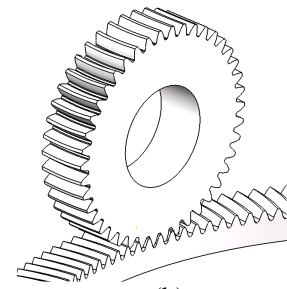
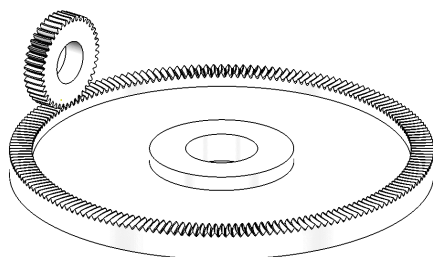


Fig.6. Face gear drive with arcuate teeth of pinion and gear

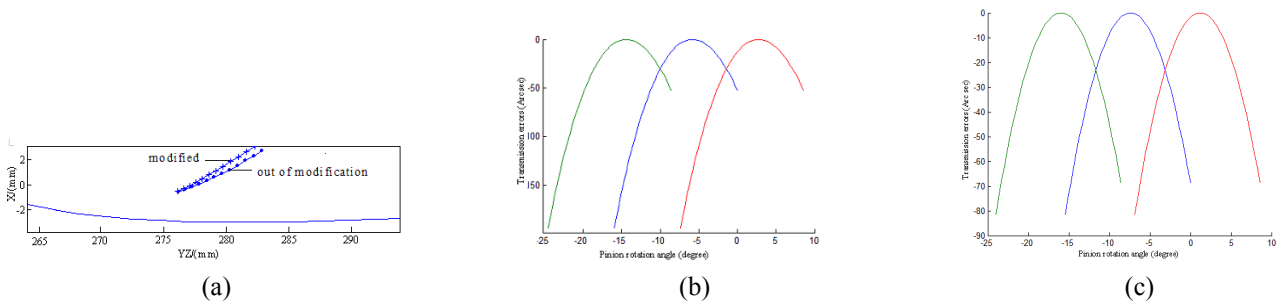


Fig.7. Output of TCA for a face gear drive: (a)Paths of contact for face gear with the profile modified or not; (b)function of transmission errors with the face gear tooth out of modification; (c)function of transmission errors for the drive with modified profile of the face gear.

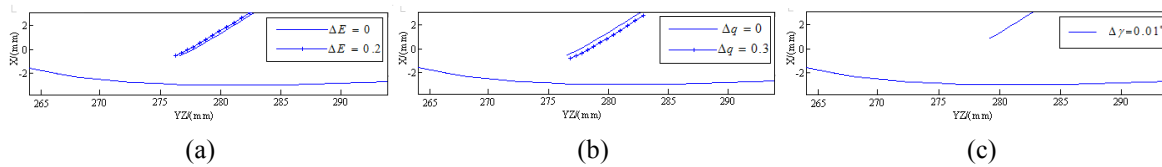


Fig.8. Influence of errors of alignment on the shift of the path of contact for a modified face gear drive with the following errors: (a)  $\Delta E$  ; (b)  $\Delta q$  ; (c)  $\Delta \gamma$

## Conclusion

The discussions above allow to draw the following conclusions:

- (1) A new type of face gear drive with arcuate tooth of face gear and pinion has been investigated. And the face gear tooth surface is generated as the envelope to the family of the imaginary gear cutter.
- (2) The function of transmission errors is a parabolic one. A low magnitude and better symmetry of the function can be obtained by application of the profile modification of the face gear.
- (3) Flank modification of the face gear can decrease the sensitivity of the gear drive to the errors of alignment  $\Delta E$  and  $\Delta q$ . The contact paths are shifted up due to the error  $\Delta \gamma$ , and this may result in stress concentration on the gear. But the sensitivity of this type face gear drive to the errors of alignment is better than others face-gear drive[3].

## References

- [1] Z. Fang, X. Cao, Y. Shen: Journal of Aerospace Power, 2010,1(25):224-227
- [2] J. Su, Z. Fang, X. Cao: Journal of Aerospace Power,2010, 6(25)
- [3] F.L. Litvin: Gear Geometry and Applied Theory. Prentice Hall, Inc., Englewood Cliffs, NJ (1994)
- [4] G.A. Korn and T.M. Korn: Mathematics Handbook for scientist and Engineers, McGraw-Hill, Inc., 2nd Ed. (1968)

## A Challenge to Design of a New Harmonic Drive Device

Shuting Li<sup>1, a</sup>

<sup>1</sup>Department of Mechanical, Electric and Electronic Engineering,  
Interdisciplinary Faculty of Science and Engineering, Shimane University,  
1060 Nishikawatsu-Cho, Matsue, 690-8504, Japan

<sup>a</sup>shutingli@ecs.shimane-u.ac.jp

**Keywords:** Gear, Harmonic Drive Device, Design, Contact stresses, Gear strength, FEM.

**Abstract.** A new silk-hat type of harmonic drive device (HDD) with arc flexspline (FS) structure is developed. Loaded gear contact analysis (LGCA) and stress calculations are made for it with three-dimensional, finite element method (3D-FEM). Basic performances and strengths tests are also made. It is found that the new structure almost has the same performances and strength as the old one.

### Introduction

HDD [1-2] has many advantages, such as lightweight, small size, high reduction ratio, low backlash etc. It is widely used in robots, aeronautic and astronautic equipments as a precise motion and power transmission. Since elastic deflection of the flexspline, a very thin-rimmed spur gear, is used to generate engagement movement of teeth, many design problems for the devices have not been solved so far. Especially, structural design and strength calculations for this device need great challenges for designers.

This paper is an introduction to the new challenge of designing a silk-hat type of HDD with arc-shaped FS structure. 3D-FEM is developed based on many years' researches. It is used to conduct LGCA (Contact problem of the HDD is different from usual solid gears. All the gear structure of the FS must be considered in the model, so, loaded gear contact analysis is used here instead of using loaded tooth contact analysis) and strength calculations of the HDD. In order to make the device have the same life everywhere, balance design and structure discussions are conducted for the HDD with the 3D-FEM. Structural discussion and strength calculation results are introduced here. Based on the results, the new HDD is made. Performance and strength tests are also made for this new structure. It is found that the new design almost has the same performance and strength as the old one.

### New Silk-hat Type of HDD with arc Flexspline

Figure 1 is the new silk-hat type of HDD with the arc-shaped flexspline. As a conventional unit type of HDD, the new HDD also consists of flexspline, circular-spline (CS), wave generator (WG), flexible ball bearing, main bearing (here, cross-roller bearing is used) and other parts [3].

As shown in Fig. 1(a), the old structure of the flexspline consists of tooth, tube and diaphragm while the new one consists of tooth and arc. This is the difference from the old one. Why to change the old structure of FS into an arc-shaped structure? Three advantages in the following are considered. (1) the new FS can be designed to be more flexible than the old one in radial direction, especially in the case that the tube is very short, so that bearing loads resulted from WG deflection can be reduced; (2) Flexible ball bearing can be inserted from both sides of the FS (the tooth side and the boss side) while it can only be inserted for the tooth side for the old structure; (3) Enlarged space of FS hollow hole at the boss side can be used for putting other parts in. On the opposite side, it is quite difficult to make the new structure of the arc-shaped FS. So, it is a great challenge to develop this new HDD.

### FEM model and Loaded Gear Contact Analysis

In order to be able to design the FS structure and calculate strength of the HDD, LGCA is made by 3D-FEM using models as shown in Fig. 2. Mathematical programming method (MPM) is developed and then used to do it based on many years' researches of the author [4-5]. In this LGCA, face-contact model of the FS teeth with the CS teeth is used. Deformation influence coefficients of the assumed contact points both on FS and CS tooth surfaces are calculated by 3D-FEM. Loads distributed on tooth surfaces are obtained by conducting MPM. Bearing ball loads are obtained through performing 3D-FEM calculations of FS structure using tooth loads and calculating reaction force on balls. Contact stresses on tooth surfaces and bearing balls are calculated with "unit area" method [6] and Hertzian formulas, respectively. Calculation results are explained in the following.

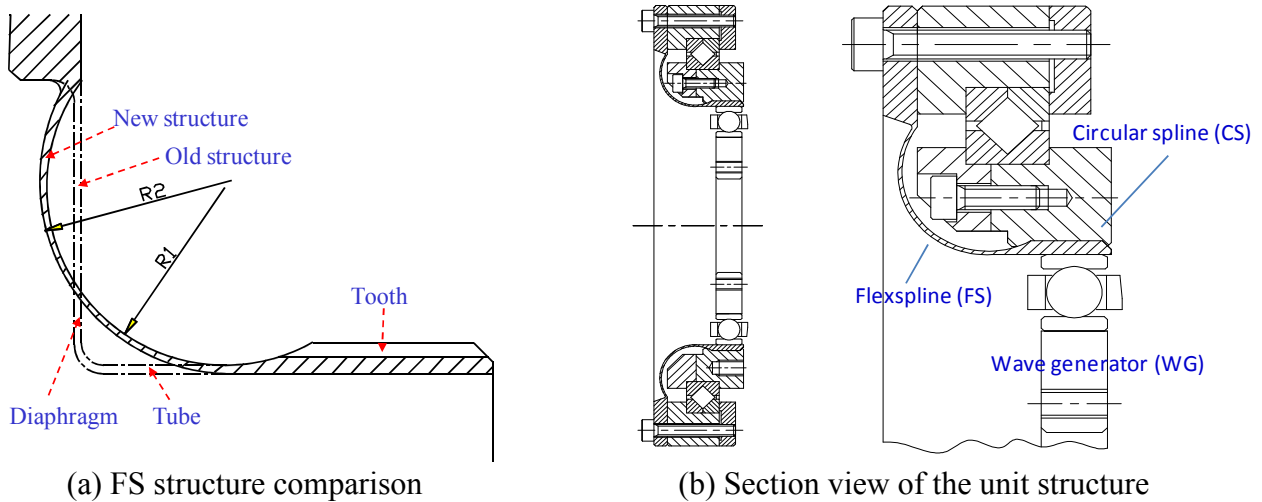


Fig.1 New silk-hat type of HDD with arc-shaped FS structure

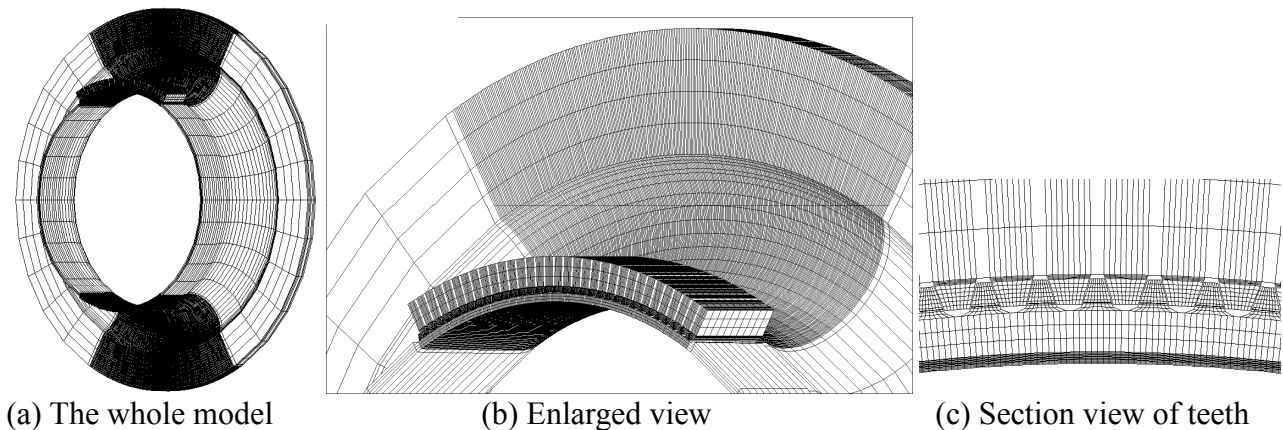


Fig.2 3D-FEM Model for loaded gear contact Analysis

### Results of Stress Analyses and Discussions

**Tooth Surface Contact Stresses.** Figure 3 is contour lines of the maximum contact stresses on every tooth surface. Abscissa and the ordinate of Fig. 3 are face width of FS teeth and angular range of contact teeth, simply called contact angle here. Major axis of the WG is located at the 0 degree of the contact angle. Position of the major axis of WG is also shown in Fig.3. From Fig. 3, it is found that FS teeth contact with CS teeth at angular range of -18 to 8 degrees. The maximum contact stress occurs at open end of FS at about 12.5 degree (FS teeth is not lead relived or crowned in the analyses).

**Tooth Root Bending Stresses.** Figure 4 is contour lines of the maximum root bending stresses for every tooth. Abscissa and the ordinate of Fig. 4 are face width of FS teeth and circumferential angle of contact teeth, simply called circumferential angle here. Major axis of the WG is located at the 90 degree of the circumferential angle. From Fig. 4, it is found that the maximum root bending stress

occurs at the positions of the major axis (circumferential angle=90degree) and flexible bearing ball. It is also found that center positions of the contour lines are agreement with the positions of the flexible bearing balls. So, it can be said that the positions of the bearing balls exerts effects on tooth root stresses directly.

**Flexspline Structural Stresses.** Bending stresses of FS structure distributed along the generating line of FS is given in Fig. 5. In Fig. 5, abscissa is number of the points on the generating line. These numbers are used to stand for the positions of the points on the generating line and they are shown in Fig. 6. Ordinate of Fig. 5 is stress level. Five stress components (Von Mises, radial, circumferential, shearing and axial stresses) are given in Fig. 5. From Fig. 5, it is found that Point 4 has greater stresses. Circumferential distribution of the stresses at Point 4 is given in Fig. 7. From Fig. 7, it is found that Mises stresses at the major axis positions are almost the same level as the ones at the minor axis positions (circumferential angle=0 and 180degrees).

**Bearing ball Loads and Contact Stresses.** Loads and contact stresses distributed on bearing balls are given in Fig. 8. In Fig. 8, abscissa is number of balls. Since the ball of No.6 is located at the position of the major axis, positions of other balls can be known simply. There are two factors to produce ball loads, the one is elliptical deflection of the WG and the other is loaded torque. Loads resulted from these two factors are calculated and given in Fig. 8, respectively. It is found that the maximum ball load and contact stress for the new structure is about 5% less than the ones of the old structure. This decrease is resulted from structural deformation of flexspline. This new structure is designed to be deformed easier than the old one.

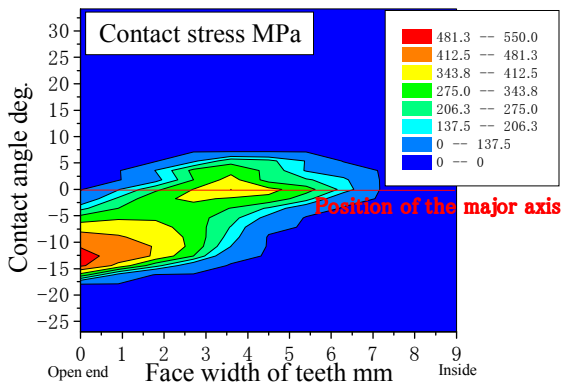


Fig.3 Contour lines of tooth contact stresses

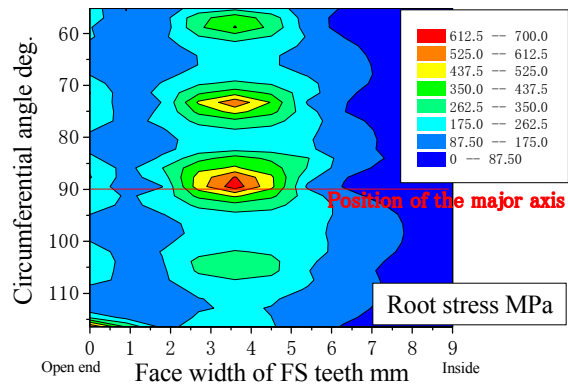


Fig.4 Contour lines of tooth root stresses

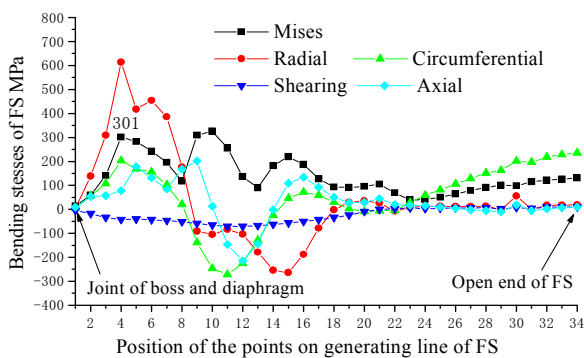


Fig.5 Stress distributed along the generating line of FS

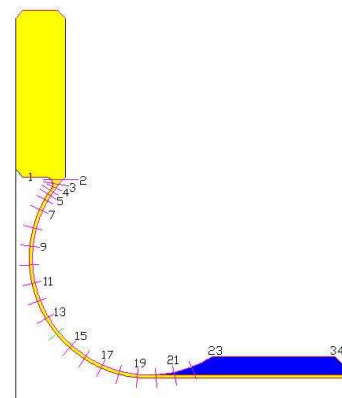


Fig.6 Tooth root bending stress

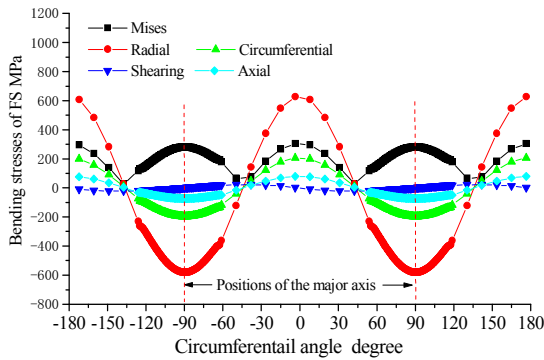


Fig.7 Stresses at Point 4

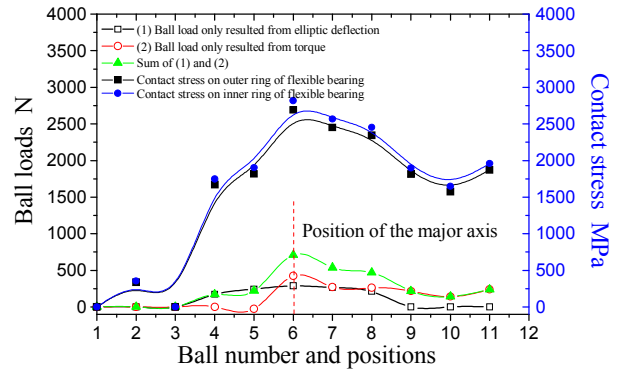


Fig.8 Loads and contact stresses on bearing balls

## Test Results

The following items are tested for the new HDD. (1) Basic performance (lost motion, backlash, transmission errors and torsional stiffness); (2) Static strength (tooth root breakage and bulking strength of the flexspline structure); (3) Fatigue strength (contact fatigue failures on tooth surfaces and bearing balls, bending fatigue failures at tooth roots and FS structure). It is found that except for bulking strength and transmission errors, the new HDD almost has the same performance and strength as the old one.

## Summary

A challenge to design a new silk type of HDD with arc-shaped FS structure is introduced in this paper. 3D-FEM is used to design the new HDD through performing loaded gear contact analyses and stress calculations. The new HDD is made through great efforts of other staffs. Performance and strength are tested for this new HDD. It is found that the new HDD can be designed as the same performance and strength levels as the conventional one.

## Acknowledgments

Thanks must be given to Mr. Joe Aubin and Mr. Fable Jim and other staffs in Harmonic Drive Technologies Inc, Boston, USA for their great efforts to make the new FS structure in 2005. Thanks must be also given to Prof. Yunwen Shen, Prof. Geng Liu and all the staffs in Machine Design Lab., Northwestern Polytechnical University for their advices in LGCA and strength calculations of HDD when the author worked there before 1994.

## References

- [1] C.W. Musser: Unite States Patent, No.2906143, Sept. 29, 1959
- [2] Y.W. Shen and Q.T. Ye: *Theory and Methods for Harmonic Drive Device Design* (China Machinery Press, Beijing 1985)
- [3] Shuting Li: European Patent EP1813836/United States Patent No.0060473
- [4] Shuting Li: Trans. ASME, J. Mech. Des., 124(3) (2002), p.511
- [5] Shuting Li: Mech. Mach. Theory. 43(9) (2008), p.1065
- [6] Shuting Li: Mech. Mach. Theory. 43(12) (2008), p.1157

## Study on Helical Tooth Profile Modification of Planetary Gear Transmission on the Basis of Gear Transmission Error

Tang Yu<sup>a</sup>, Chang Shan<sup>b</sup>, Wang Zhi-qiang<sup>c</sup>, Zhang Kun<sup>d</sup>

Harbin Marine Boiler & Turbine Research Institute, Harbin 150078, China

<sup>a</sup>heilj.t@163.com, <sup>b</sup>changshan703@163.com, <sup>c</sup>stu10@sina.com, <sup>d</sup>zhangkun19851027@163.com

**Keywords:** Planetary transmission, Gear transmission error, Modification curves, Reduce vibration and noise

**Abstract:** In order to minimize the fluctuation of gear transmission error (*GTE*) about the planetary gear transmission. A method was developed to deciding tooth profile modification curves of planetary transmission. According to the condition of the invariable design load, computing the dynamic characteristics of the planetary transmission system under modified and un-modified gear. At the same time, the compare is carried through of the dynamic characteristics for modified and un-modified gear. The results of the dynamic calculation indicate that the profile modification method can make the amplitudes of gear mesh stiffness change calmness and reduce the amplitudes of gear mesh stiffness by this method in paper. At last, the conclusion can be obtained that the tooth profile modification can reduce the vibration and noise of the planetary transmission system.

### Introduction

Dynamic characteristic of gear transmission is the important research content of the warship power transmission. Scholars have accepted and approved that the *GTE* is the predominant source of system excitation and via a complex transfer function produces vibration and noise in the power train system [1]. In order to reduce fluctuation of *GTE* in the process of gear transmission; the theory of tooth profile modification is applied to gear system. By tooth modification, the fluctuation of *GTE* is reduced to least. The tooth modification can improve the change of time-varying mesh stiffness during the gear mesh. In paper, the planetary transmission system is founded by the finite element method; the dynamics simulation is carried through of the un-modified planetary transmission system, and obtains the displacement of gear components. The parameters of the profile modification can be gained by the above analysis. The simulation is carried through of the modified gear system; the compare is executed of the dynamic response of modified and un-modified gear, the result proves the gear profile modification is an effective method to reduce the vibration and noise of the gear system.

### The Transmission Error of the Gear System

Gear transmission error (*TE*) is defined as the difference between the actual position of the output gear and the position it would occupy if the gear drive were perfect [2]. The difference is expressed with  $\text{sign}\Delta\theta$ , the  $\Delta\theta$  can be translated into displacement on the mesh action line, it is called the linear transmission error, and is expressed with *TE*. So the *TE* is expressed as the Eq. 1.

$$TE = r_{b2}\Delta\theta \quad (1)$$

Here  $r_{b2}$  is the driven gear base circle radius.

*TE* is a variable during the gear transmission. When *TE* is constant, the vibration of gear system will disappear. The objective of gear modification is to reduce the fluctuation of transmission error of the planetary transmission system, and control the fluctuation quantity to reach least.

In the mesh area of the gear transmission, the hypothesis is employed that the most value of *TE* is  $\Delta\theta_{i\max}$  during the mesh of the number *i* gear pair.  $\Delta\theta_i$  is a *TE* on the random mesh point during the gear mesh. In the course of mesh, the fluctuation quantity of *TE* is Eq.2.

$$\Delta_i = \Delta\theta_{i_{\max}} - \Delta\theta_i = \frac{TE_{i_{\max}} - TE_i}{r_{b2}} \quad (2)$$

The linear  $TE$  of the random mesh point should equal to synthesis deformation  $\delta_i$  of the gear tooth of the standard assembly for theory involutes gear transmission i.e. the summation of the deformation on the mesh line for the drive and driven gears. Eq. 3 can be obtained on the basis of the Eq. 2.

$$\Delta_i = \frac{TE_{i_{\max}} - \delta_i}{r_{b2}} \quad (3)$$

The summation of modification quantity is  $E_i$  on the mesh line for the drive and driven gears for the random mesh point of the number  $i$  mesh tooth profile after the modified gears. The  $E_i$  is called gear tooth synthesize modification quantity. At the same position, the gear tooth synthesize deformation is  $\delta_i$ . After the gears are modified, the fluctuation quantity of  $TE$  can be express with underside Eq. 4.

$$\Delta_i = \frac{TE_{i_{\max}} - (\delta_i + E_i)}{r_{b2}} \quad (4)$$

In order to achieve to reduce vibration of gear system to the modified gears, the fluctuation value of  $TE$  equal to zero for the random mesh course of gear pair. The Eq. 5 can be gained.

$$TE_{\max} = \delta_i + E_i = \text{constant} \quad (5)$$

### Make Certain Modification Curve of Gear Tooth Profile

The assumption is done that the tooth system runs under the constant load, the most linear transmission error ( $TE_{\max}$ ) is ensured firstly. In paper, the  $TE_{\max}$  is ensured by the finite element method. The  $TE_{\max}$  will present to input-mesh and output-mesh position of gear pair on the basis of literature [4]. It can be expressed with Eq. 6.

$$TE_{\max} = \max \{ \delta_i \} \quad (6)$$

In paper, the geometry parameter of the planetary transmission is listed table 1.

Table 1 Geometry parameter of gear transmission

|                          | Sun                   | Pinion | Ring |
|--------------------------|-----------------------|--------|------|
| Tooth number             | 27                    | 35     | 99   |
| Press angle (°)          | 20°                   |        |      |
| Modulus (mm)             | 3                     |        |      |
| Helix angle (°)          | 26°                   |        |      |
| Tooth face width (mm)    | 25                    |        |      |
| Input torsion (N·mm)     | 1.83×10 <sup>6</sup>  |        |      |
| Input rotate speed (RPM) | 1.623×10 <sup>3</sup> |        |      |

The sun is an input gear, the ring is fixed and the carrier is an output component. The synthesis deformation quantity  $\delta_i$  is periodically variation on the mesh action line between mesh gears before the gears are modified on the basis of the calculation of the finite element method.

In the fig. 1, the  $TE_{max}$  equal to 0.07695 (mm) in the course of gears mesh for sun and pinion, and the  $TE_{max}$  equal to 0.07421 (mm) in the course of gears mesh for ring and pinion. The  $TE_{max}$  is a steady value when the gear system runs steadily. The synthesis modification quantity is computed by Eq. 5. The curve figure of the synthesis modification quantity is showed as the fig. 2.

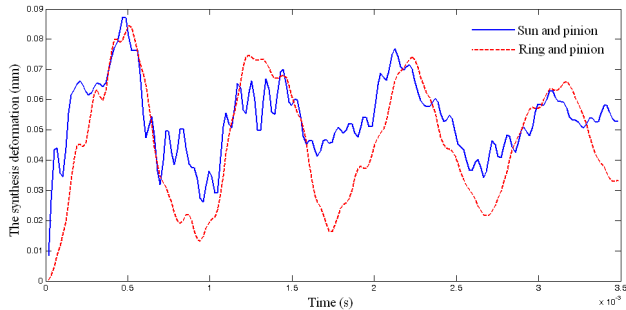


Fig.1 The synthesis deformation of gear on the mesh line

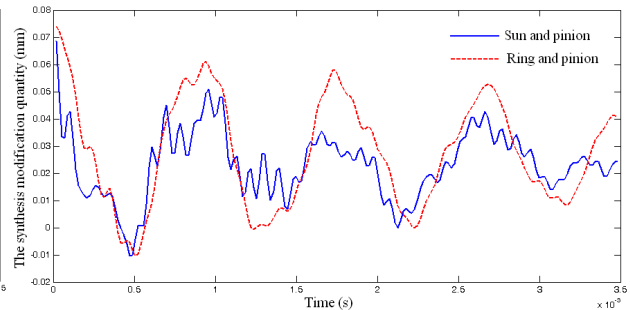


Fig.2 The synthesis modification quantity of gear on the mesh line

When the  $TE_{max}$  curve is made sure, the modification curve of single gear profile will be ascertained on the mesh action line too. The literature [3] thinks that the  $TE_{max}$  is distributed averagely to the drive and driven gears of mesh gears on the mesh action line is feasible. The tooth is modified only at the input-mesh and output-mesh position. The modification quantity curve of the normal direction can be showed as the fig. 3, fig. 4, fig. 5.

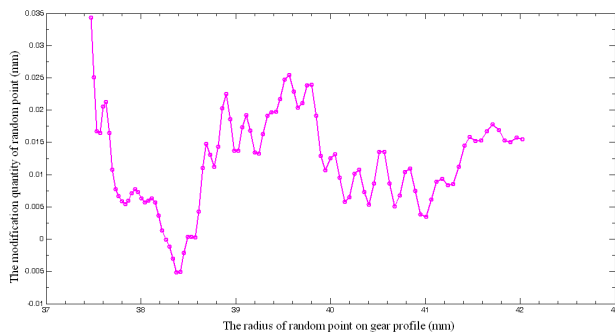


Fig.3 The modification quantity of sun gear profile of normal direction

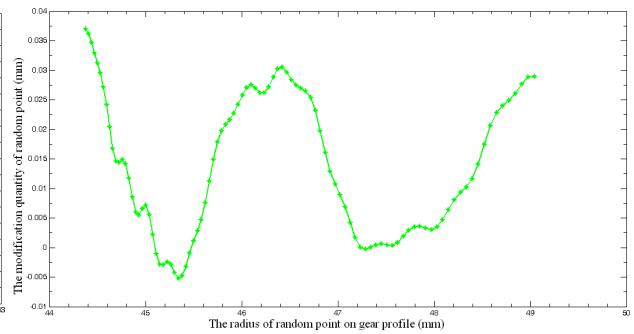


Fig.4 The modification quantity of pinion gear profile of normal direction

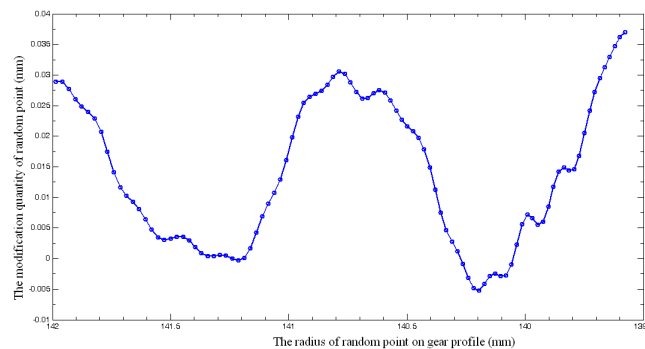


Fig.5 The modification quantity of ring gear profile of normal direction

### The Characteristic Analyze of Planetary Transmission System

In paper, the dynamic characteristic is compared of modified and un-modified gear about the upper example. The response of modified gears can be obtained by the simulation calculation.

The mesh stiffness curve of mesh gears can be gained by calculation. The synthesis mesh stiffness is carried through the Fourier Transform ( $FFT$ ) in the frequency filed to convenient for compare. The frequency response is showed as the fig.6, fig.7.

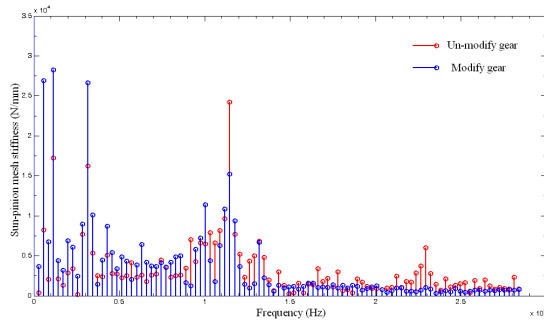


Fig.6 The synthesis mesh stiffness between sun gear and pinion gear

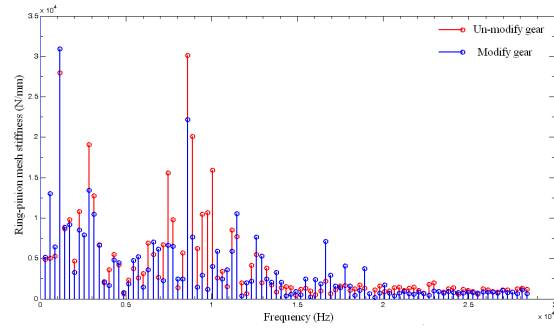


Fig.7 The synthesis mesh stiffness between ring gear and pinion gear

The amplitudes of the synthesis mesh stiffness will be reduced after the gears are modified from fig.6, fig.7, and the change of mesh stiffness becomes calm down. So the gear modification is effective to reduce vibration and noise of gears system.

### Conclusion

The fluctuation can induce vibration and noise of gear transmission system; the synthesis modification curve of gear profile is obtained on the base of the constant of transmission error. The modification can reduce observably the fluctuation of *GTE*. So the gear modification can reduce vibration and noise of gear transmission system.

### References

- [1] J. Peeters, D. Vandepitte and P. Sas: Wind Energy (2006), p. 141
- [2] J.D. Smith: Gear noise and vibration, 2nd edition (2003)
- [3] Y.H. Sun and C. Zhang: Journal of Tientsin University (2001), p. 214

## Optimization Procedure for Complete Planetary Gearboxes with Torque, Weight, Costs and Dimensional Restrictions

Ulrich Kissling<sup>1,a</sup>, Inho Bae<sup>1,b</sup>

<sup>1</sup>KISSsoft AG, Uetzikon 4, 8634 Hombrechtikon, Switzerland

<sup>a</sup>ulrich.kissling@kisssoft.ch, <sup>b</sup>inho.bae@kisssoft.ch

**Keywords:** Micro Planetary Gearbox, Wind Turbine Gearbox, Gearbox Design, Optimization, Weight Reduction, Manufacturing Cost, Dimensional Restrictions.

**Abstract.** In a gear box design, it is quite difficult for a designer to quickly find an optimum solution, while the space restriction is given and the weight is to be minimized. Also the manufacturing cost, total power loss and other relevant factors have to be considered. Solving such a problem is very time-consuming, if different variants of reducers have to be evaluated carefully. A new optimization tool, based on KISSsys software, permits to layout automatically a complete gearbox using functions for the layout of gear stages, shaft dimensions and bearings, if the required torque capacity, life time, safety factors and the total ratio are given. This tool is used to generate a complete set of different variants of gear reducers. The main results are displayed in 3D graphics, showing weight, costs and efficiency of the different variants. Another graph shows the casing dimensions of the variants in three dimensions in order to check the compliance with space restriction. The use of this tool in two typical engineering applications gives very good results; the potential for weight reduction is higher than expected, going up to 30%. Manufacturing price reduction is even higher, going up to 50%.

### Introduction

A gearbox design, for example a planetary gearbox design with the total reduction ratio of 60:1, is quite difficult for a designer to quickly find an optimum solution, when the maximum space restrictions are given and the weight is to be minimized, and even the manufacturing costs, total power loss and other relevant factors have to be considered. Is it better in such a case to design a two-stage reducer, with relatively high reduction per stage, or a three stage reducer?

Solving such a problem is very time-consuming, because a large number of different variants have to be evaluated carefully. A new optimization tool, based on KISSsys software, permits to layout automatically a complete gearbox using the layout functions of gear-stages, shaft dimensions and bearings from the given torque capacity, life time, safety factors and total ratio. The casing and the planet carrier is also automatically dimensioned, and the gross manufacturing price is calculated based on per kg-prices for gears, shafts, planet shafts, carrier and bearings.

In the first step, the number of gear stages is defined. If the number of stages is not clearly defined, variants with different number of stages are checked. Furthermore the distributions of the reductions  $i_{\text{stage}}$  over the individual stages can be different and should be checked with different variants. Other parameters giving big influence on size and weight of reducers are the face width to center distance ( $b/a$ ) and the face width to reference diameter ( $b/d$ ) ratio; therefore also these parameters are varied. The automatic optimization procedure then generates the gearbox variants for a given output torque and total ratio, depending on the required variation range of parameters ( $b/a$ ,  $i_{\text{stage}}$ ) and the number of stages, each with its weight, efficiency, dimensions and costs. The main results are displayed in 3D graphics showing weight, costs and efficiency of all the variants. Another graph shows the casing dimensions of the variants in three dimensions for checking the compliance with external space restrictions. Furthermore, Excel compatible tables are produced with details for additional analysis of the results.

### A ‘Gearbox-Variant-Generator’ based on KISSsys

In the calculation software KISSsoft [1], a tool for the optimization of gear stages (pairs of gears and planetary stages) called ‘Fine-Sizing-Routine’ was developed already in 1987 [2]. Now, this function became one of the most powerful features in KISSsoft. Based on a user-defined range of parameters (module, helix angle, etc.) the software presents a large number of possible solutions covering the full parameter space and presents a list with many data (geometry, safeties, characteristics as sliding, losses, price, transmission error) including a qualification of every solution based on required characteristics. So the user can investigate all the near-best solutions and then select the optimal variant, which best fits his needs. In order to assist the engineer during this task, the program offers filter and sorting functions. KISSsoft was the first professional gear software worldwide proposing such a concept [2]. When the ‘Fine-Sizing-Routine’ was first developed, it was impossible to imagine a similar feature for the layout of complete gearboxes. But with the evolution of the computing power of today, the more powerful tools have been developed. KISSsys [1, 4] is such software available since 2000 for the calculation of complete power transmissions. The KISSsys software combines kinematic analysis, lifetime calculation, 3D graphics and user defined tables / dialogues with a programming language (Fig. 1). Due to its flexibility, it is the tool of choice for strength and lifetime analysis of various kinds of drive trains and gearboxes.

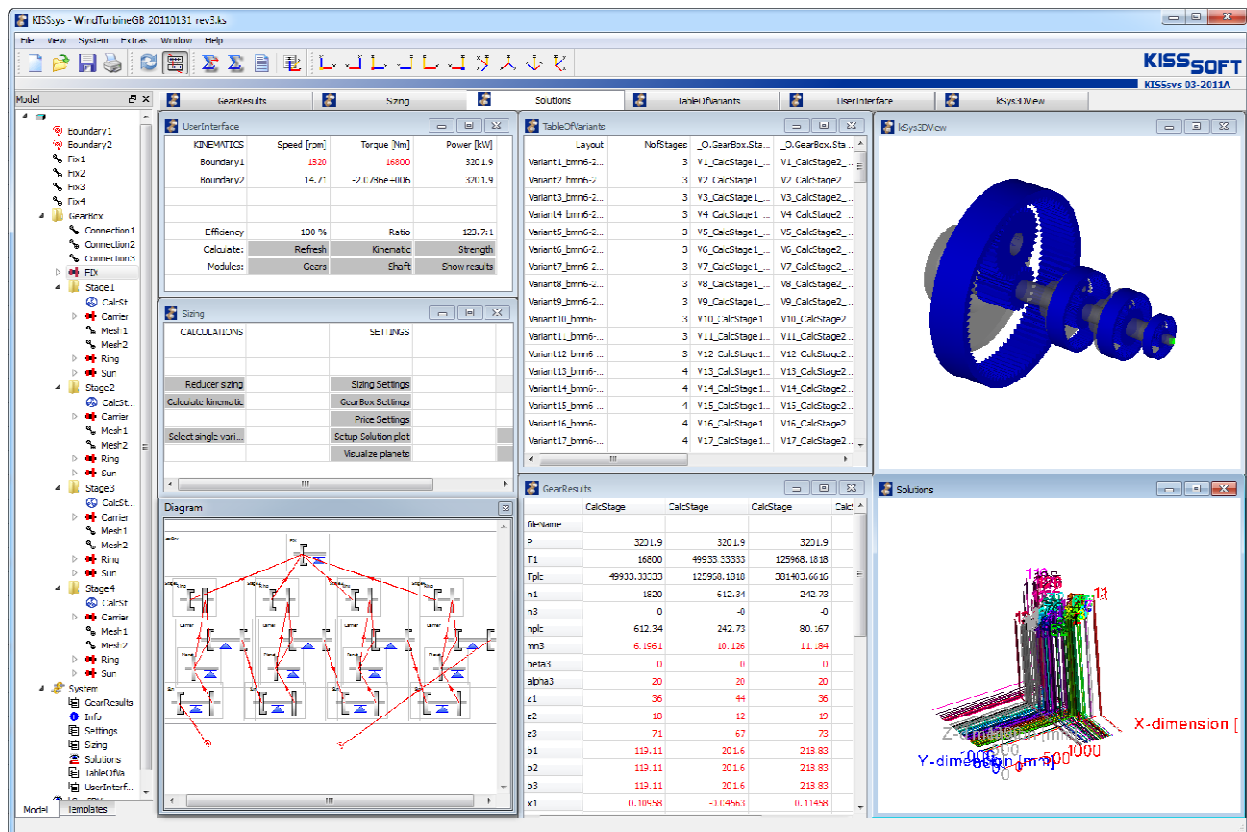


Fig. 1. KISSsys windows of the Gearbox-Variant-Generator

User Interface: Provides for input of required torque and speed

Sizing: Includes the various sizing functions and functions for user data input

Table of Variants: List of the different reducers, of which any solution can be selected

Solutions: 3D display of main results for the 90 reducer variants calculated

### Optimization of a Compact Micro-Planetary-Gearbox

The tool was used in a project for a Chinese company, producing small compact gear reducers with a high speed reduction. Such reducers, having an outer diameter of 50 mm and less are called as Micro-Planetary-Gearboxes. Normally the ring gear is the housing of these reducers, and all the stages must have the same ring gear geometry to simplify the manufacturing process (cutting the inner gear

tooth form with a needle out of a steel tube). The design data for one of the required gearbox was: Output speed 31 rpm and 16 Nm torque. On the input side, a 50 W with 5000 rpm motor should be used. Therefore, the required total reduction is  $i = 160$ . Since a single planetary stage has normally a reduction between 2.5 to 7.0, the reducer can be built as a 3-, 4- or 5-stage-reducer. There are many possibilities how the total reduction is distributed over each planetary stage.

The tool proposes in the first step different possibilities for the ratio distribution over the stages (Fig.2). The proposal can be easily modified by the project engineer. The user can request a special design to share the same ring gear for all stages. Additionally other design parameters can be varied, for example the b/a ratio. Then all the different gear reducers are automatically designed for the required torque, and then the weight and manufacturing price are calculated. In this example, 42 reduction ratio variants combined with 4 different b/a ratio results in 168 different reducers. All the solution can be visualized and in 3D graphics with showing the different characteristics. As shown in Fig. 2, the 5-stage solutions are the most economic.

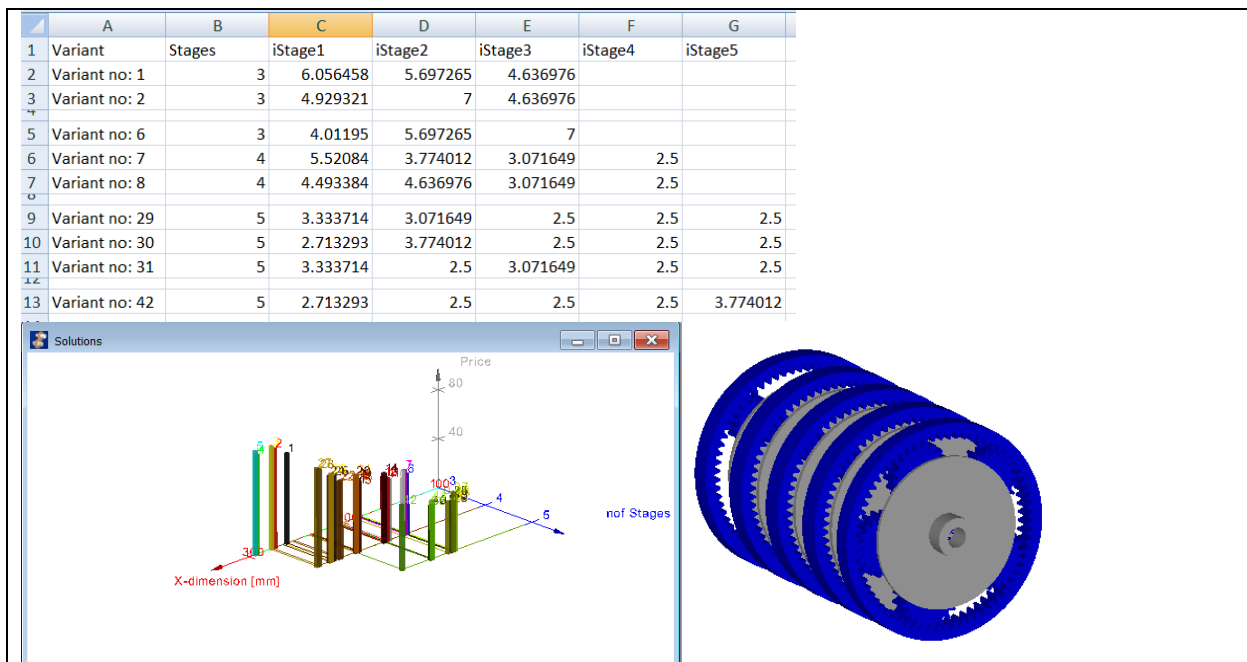


Fig. 2. Micro-Planetary-Gearbox with common outer ring (Analyzing 168 different reducer-variants)

Above: Proposed stages and ratio variants.

Below: Manufacturing prices of the different reducers (left), 3D-model of the selected variant (right)

### Optimization of a 3-MW Wind Turbine Gearbox

One of the most important criteria in wind turbine design is weight reduction. Normally lower weight of the gearbox is even more important than lower manufacturing cost, because when the reducer is lighter, this reduces the cabin and tower construction costs. The wind turbine gearbox can have various configurations, and we decided to design a 3- or 4-stage planetary gearbox with no restriction on the ring gear geometry. The design data for the gearbox was: Input speed 15 rpm and output power 3.2 MW. The required total gear ratio is  $i = 120$  (speed increaser). The number of planets of all the stages is set to 3 to simplify the design.

The tool proposes 153 different gearboxes from 51 ratio variants combined with 3 different b/a-ratio from 0.3 to 0.7 with the step of 0.2. Fig. 3 shows the minimum and the maximum priced variants for each b/a ratio. The average prices of the 3- and 4-stage gearboxes are  $1.51 \times 10^5$  and  $1.73 \times 10^5$ , and have less than 13% of difference. However, it is surprising that the difference of the minimum and the maximum prices is over 4 times ( $1.05 \times 10^5$  and  $4.44 \times 10^5$ ) with the similar level of safeties. In addition, it should be noted that the minimum price gearbox was found in 4-stage variants, not in 3-stage. Thus, the proper selection of the design is most important to reduce the gearbox price, and it's inevitable to use the tool in order to achieve the optimal gearbox design.

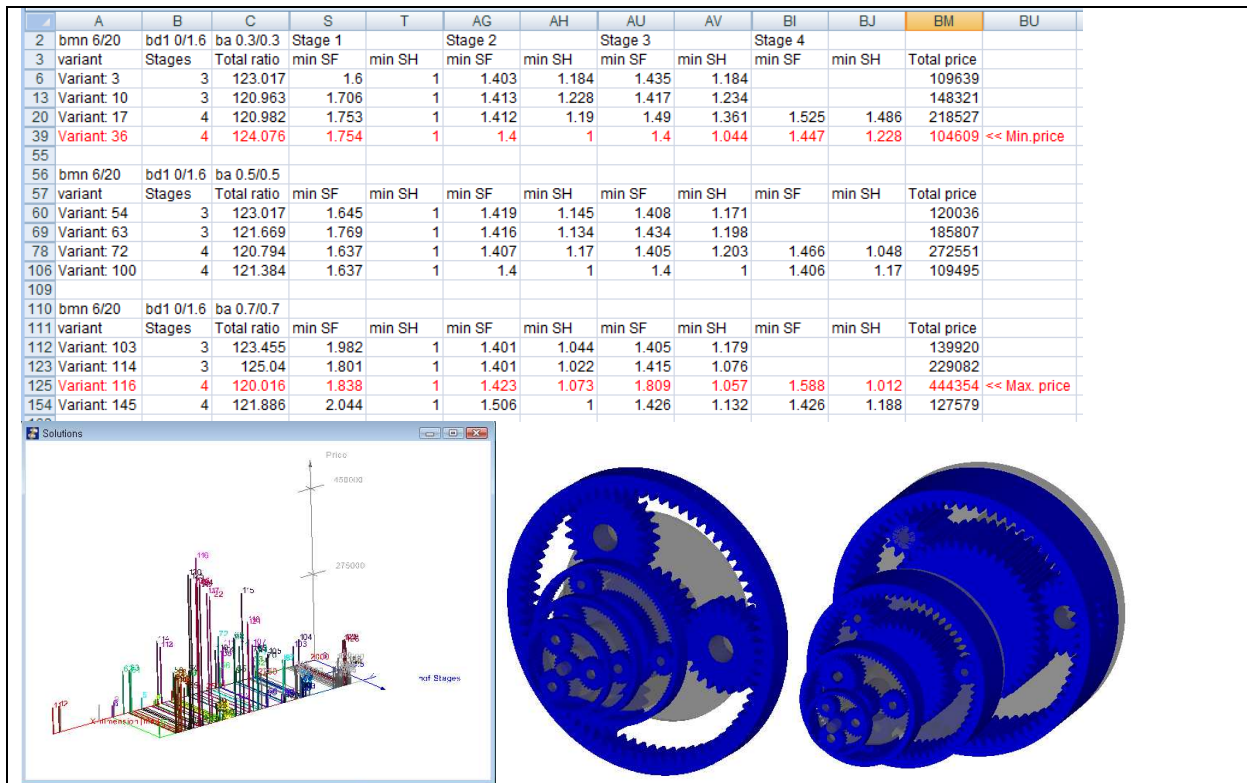


Fig. 3. Wind turbine gearbox variants

Above: Gearbox variants with minimum and maximum masses.

Below: Price of the gearboxes (left), 3D-models of the minimum(center) and maximum prices (right)

## Conclusions

A new tool, a Planetary-Variant-Generator permits an arbitrary number of completely defined planetary gearbox variants to be created automatically using functions for the layout of gear-stages, shaft dimensions, bearings and planet carrier; given the required torque capacity, life requirement, safety factors and the total ratio. As specified by the user, gearbox variants with different number of stages and different distribution of the ratios over the stages are calculated. The results such as weight, power loss, manufacturing price, torque capacity can be visualized in 3D-diagrams, in which the numbered variants are displayed. Thus the user can review the best proposition, but he can also see all the near-best solutions and then select the optimal variant, the one that best fits his needs.

The use of this tool in two typical engineering applications gives very good results; the potential for weight reduction is higher than expected, going up to 30%. Manufacturing price reduction is even higher, going up to 50%. This product will be enhanced with some additional features and be available for general use.

## References

- [1] <http://www.kisssoft.ch/english/products/>
- [2] U. Kissling: Konzept für die effiziente Auslegung und Optimierung von Planetengetrieben nach verschiedenen Kriterien (VDI-Berichte Nr.1460, VDI-Verlag, Germany, 1999).
- [3] U. Kissling: Entwurf von Getrieben in engen räumlichen Randbedingungen mit gleichzeitiger Herstellkosten-Schätzung (SimPEP Kongress 2007, Würzburg, 2007).
- [4] U. Kissling: Automatic Optimization Procedure of a complete Gearbox for Weight, Efficiency, Costs and Dimensional Restrictions (Int. Gear Conference, Munich, 2010).
- [5] T. H. Chong, I. Bae and G. J. Park: Mechanism and Machine Theory, Vol. 37 (2002), p 295

## Analysis System of Marine Planetary Gear Trains

LIU Geng<sup>1, a</sup>, CHANG Shan<sup>2, b</sup>, WU Liyan<sup>1, c</sup> and LI Yingsheng<sup>2, d</sup>

<sup>1</sup>School of Mechanical Engineering, Northwestern Polytechnical University, Xi'an, China

<sup>2</sup>703th Research Institute of China Shipbuilding Corporation, Harbin, China

<sup>a</sup>npuliug@nwpu.edu.cn, <sup>b</sup>changshan1@163.com, <sup>c</sup>wuliyan@nwpu.edu.cn, <sup>d</sup>lys703-35@126.com

**Keywords:** analysis system, performance simulation, marine planetary gear train

**Abstract.** Planetary gear train (PGT) with herringbone gears is one of typical transmission styles used in marine power transmission. How to effectively design a PGT with lighter structures and lower vibration and noise is a fatal task for heavily loaded marine gearing. An analysis system which was developed in the past decades is introduced in this paper to simulate the performance of planetary herringbone gear trains. The effects of main crucial parameters on the static and dynamic characteristics of planetary herringbone gear trains are studied by using the analysis system. The results are discussed and show that the presented system is effective and can be used in design of planetary herringbone gear trains.

### Introduction

Planetary gear train (PGT), including power-split PGT, has been widely applied in industry. Many works have been done on simulating the performance of PGT. These researches were mainly focused on the PGT with spur gears <sup>[1-2]</sup> or helical gears <sup>[3-5]</sup>. But for marine power transmission, PGT with herringbone gears (HPGT) is more applicable because of its heavily loaded working circumstance. Establishing an effective analysis system is a crucial issue in design of marine planetary herringbone gear trains with lighter structures and lower vibration and noise.

An analysis system is introduced in this paper for analyzing static and dynamic characteristics of marine planetary herringbone gear trains. Some crucial factors, like gravity, random distribution of manufacturing errors and coupling influence between two stages, are studied and discussed.

### Analysis System

The schematic diagram of the analysis system is shown in Fig.1.

**Classical formulas based analyses.** After inputting the basic parameters and transmission type of marine PGT, the load capacity, stiffness and stresses of all typical components, including gears, carriers, shafts and couplings, can be calculated by the classical formulas.

**FEM based static and dynamic analyses. Parametric Modeling.** A set of parameters are designed to control the geometries and structures of HPGT gears and parts. Three-dimensional models of the HPGT gears and parts then can be easily generated by inputting rational parameters. CAE works of the gear trains can be flexibly carried out by using these models, such as the FE analyses, structural optimizations, *et al.*.

**Three Dimensional Optimization Modifications.** According to different purpose, different gear modification means of HPGT can be selected, including tooth flank modification, tooth axial modification and 3-D optimization modification.

*Tooth Static Load Analysis.* The mesh stiffness, load distributions along different contact lines and load sharing ratio on different teeth in one engagement position are computed based on linear programming technique.

*Dynamic Analyses of Gear System.* Lumped mass models for the dynamic analysis of gear systems of herringbone gear trains are established. The influences of main crucial factors in marine herringbone gear trains, such as film stiffness of journal bearing, gravity, random distribution of manufacturing errors, coupling influence between two stages, et al., are taken into consideration.

*Stiffness and Strength Analysis.* Static and dynamic stiffness and stresses of gears and gear train parts are computed in this module. The means for calculating the steady-state displacement and stress responses of gear structures and gear train parts by commercial software is developed.

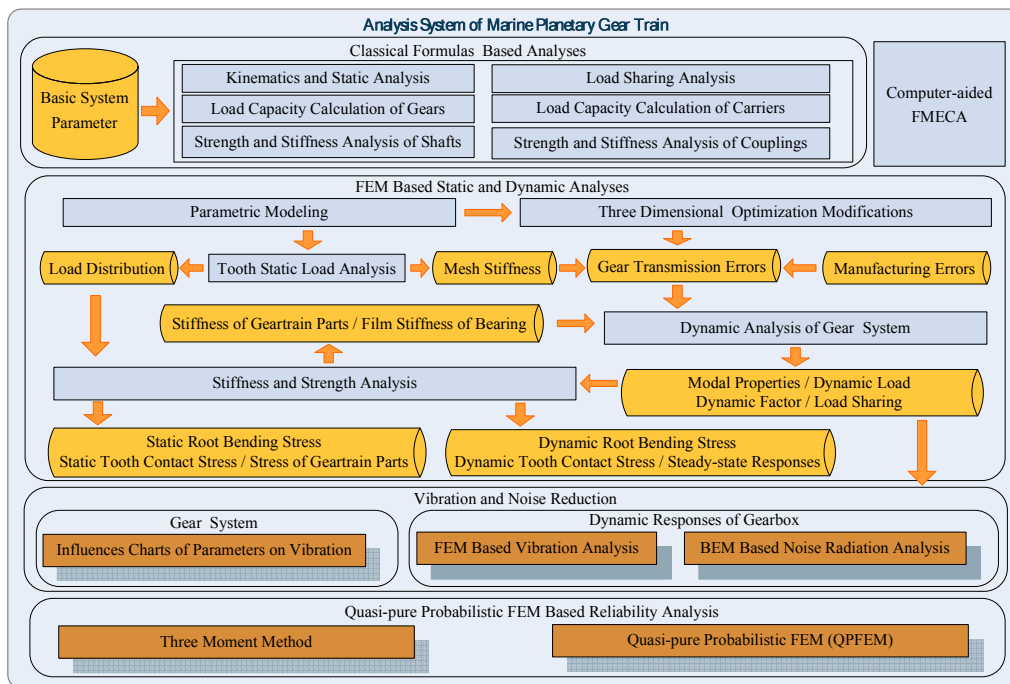


Fig.1 The schematic diagram of the analysis system

**Vibration and noise reduction.** *Influence Charts of Parameters on Vibration.* Based on the analysis of one gear pair<sup>[6]</sup>, the general concept of the vibration chart is presented. Integrated with dynamic analyses of gear system, the influence of main parameters on vibration can be drawn in chart forms.

*FEM Based Vibration Analysis of Gearbox.* The dynamic response of gearbox is calculated by using FEM with spring element to simulate the vibration isolators. The time history of the vibration acceleration and the noise spectrums are obtained by using FEM.

*BEM Based Noise Radiation Analysis of Gearbox.* Taking the vertical vibration acceleration of gearbox as boundary condition, the noise radiation of the gearbox structure is analyzed by using BEM. The contributions of path, modal and panel to the noise radiation at a specified field point are gained simultaneously.

**Quasi-pure Probabilistic FEM based Reliability Analysis.** *Three Moment Method.* This method considers not only the means and variances of random variables, but also the influence of skewness of probabilistic distribution of the variables. The experiments showed that the method can greatly increase the precision of reliability analysis.

*Quasi-pure Probabilistic FEM.* Based on the three moment method, the basic theory and calculation procedure of quasi-pure probabilistic FEM is derived and implemented to increase the speed and accuracy of the reliability analysis of complex structures.

**Computer-aided FMECA.** Based on the typical failure and knowledge management theory, the computer-aided Failure Mode Effects and Criticality Analysis (FMECA) for marine power transmission is developed.

**Results and Discussion**

*The parametric models of HPGT.* The parametric model of a herringbone gear is shown in Fig.2. The assembly model of the power-split HPGT is shown in Fig.3. This virtual prototype can achieve the virtual assembling and movement.

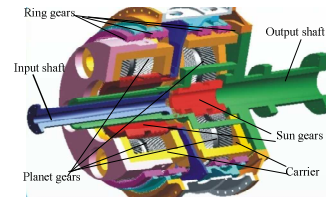
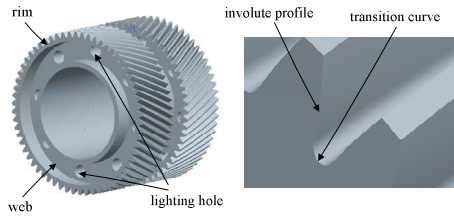
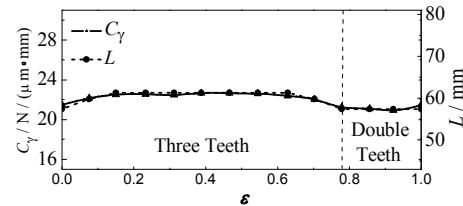
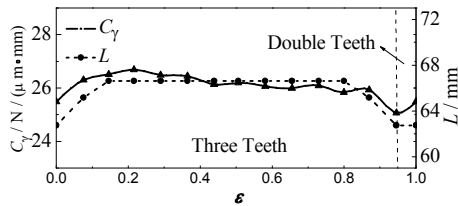


Fig.2 The model of a herringbone gear

Fig.3 The virtual prototype of a power-split HPGT

*The mesh stiffness analysis.* The influences of the structural sizes and basic parameters on mesh stiffness of herringbone gear pair are studied, including rim, web, lighting holes, helical angle, *et al.*. The comparison of mesh stiffness and contact length of gears is shown in Fig.4. The results show that the sum length of all contact lines in one engagement position is the most significant factor to affect the mesh stiffness of the position. The mesh stiffness decreases slightly when the tooth comes into or exits the engagement.



(a) The external gear pair

(b) The internal gear pair

Fig.4 The mesh stiffness and contact length of helical gears

*Dynamic responses of power-split HPGT.* It can be seen from Fig.5 that when the random distribution of manufacturing errors is introduced, the dynamic forces at different meshing cycles are different. It fits more real working situation of the HPGT. The dynamic load factors with different input speeds of the sun-planet pair in encased stage are shown in Fig.6. There are several potential resonance frequencies in the planetary gear train.

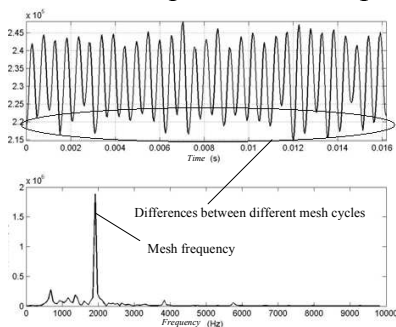


Fig. 5 The dynamic force

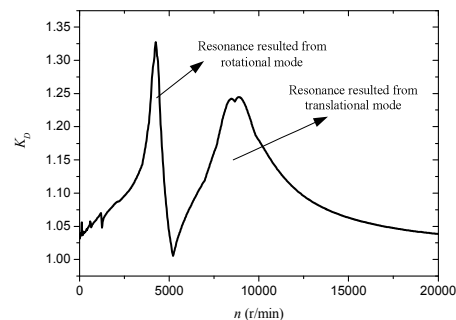


Fig.6 The dynamic load factor

*Influence of modification on dynamic response.* Table 1 gives the dynamic load factor and vibration accelerations with different modification means. The tooth frank and 3-D modifications can decrease the vibration accelerations distinctly. The decreased ratio of dynamic load factor is less than 5% after the tooth axial modification due to the high contact ratio of herringbone gears.

Table 1 The dynamic load factor and vibration accelerations with different modification

| Modification means | Dynamic load factor | Ratio  | Vibration accelerations | Ratio   |
|--------------------|---------------------|--------|-------------------------|---------|
| None               | 1.2414              | -      | 21.1015                 | -       |
| Tooth frank        | 1.1949              | -3.72% | 17.9401                 | -14.98% |
| Tooth axial        | 1.2284              | -1.02% | 20.2916                 | -3.84%  |
| 3-D modification   | 1.1840              | -4.60% | 17.0471                 | -19.21% |

*Influence charts.* Fig. 7 shows the influences of input speed and the bending stiffness of input shaft on input bearing vibration. Fig. 8 is the influence charts of mass ratio and input speed on dynamic load factor.

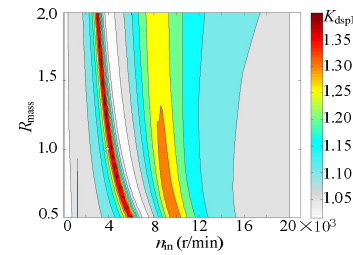
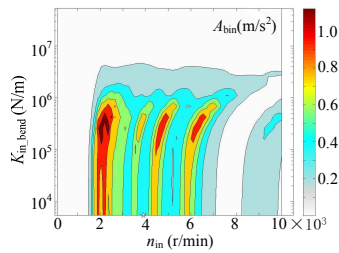


Fig.7 Influence chart of input shaft bending stiffness      Fig.8 Influence chart of mass ratio

*Acoustic analysis of the gear box.* Three models of the gear box, including assembly, FEM and BEM models, are shown in Fig.9 respectively. To apply the load more conveniently, the coupling is defined between the nodes of the output shaft bearings and holes of the planet gear axis. The effects of the coating layer thickness of damping material, the amounts of ribs, and the wall thickness on the noise radiation are studied to optimize the structure size and local material.

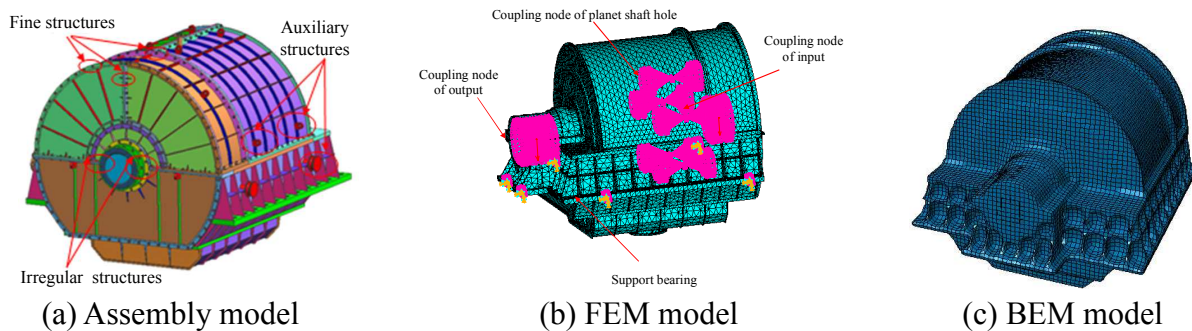


Fig.9 Three models of gear box for power-split HPGT.

## Conclusions

An analysis system of marine planetary gear train is developed in this paper. The system includes classical formulas based analyses, FEM based analysis, vibration and noise reduction, quasi-pure probabilistic FEM based reliability analysis and computer-aided FMECA. The effectiveness of the system has been demonstrated by performance simulation for power-split HPGT. The analysis system can be used for innovation design of marine planetary gear trains.

## References

- [1] J. Lin and R. G. Parker. Journal of Vibration and Acoustics Vol.121-7 (1999), p.316.
- [2] J. Lin and R. G. Parker. Journal of Sound and Vibration, Vol.233-5 (2000), p.921.
- [3] A. Kahraman. Journal of Mechanical Design Vol.116 (1994), p.713.
- [4] A. Saada and P. Velez. Journal of Mechanical Design Vol.117-6 (1995), p.241.
- [5] T. Eritenel, R. G. Parker. Journal of Sound and Vibration Vol.325 (2009), p.397.
- [6] K. Umezawa, T. Sato and K. Kohna. The Japan Society of Mechanical Engineers Vol.27-225 (1984) p.569, Vol.28-243 (1985), p.2143, Vol.28-246 (1985), p.3018.

# Application Probing of Advanced Helicopter Transmission System Technology

Wenqiang Ding<sup>1,a</sup>

<sup>1</sup>China Aviation Powerplant Research Institute, Zhuzhou, Hunan, 412002, China

<sup>a</sup>www.wl@yeah.net

**Keywords:** helicopter transmission system; design train of thought; component structure

**Abstract.** This paper performs analyses and studies to a part of the foreign advanced helicopter transmission system technology. It introduces the design train of thought, main component structures and relevant parameters. It will give a reference to engineering technical personnel of the helicopter transmission system.

## Introduction

Transmission system is one of three key dynamic components of helicopter. The requirements of helicopter are higher and higher in the world, such as the reliability, security, economy, comfort ability, environment ability and so on. The requirements of transmission system are also getting higher, for instance light weight, long life, high TBO(Time Between Overhaul), high survivability and low noise. The investment and research percentage of transmission system are also increased by every helicopter company in the world. Therefore the new technique of the helicopter transmission system is appearing time and again. Now we are performing analysis and application probing of a part of advanced helicopter transmission system technique on the world.

## The Circular Arc Gear Technique

The circular arc gear transmission could be divided into single and double circular arc gear transmission.

**The Single Circular Arc Gear.** The single circular arc gear is called into Novikov gear or W-N gear (Wildhaber-Novikov) or conformal gearing. Its engagement transmission is performed by the contact of concave and convex gear surface. The pinion is convex gear and the driven gear is concave gear, shown as Fig. 1. The engagement transmission of involute gear is contact by convex gear and convex gear. Its stress is larger than the circular arc gear on unit area, shown as Fig. 2 and Fig. 3. There are many advantages which the circular arc gears compared with the involute gears, so it has been successfully used in the helicopter transmission system. For example, the Lynx helicopter main gearbox that used the circular arc gear which is made by Westland Helicopter Company and Ka-type helicopter main gearbox that used the circular arc gear which is made by Russia Helicopter Company.

The Lynx helicopter main gearbox is the earliest application of the single circular arc gear in the world. According to Chief engineer D. Berrington introduction of the Westland Helicopter Company, "In order to ensure safety and reliability of the whole helicopter, we applied the single circular arc gears on the Lynx helicopter main gearbox. By means of several gears studies to circular arc gears, Westland Helicopter Company has matured design technology and manufactures

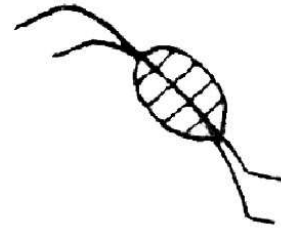
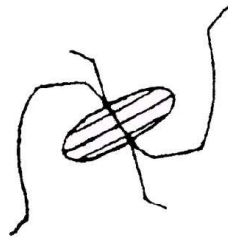
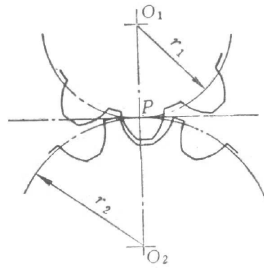


Fig.1 Single circular arc gears    Fig.2 Involute gear stress    Fig.3 Circular arc gear stress

experience of circular arc gears which can ensure the helicopter safety for flight. After the application the circular arc gears on the helicopter main gearbox, the advantage is that it is simple to main gearbox drive construction and reduction the part numbers. On the other hand, it can reduce the height of the main gearbox. It compare with application planet system on the main gearbox which can be reduced the height about 250mm. Therefore, it can increase reliability and maintenance and reduce the weight of main gearbox.

From the text above, there are main advantages after application the single circular arc gears on the Lynx main gearbox as follows:

(1) The single drive ratio could be very large if main gearbox is used the circular arc gears. The gear numbers could be one. In the theory speaking, there are not limit situation on the minimized tooth numbers. But taking into account reducing weight and gear's strength and rigidity, the gear ratio couldn't have not limit. The single circular arc gear ratio could be larger to 1:9, and the Lynx main gearbox single stage gear ratio is only chosen 1:7.

(2) The Lynx main gearbox (MGB) drive stage number only has two stages. It can reduce the part numbers. The Lynx MGB are compared with "Seaking" MGB, the drive part number reduced to 40 percent, shown as Table 1.

Table 1 Comparison with Seaking MGB and Lynx MGB

| Item         | Helicopter | "Seaking" MGB | "Lynx" MGB |
|--------------|------------|---------------|------------|
| Component No |            | 44            | 26         |
| Gear No      |            | 16            | 7          |
| Bearing No   |            | 28            | 19         |
| Total        |            | 88            | 52         |

(3) The circular arc gear engagement is very stable, only has small period dynamic loads. At the same time, it's easy to form elastic fluid oil film. Therefore the gears are not easy to appear failures of spall and scoring.

(4) The gear surface has higher loads capability due to the circular arc gear having very large radius of equivalent curvature. The single circular arc gear form is adopted in the Lynx main gearbox, and the gear surface has high hardness (HRC58) after carburized and quench. The capacity of circular arc gear surface has greatly increased comparing with soft gear surface (HRC35).

(5) After application the circular arc gear should take into account the forces composed in order to reduce loads of bearing and houses, so as to increase the life of bearings and houses. Parallel shaft drive should be adopted among the combined gears. It could reduce the radial forces, shown as Fig.4.

(6) The spiral direction of combined gear is right hand, when it transfers the power could make the axial forces go down. It is opposite with main rotor thrust direction, so that it could reduce the loads of main rotor shaft ball bearings within the most operation time. Therefore it could increase and extend the application life of the main rotor shaft ball bearings.



(5) Just because of the merits of face gear transmission as described above, many universities and enterprises in China carried out related researches also. They established the method of calculation of contact strength, bending strength and scoring strength. There are some enterprises are now doing researches on teeth grinding machine for face gears. All these have laid the good foundations for the application and extension of face gear in China.

Table 2 Comparison of spiral level gear and face gear

|               | Spiral Level Gear | Face Gear        |
|---------------|-------------------|------------------|
| Spilt-torque- | no merits         | having merits    |
| Weight        | heavy             | light            |
| Noise         | high              | low              |
| Cost          | high              | low              |
| Reliability   | high              | high             |
| Axial force   | large             | small(pinion no) |
| Bearing life  | short             | long             |

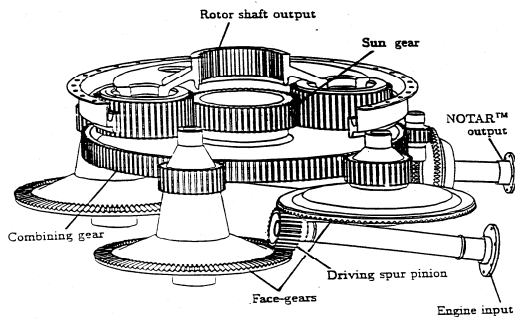


Fig.6 Face Gear Application of Main Gearbox (three stages)

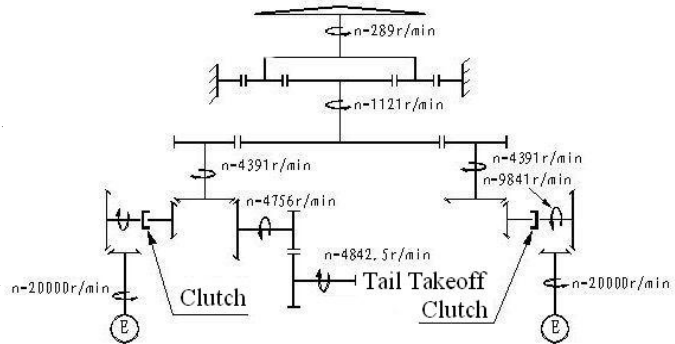


Fig.7 Original Main Gearbox Transmission Scheme of Apache Helicopter (four stages)

**Integrated Design Technique**

Accompanying the unceasing development of the transmission system of helicopters, integrated design technique had been widely adopted in main gearbox design (Fig.8~10). For example, the main gearbox of French “Tiger” helicopter had adopted large amount of this technology, i.e. spiral bevel gear-ball bearing inner race-spur gear-helical gear-roller bearing inner race five functions in one design. Fig.11 shows the details. Integrated design can reduce the number of parts, weight and increase reliability of main gearbox.

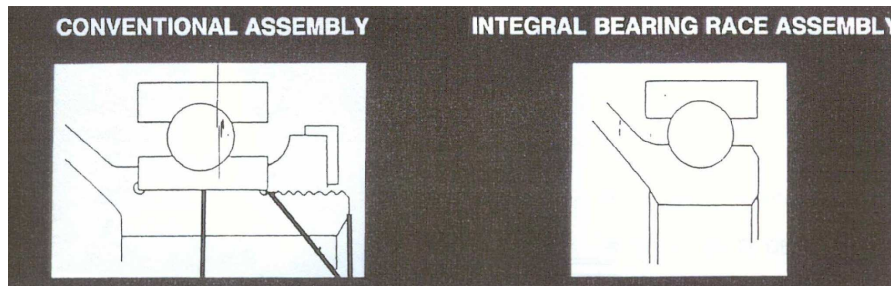


Fig.8 Comparison between a conventional bearing assembly and an assembly with an integral bearing race

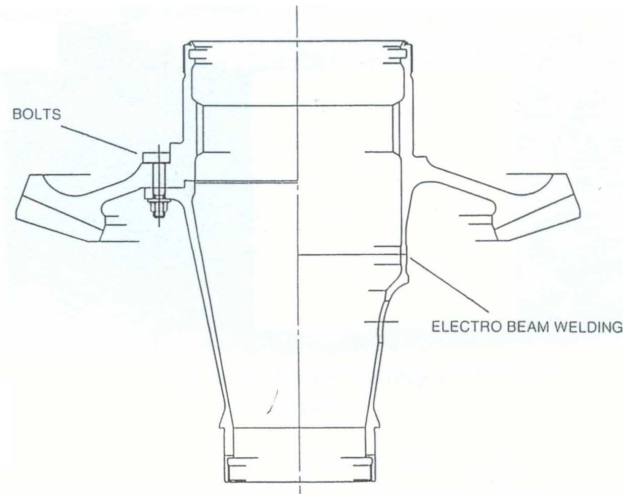


Fig.9 Integrated design structure of a combined gear

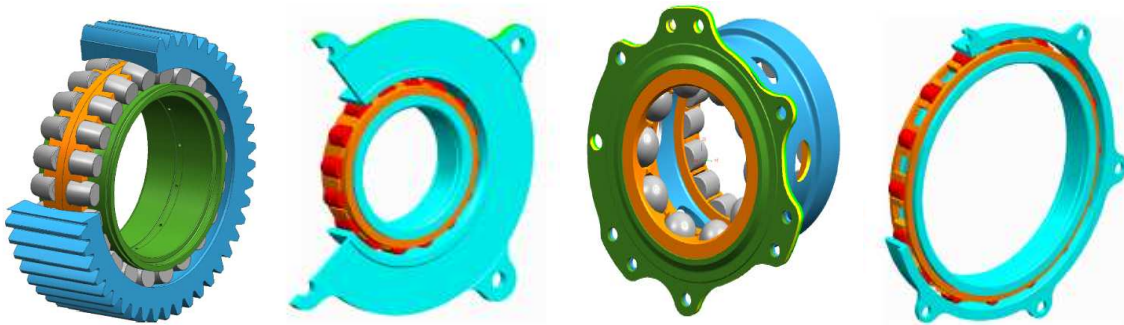


Fig.10 Bearing integrated technique

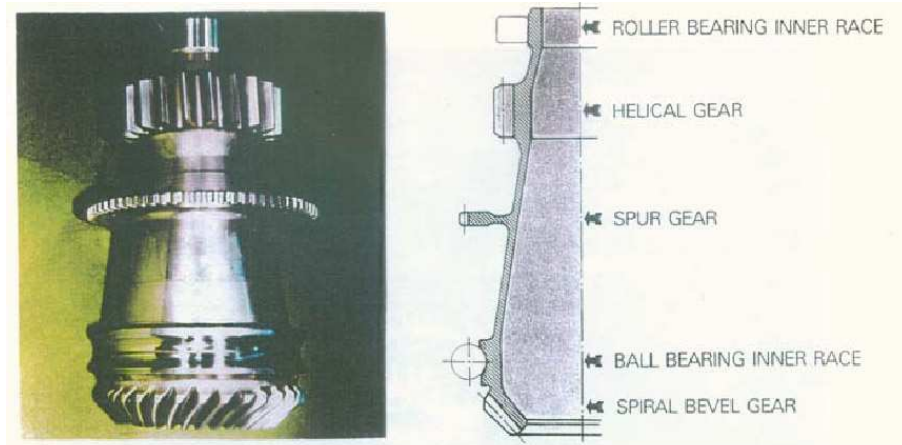


Fig.11 Integrated technique of main gearbox tail take-off component

### Dry-running Technique

For either civil or armed force users the duration of dry-running of helicopter gearbox should be no less than 30 minutes at present in foreign countries. Dry-running is one of the key techniques in helicopter gearbox design. Everybody knows that helicopter gearbox will be in dry-running condition in a short time when damaged by a shot. Due to rapid temperature rise, bearing expand and get stuck quickly, gears lose their working clearance, and the gearbox will be damaged in a few minutes and stop working. This result will be a terrible catastrophe. Therefore, gearbox gears must have a longer dry-running capability to secure the safety of helicopters, customers and pilots. Foreign helicopters companies take mainly the following measures in design:

(1) Increase moderately the clearance of spiral bevel gear of high speed input stage, to prevent gear interference or get stuck due to high temperature rise when dry-running.

(2) Increase moderately the axial and radial play of all the bearings of high speed input stage, ceramic bearing can also be used. In order to extend the time of dry-running, the steel-made cage of bearings is silver plated.

(3) High temperature resistant and low friction coefficient materials, such as M50NiL and CSS-42L steel are adopted.

(4) Ring shaped oil reserve trough on the casing of input stage and oil collect cavity or wickness in the shaft measures are made, when lubrication system suffers a shot, oil will flow slowly into bearings or on gears by centrifugal force under no pressure condition. The dry-running time thus will be extended. Fig.12 shows the nose gearbox of Apache helicopter.

(5) Gear shaft is placed with simple support; ball bearings and roller bearings are adopted for the support of gear shafts. In high speed input stage tapered roller bearings will not be used if possible. Grease lubrication is adopted on the tail drive system also.

(6) Redundancies structure design is adopted for example: Modular structure of the left and right input stage can be designed into symmetry. Two independent lubrication system and methods of multi-paths transmission power are adopted in the main gearbox, e.g. after the OH-58C helicopter main gearbox which is made by USA is modified from three planet gears change into four, the dry-running time can increase three times.

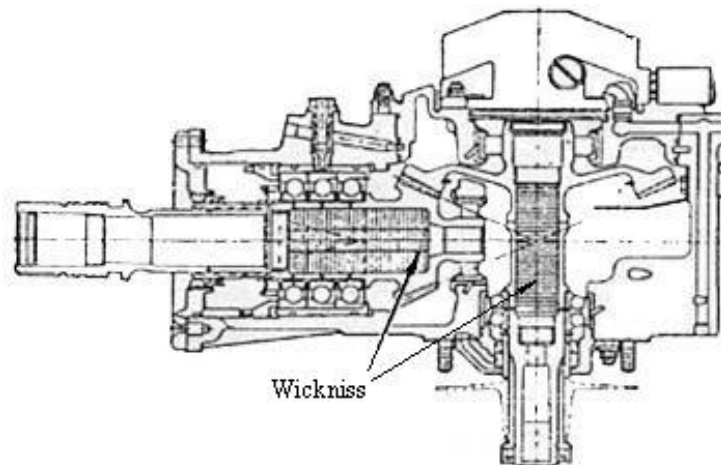


Fig.12. Wickness of input stage of apache main gear box

## References

- [1] B.A. Shotter: *The Lynx Transmission and Conformal Gearing*, SAE 781041, 1978.
- [2] A.Garavaglia and G. Gattinoni: *Design Criteria of the 129 Helicopter Drive System*, AGARD-CP-302, 1991.
- [3] T.L. Krantz and J.G. Kish: *Advanced Rotorcraft Transmission (ART) Program Summary*, AIAA Paper, AIAA-92-3365, 1992.
- [4] Gilbert J.Weden and John J. Coy: *Gears and Power Transmission System for Helicopters and Turboprops*, AGARD-CP-369, 1992.
- [5] J.H. Shao: *The Circular Arc Gears* (China Machine Press, China, 1994).

## Initial Pressure Influence on Pressure Flow Factor Used in Mixed-Lubrication Model

Fanming Meng<sup>1, a</sup>, Yuanpei Chen<sup>1, b</sup>

<sup>1</sup>The State Key Laboratory of Mechanical Transmission,  
Chongqing University, Chongqing 400044, China  
<sup>a</sup>fmmeng@cqu.edu.cn, <sup>b</sup>ypc\_1987@126.com

**Keywords:** initial pressure, pressure flow factor, measured surface, mixed-lubrication.

**Abstract.** The average flow model proposed by Patir and Cheng offers a great convenience for the mixed-lubrication analysis of rough surfaces. The pressure flow factor introduced by Patir and Cheng helps to analyze the influence of roughness on the average pressure and average flow of a lubricant between surfaces. This paper reports how to reasonably choose initial pressure in computing the pressure flow factor. The numerical results show that the pressure distribution and further pressure flow factor value are sensitive to an initial pressure in solving the pressure flow factor, and the initial pressure of a constant value is not suitable for the pressure flow factor calculation for a measured surface with many sample points. Meanwhile, the pressure flow code is demonstrated by the comparison of the pressure obtained numerically with the analytical solution of pressure.

### Introduction

The average flow model developed by Patir and Cheng [1] (referred to as PC hereafter) has been used in mixed-lubrication analyses for tribological pairs more than thirty years, where pressure and shear flow factors were introduced by PC to express the influence of roughness on the average pressure and average flow of a lubricant between surfaces. Based on the PC flow factors, some improved flow factors were given to be suitable for special operation conditions in the past by using a statistical model [1], deterministic model [2] and perturbation analysis method [3].

Despite these improvements, so far very little work has been done in the description of details of numerically solving flow factors, except PC's original work. This brings out a difficulty for the flow factor innovators who are not familiar with the numerical details of the flow factors. The authors' calculation experience show that the solution process of the shear flow factor is usually smooth due to the fact that the inlet pressure of a lubricant is defined to be equal to the outlet pressure of the lubricant according to PC's flow factor theory. Some numerical difficulties, however, will occur in solving the pressure flow factor, especially for one used for a measured surface with a large number of sample points, since the inlet pressure is defined by PC not to equal the outlet pressure for the pressure flow factor calculation. Therefore, important details in solving the pressure flow factor need to be revealed to be convenient for flow factor's application or improvement. In the present work, only the choice of initial pressure in solving pressure flow factor will be analyzed, since the initial pressure plays an important role in achieving the reasonable pressure flow factor value.

### Review of the Pressure Flow Factor

Figure 1 shows two surfaces in a lubricated interface. The upper and lower boundaries of the mating surfaces are denoted by surfaces A and B, respectively, with velocities  $u_2$  and  $u_1$  along the  $x$  direction, as shown in Fig.1, where the nominal film thickness between the upper surface A and lower surface B is denoted by  $h$ .

If the roughness amplitudes of surfaces A and B are represented, respectively, by variables  $\delta_2$  and  $\delta_1$ , which are separately distributed with standard deviations  $R_{q1}$  and  $R_{q2}$  from their mean levels, the local film thickness  $h_r$  can be expressed as

$$h_r = h + \delta_1 + \delta_2. \quad (1)$$

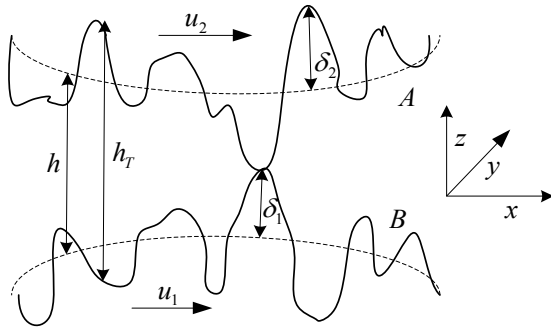


Fig.1 Two surfaces in a lubricated interface

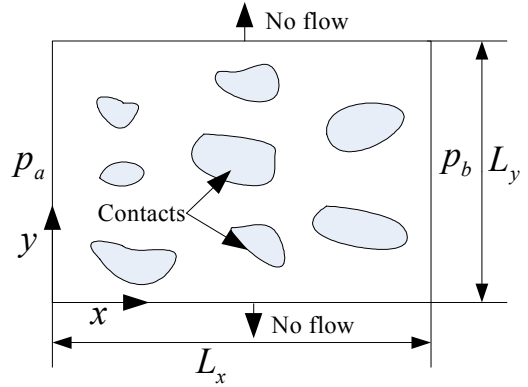


Fig.2 Boundary conditions

The lubrication theory for continuous, homogeneous and Newtonian fluid, neglecting the dependency of lubricant density on oil film pressure, leads to the following Reynolds equation for the average pressure [1] used for pressure flow factor

$$\frac{\partial}{\partial x} \left( \frac{h_T^3}{12\eta} \frac{\partial p}{\partial x} \right) + \frac{\partial}{\partial y} \left( \frac{h_T^3}{12\eta} \frac{\partial p}{\partial y} \right) = \frac{u_1 + u_2}{2} \frac{\partial h_T}{\partial x} + \frac{\partial h_T}{\partial t} \quad (2)$$

where  $p$  is the average pressure,  $\eta$  is the lubricant viscosity, and  $t$  is the time. For simplifying calculation, the pure rolling condition is used here, that is,  $u_1 = u_2 = \bar{U}$ , as proposed by PC. The  $\delta_1$  and  $\delta_2$  are the functions of position on each moving surface with time dependence relative to a stationary referenced place. This time dependence can be written as

$$\delta_i = \delta_i(x - \bar{U}t, y), \quad i = 1, 2. \quad (3)$$

so that

$$\frac{\partial \delta_i}{\partial t} = -\bar{U} \frac{\partial \delta_i}{\partial x}, \quad i = 1, 2. \quad (4)$$

Thus, by using Eqs.3 and 4, along with the above pure rolling condition, Eq.2 can be reduced to

$$\frac{\partial}{\partial x} \left( \frac{h_T^3}{12\eta} \frac{\partial p}{\partial x} \right) + \frac{\partial}{\partial y} \left( \frac{h_T^3}{12\eta} \frac{\partial p}{\partial y} \right) = 0. \quad (5)$$

To solve the Eq.5 for pressure and further for pressure flow factor, the following boundary conditions shown in Fig.2 are employed, i.e.,

$$\begin{cases} p = p_a & \text{at } x = 0 \\ p = p_b & \text{at } x = L_x \\ \frac{\partial p}{\partial y} = 0 & \text{at } y = 0, y = L_y \text{ (no flow)} \end{cases} \quad (6)$$

For simplicity,  $p_a$  and  $p_b$  are taken to be unit, and zero, respectively. Once Eq.5 is solved for pressure using the boundary conditions expressed by Eq.6, the pressure flow factor  $\phi_x$  (or  $\phi_y$ ) can be determined.

The pressure flow factor in  $x$  direction is

$$\phi_x = \int_0^{L_y} \int_0^{L_x} h_T^3 \frac{\partial p}{\partial x} dx dy / (h^3 (p_b - p_a)). \quad (7)$$

Note that the pressure flow factor in the  $y$  direction can be obtained from the equation  $\phi_y(\gamma, h / \sigma) = \phi_x(1 / \gamma, h / \sigma)$  due to geometric similarity of the computation domain.

## Results and Discussion

Equation 5 can be solved under relaxation iteration in row by row procedure with the first-order backward scheme. The pressure flow factor code was validated in reference[2], where a basic agreement between the results from present code and PC method can be found. In numerically simulating the pressure flow factor, the origin of coordinates is located at the beginning of the bottom surface in Fig.1, i.e., the inlet of the lubricant. The boundary conditions given in Eq.6 are applied when solving Eq.5 for the pressure. For simplicity and without losing generality, let  $L_x=L_y=1$ .

Since the right-hand side of Eq.5 is zero, the equation has special characteristics. The authors' numerical practice shows that Eq.5 can be solved for the pressure used for the calculation of the pressure flow factor on the condition of many initial pressure values, among which the appropriate initial pressure needs to be discussed and chosen out in the following section. In the analysis, the  $h_T$  value varies, and a measured rough surface with transverse orientation is used with  $1001 \times 521$  sample points along the  $x$ - and  $y$ -directions, until otherwise specified. Meanwhile, the non-dimensional form of pressure is represented by  $p / p_a$ . Here,  $p_a$  and  $p_b$  are still taken to be unit and zero for simplifying the analysis.

Case 1:  $h_T = c_1$

Here,  $c_1$  is a constant value. In this case, the roughness is not considered. Thus, a linear pressure distribution of  $p = ((p_a - p_b)x / L_x + p_b / L_x)$  can be obtained.

Case 2:  $h_T \neq c_1, p_0 = c_2$

Here,  $c_2$  is a constant value. In this case, an arbitrary initial constant pressure  $p_0$  can meet Eq.5. This implies the final pressure flow factor value is affected greatly by the initial pressure  $p_0$ .

Case 2.1:  $p_0 = 0$

The initial pressure  $p_0$  is first assumed to be zero. Numerical results show that the calculated pressure does not reflect the orientation of the transverse surface. The unreasonable pressure distribution implies that the final flow factor value from the initial pressure of zero will be incorrect.

Case 2.2:  $0 < p_0 < p_a$

The initial pressure between  $0 < p_0 < p_a$  is used. In this case, the pressure flow factor  $\phi_x$  versus  $H$  is given in an Fig.3, where  $p_0$  is equal to 0.2. The  $\phi_x$  value approaches unit when the  $H$  value becomes larger. This is similar to conclusion obtained in reference [1] and therefore seems to be correct. Figure 4 gives the corresponding pressure distribution for  $H=0.3$  and when the non-dimensional value of  $p_0$ ,  $p_0 / p_a$ , equals 0.2, its convergence precision  $\varepsilon$  still being  $1.0 \times 10^{-6}$ . The pressure distribution with the unreasonable plateau does not show the orientation of the transverse surface, which implies the obtained pressure flow factor shown in Fig.3 is not reasonable.

Case 2.3:  $p_0 > p_a$

In this case, the pressure flow factor  $\phi_x$  versus  $H$  is given in Fig5, where initial non-dimensional pressure  $p_0 / p_a$  equal to 3 is used for every  $H$  value. Further, Fig.6 gives the pressure distribution at  $H=0.3$  when the non-dimensional value of  $p_0$  is taken to be 3, its convergence precision  $\varepsilon$  still being  $1.0 \times 10^{-6}$ . The orientation of the transverse surface does not be reflected in Fig.6. This unreasonable pressure implies the obtained pressure flow factor shown in Fig.5 is unreasonable.

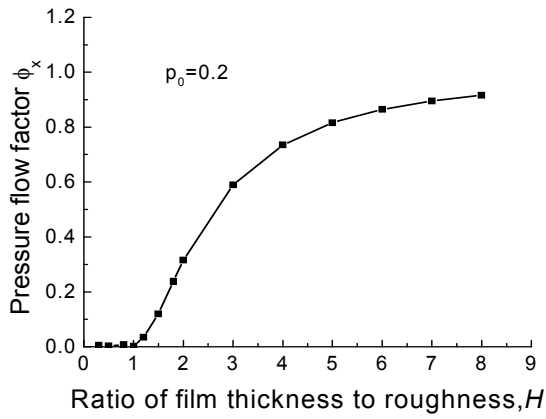


Fig.3. Pressure flow factor for transverse surface when the initial non-dimensional pressure is 0.2

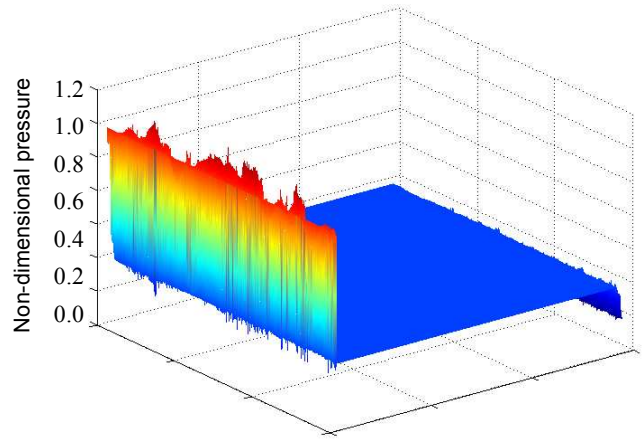


Fig.4. Pressure distribution computed for  $\epsilon=1.0 \times 10^{-6}$  when the initial non-dimensional pressure is 0.2

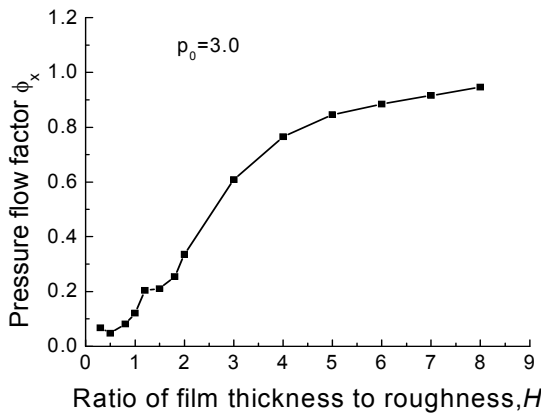


Fig.5 Pressure flow factor for the transverse surface when the initial non-dimensional pressure is 3

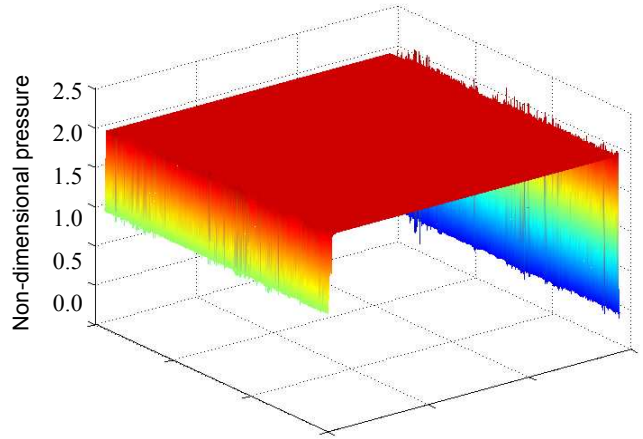


Fig.6 Pressure distribution computed for  $\epsilon=1.0 \times 10^{-6}$  when the initial non-dimensional pressure is 3

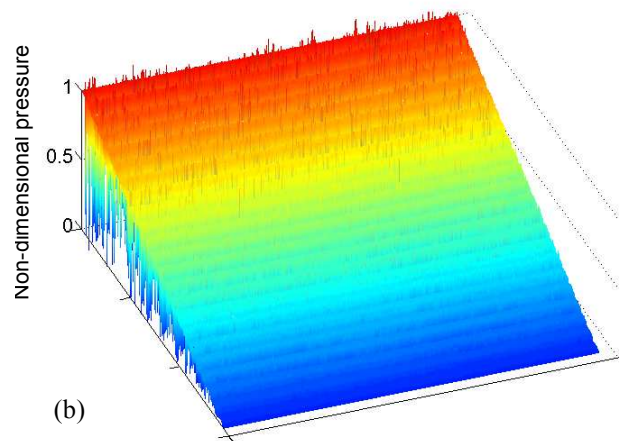
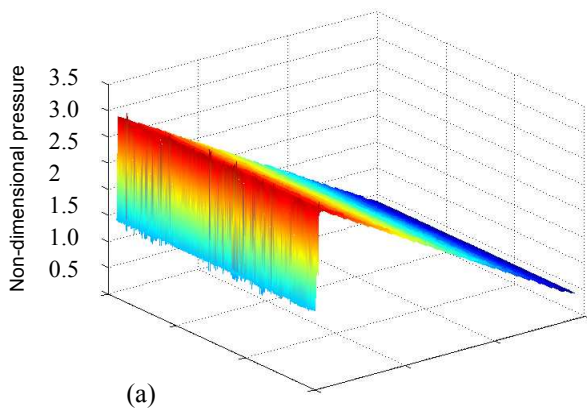


Fig.7 Pressure distribution computed for  $\epsilon=1.0 \times 10^{-6}$  using equation (16). (a):  $p_0=3$ ; (b):  $p_0=1$

Case 3:  $h_T \neq c_1, p_0 \neq c_2$

Further the varied film thickness is used, and the initial pressure is a function of  $x$ , that is

$$p_0 = c \cdot ((p_a - p_b)x / L_x + p_b / L_x). \tag{8}$$

In Eq.8, the coefficient  $c$  is set as a varied constant value. There are three cases for the  $c$  value, that is,  $c > 1$ ,  $c = 1$ ,  $c < 1$ . In this discussion, the pressure convergence precision  $\varepsilon$  for the three cases is  $1.0 \times 10^{-6}$ .

Fig.7 gives the pressure distribution for  $H = 0.3$  when the initial non-dimensional pressure is separately taken to be approximately 3 and 1. The pressure distributions show basically the orientation of the transverse surface. The boundary pressures at  $x = 0$  in Fig.7(a) and (b) are separately 3 and 1. Meanwhile, the approximate linear pressure distribution along  $x$  axis can be seen in Fig.7 (a) and (b). If the initial non-dimensional pressure is taken to be 0.3, the boundary pressures at  $x = 0$  is about 3.

To choose the reasonable pressure, a symbol is used first, that is  $e = \delta/h$ . Thus, the local film thickness can be expressed as  $h_t = h(1 + e)$ , where  $\delta$  is the composite roughness amplitude of the upper and lower surfaces. By using a Taylor series, the pressure  $p$  of an arbitrary node in the neighborhood of a fixed point  $f$  can be expanded as

$$p = p_f + \Delta x \cdot \left. \frac{\partial p}{\partial x} \right|_f + \Delta y \cdot \left. \frac{\partial p}{\partial y} \right|_f + \frac{1}{2} \Delta x^2 \cdot \left. \frac{\partial^2 p}{\partial x^2} \right|_f + \frac{1}{2} \Delta x \cdot \Delta y \cdot \left. \frac{\partial^2 p}{\partial x \partial y} \right|_f + \frac{1}{2} \Delta y^2 \cdot \left. \frac{\partial^2 p}{\partial y^2} \right|_f + \dots \quad (9)$$

where  $\Delta x$  and  $\Delta y$  are separately intervals between neighboring nodes along  $x$ - and  $y$ - axes. When the number of nodes approaches very larger values (for example  $1001 \times 521$  along  $x$  and  $y$  axes in the present study), the  $p$  value must approach  $p_f$  due to  $\Delta x \rightarrow 0$  and  $\Delta y \rightarrow 0$ . By observing Fig.7(a) and (b), along with the above analysis, only the pressure distribution shown in Fig.7 (b) can meet this rule. Therefore, only the initial pressure of  $((p_a - p_b)x/L_x + p_b/L_x)$  is acceptable.

## Conclusions

- (1) The pressure distribution and further pressure flow factor value are sensitive to an initial pressure in solving the pressure flow factor.
- (2) Reasonable pressure distribution and further reasonable pressure flow factor is obtained only when the used initial pressure in solving the pressure flow factor is taken to be the pressure solution obtained under the smooth surface condition.

## Acknowledgements

This work is supported by the Fundamental Research Funds for the Central Universities of P.R.China (Project No. No. CDJZR10 285501).

## References

- [1] N.Patir and H.S. Cheng: ASME, J. Lubr. Technol., Vol. 100 (1978), p. 12
- [2] F.M. Meng, W.Z Wang, Y.Z. Hu and H.WANG: Proc. Instn Mech. Engrs, Part C, J. Mechanical Engineering Science, Vol. 221 (2007): p.15
- [3] Q. Wang and H. S. Cheng: STLE Tribol. Trans., Vol. 38 (1995), p. 654

## Asymmetric Gears: Parameter Selection Approach

Alexander Kapelevich, AKGears, LLC,  
316 Oakwood Drive, Shoreview, MN 55126, USA  
ak@akgears.com

**Keywords:** Gears, Asymmetric Teeth, Direct Gear Design, Gearbox

**Abstract.** In many gear transmissions the tooth load on one flank is significantly higher and is applied for longer periods of time than for the opposite one. An asymmetric tooth shape reflects this functional difference. This paper describes an approach to rationalize the asymmetric gears parameter selection to meet a variety of operating conditions and requirements to custom high performance gear drives.

### Introduction

In many gear transmissions the tooth load on one flank is significantly higher and is applied for longer periods of time than for the opposite one. There are many publications about gears with asymmetric teeth [1, 2], where the asymmetric teeth design is defined by the preselected asymmetric generating (tooling) gear rack parameters, - a common method for conventional gears with symmetric teeth. The modified asymmetric tooling gear racks cannot satisfy all possible applications and requirements of such gear drives.

The Alternative Direct Gear Design<sup>®</sup> method is not bounded with the preselected basic rack parameters and provides the gear tooth geometry optimized for specific gear train application. Its application to the gears with the asymmetric teeth is described in articles [3, 4].

This paper describes an approach to rationalize the asymmetric gears parameter selection to meet a variety of operating conditions and requirements to custom high performance gear drives.

### Asymmetric Gear Torque Transmission Conditions

Asymmetric tooth profiles make possible to increase the operating pressure angle (with the given transverse contact ratio  $> 1.0$ ) beyond the conventional symmetric gears' limits. This allows to reduce drive flank contact stress and sliding velocity reduction. As a result, asymmetric gears have higher tooth surface endurance to pitting and scoring. Their application increases transmission density and makes the gearbox smaller and lighter.

Different torque transmission condition cases for one pair of the 24 tooth spur gears are presented in the Table 1.

**Cases #1 and #2.** The gear teeth are symmetric and their surface durability is identical for both tooth flanks. Case #1 presents the traditionally designed 25° pressure angle gears with the full radius fillet. This case is considered as a baseline and its Hertz contact stress, bearing load, and specific sliding velocity are assumed as 100% for comparison with other gear cases. These types of gear profiles are used in the aerospace industry because they provide better bending strength and flank surface endurance in comparison with the standard 20° pressure angle gears typical for commercial applications. Case #2 is high 32° pressure angle symmetric gears, optimized by the Direct Gear Design method. Its Hertzian contact stress is about 8% lower and specific sliding velocity is about 6% lower than for the baseline gear pair. They should have better flank tooth surface pitting or scoring resistance. However, their bearing load is 7% higher.

**Case #3.** These asymmetric gears are mostly for unidirectional load transmission by a 40° pressure angle driving tooth flanks providing the advantages of 12% contact stress reduction and 25% sliding velocity reduction. However, these parameters for the coast flanks are practically the

same as for the baseline gears and should provide similar tooth surface load capacity. These types of gears may find applications for drives with one main load transmission direction that should be capable to carry lighter load for shorter periods of time in transmission direction.

**Case #4.** These asymmetric gears have driving tooth flanks with a 46° pressure angle that reduces the contact stress by 14% and sliding velocity by 32%. The disadvantage of such teeth is a very high (+30%) bearing load. These types of gears are only for unidirectional load transmission. Their coast 10° pressure angle flanks have insignificant load capacity. These types of gears may find applications for drives with only one load transmission direction that may occasionally have no load coast flank tooth contact, like in the case of a tooth bouncing in high speed transmissions.

Table 1

| Case #                       | 1                    | 2         | 3                            | 4                         | 5                |
|------------------------------|----------------------|-----------|------------------------------|---------------------------|------------------|
| Tooth profile                | Symmetric (baseline) | Symmetric | Asymmetric                   | Asymmetric                | Asymmetric       |
| Pressure angle, °            | 25                   | 32        | 40/24*                       | 46/10*                    | 60/-**           |
| Asymmetry coefficient        | 1.0                  | 1.0       | 1.19                         | 1.42                      | -**              |
| Contact ratio                | 1.35                 | 1.2       | 1.2/1.44*                    | 1.2/1.0                   | 1.2/-**          |
| Hertz contact stress, %      | 100                  | 92        | 88/102*                      | 86/150*                   | 94/-**           |
| Bearing load, %              | 100                  | 107       | 118/99*                      | 130/92*                   | 181/-**          |
| Specific sliding velocity, % | 100                  | 94        | 75/108*                      | 68/97*                    | 49/-**           |
| Torque transmission flanks   | both                 | both      | drive, coast with lower load | drive, coast with no load | drive flank only |

\* for drive/coast tooth flanks;

\*\* coast flank mesh does not exist.

**Case #5.** Asymmetric gears have only driving tooth flanks with the extreme 60° pressure angle with no involute coast tooth flanks at all. They may not be considered for any particular practical applications, they demonstrate an extreme case of the asymmetric spur involute gears.

### Asymmetric Gears in Chain and Planetary Arrangements

The nominal contact stress at the pitch point is [5]

$$\sigma_H = z_H z_E z_\epsilon z_\beta \sqrt{\frac{F_t}{d_{w1} b_w} \frac{u \pm 1}{u}}, \tag{1}$$

Where,

$$z_H = \sqrt{\frac{2 \cos(\beta_b) \cos(\alpha_{wt})}{\cos(\alpha_t)^2 \sin(\alpha_{wt})}} \text{ - zone factor, for the directly designed spur gears}$$

$$z_H = \frac{2}{\sqrt{\sin(2\alpha_w)}}; \tag{2}$$

- $Z_E$  - elasticity factor that takes into account gear material properties (modulus of elasticity and Poisson's ratio);
- $Z_\epsilon$  – contact ratio factor, its conservative value for spur gears is  $Z_\epsilon = 1.0$ ;
- $Z_\beta$  – helix factor, for spur gears  $Z_\beta = 1.0$ ;
- $F_t$  – nominal tangent load, that at the pitch diameter  $d_{w1}$  is  $F_t = \frac{2T_1}{d_{w1}}$ ;
- $T_1$  – driving gear (pinion) torque;
- $b_w$  – contact face width;
- sign “+” for external gearing, sign “-” for external gearing.

Then for the directly designed spur gears the nominal contact stress at the pitch point can be presented as

$$\sigma_H = z_E \frac{2}{d_{w1}} \sqrt{\frac{2T_1}{b_w \sin(2\alpha_w)} \frac{u \pm 1}{u}} \quad (3)$$

In the chain gears, the idler gear transmits the same load by both tooth flanks. This arrangement seems unsuitable for asymmetric gear application. However, in many cases, the idler's mating gears have a significantly different number of teeth (Fig. 1). This allows asymmetric gears to equalize the contact stress and achieve maximum load capacity.

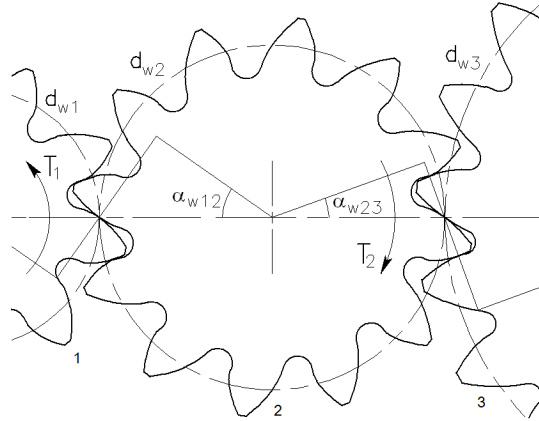


Fig. 1. Chain gear arrangement; 1 – input pinion; 2 – idler gear; 3 – output gear

The pitch point contact stress in the pinion/idler gear mesh is

$$\sigma_{H12} = z_E \frac{2}{d_{w1}} \sqrt{\frac{2T_1}{b_{w12} \sin(2\alpha_{w12})} \frac{u_{12} + 1}{u_{12}}} \quad (4)$$

and in the idler/output gear mesh is

$$\sigma_{H23} = z_E \frac{2}{d_{w2}} \sqrt{\frac{2T_2}{b_{w23} \sin(2\alpha_{w23})} \frac{u_{23} + 1}{u_{23}}} \quad (5)$$

or, ignoring gear mesh losses

$$\sigma_{H23} = z_E \frac{2}{u_{12} d_{w1}} \sqrt{\frac{2u_{12} T_1}{b_{w23} \sin(2\alpha_{w23})} \frac{u_{23} + 1}{u_{23}}}, \quad (6)$$

where the subscript indexes “<sub>12</sub>” and “<sub>23</sub>” are for the pinion/idler gear and the idler/output gear meshes accordingly.

When  $\sigma_{H12} = \sigma_{H23}$ , from (4) and (6), considering that all gears are made from the same material, the idler gear pressure angle ratio is

$$\frac{\sin(2\alpha_{w23})}{\sin(2\alpha_{w12})} = \frac{b_{w12}}{b_{w23}} \frac{u_{23} + 1}{u_{23}(u_{12} + 1)}. \quad (7)$$

For example, if the pinion number of teeth is  $n_1 = 9$ , the idler gear number of teeth is  $n_2 = 12$ , the output gear number of teeth is  $n_3 = 20$ , the contact face width ratio is  $b_{w12}/b_{w23} = 1.2$ , and the pinion/idler gear pressure angle is  $\alpha_{w12} = 35^\circ$ , the idler/output pressure angle is

$$\alpha_{w23} = \frac{1}{2} \arcsin\left(\sin(2 \times 35^\circ) \times 1.2 \times \frac{\frac{20}{12} + 1}{\frac{20}{12} \times (\frac{12}{9} + 1)}\right) = 25.3^\circ.$$

Similar contact stress equalization technique can be applied for the planetary gear arrangement (Fig. 2), because the planet gear is considered as the idler gear engaged with the sun gear and the ring gear.

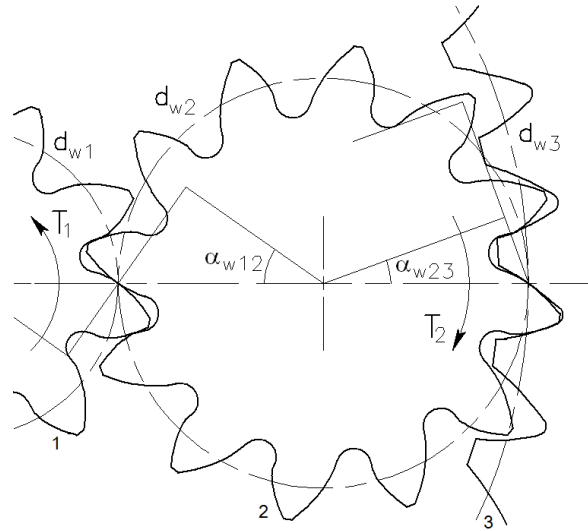


Fig. 2. Planetary gear attangement; 1 – sun gear; 2 – planet gear; 3 – ring gear

In this case, the planet and ring gears are in the internal mesh and equation (7) looks like

$$\frac{\sin(2\alpha_{w23})}{\sin(2\alpha_{w12})} = \frac{b_{w12}}{b_{w23}} \frac{u_{23} - 1}{u_{23}(u_{12} + 1)}. \quad (8)$$

For example, if the sun gear number of teeth is  $n_1 = 9$ , the planet gear number of teeth is  $n_2 = 12$ , then the output gear number of teeth is  $n_3 = n_1 + 2n_2 = 33$ , the contact face width ratio is  $b_{w12}/b_{w23} = 1.8$ , and the pinion/idler gear pressure angle is  $\alpha_{w12} = 40^\circ$ , the idler/output pressure angle is

$$\alpha_{w23} = \frac{1}{2} \arcsin\left(\sin(2 \times 40^\circ) \times 1.8 \times \frac{\frac{33}{12} - 1}{\frac{33}{12} \times (\frac{12}{9} + 1)}\right) = 14.5^\circ.$$

## Summary

- (1) This paper introduces the Direct Gear Design approach for the asymmetric gear design.
- (2) Different cases of possible load transmission conditions for asymmetric gears are described.
- (3) Contact stress equalization for the chain and planetary arrangements with the asymmetric gears and numerical examples are presented.

## References

- [1] G. DiFrancesco and S. Marini: Gear Technology, September/October (1997), p. 47
- [2] F. Karpat, K. Cavdar, and F.C. Babalik: VDI Berichte, 1904 I (2005), p. 145
- [3] A.L. Kapelevich: Mechanism and Machine Theory, Issue 35 (2000), p. 117
- [4] A. L. Kapelevich: The JSME International Conference on Motion and Power Transmissions, Matsushima, Japan, May 13-15 (2009).
- [5] Standard ISO 6336-2: (2006).

## Failures in the Development and Service of the Helicopter Transmission System

Xue Tongbo<sup>1,a</sup>, Li Gaiqi<sup>1,a</sup>

<sup>1</sup>AVIC Aviation Powerplant Research Institute, Zhuzhou, 412002, China

<sup>a</sup>capi@608.163.net

**Keywords:** transmission system; failure; mode; cause; corrective action

**Abstract.** In this paper the failures which may occur in the development and service of the helicopter transmission system are discussed. The mode, characteristic, cause and corrective action for the failures are summarized. Besides, the measures of the design and manufacture to eliminate the failures are recommended.

### Introduction

According to specifications, the failure of the transmission system means that the time or status as the product or part of the product of the transmission system cannot accomplish the required performance. According to their macro characteristic, the failures could be divided into three types: surface damage, breakage and excessive deformation. The main failure modes, effects and causes of the transmission parts are as listed in Table 1.

Table1 Failure modes, effects and causes of the transmission parts

| Parts   | Failure modes                 | Failure effects and hazards   | Main causes of the failure  | Failure classification |
|---------|-------------------------------|---|---|------------------------|
| Gear    | Tooth surface pitting         | It may lead to spalling and other severe defects and could be detected by chip detector.  | Excessive surface stress and/or insufficient tooth surface durability       | Minor                  |
|         | Tooth surface spalling        | Affecting gear meshing, enlarging vibration and may leading to tooth breakage .   |   | Major                  |
|         | Tooth surface Scratch/scoring | Scratch's further deterioration may lead to scoring and other severe defects affecting gear meshing, enlarging vibration and leading to tooth breakage. | Load concentration or insufficient lubrication.                             | Major                  |
|         | Tooth breakage                | Loss of transmission function   | Excessive loading, insufficient tooth load capacity or excessive vibration. | Catastrophic           |
|         | Gear rim and web breakage     | Loss of transmission function   | Excessive vibration   | Catastrophic           |
| Bearing | Spalling                      | Affecting or total loss of supporting/ centering functions  | Excessive surface contact stress and/or insufficient load capacity          | Major                  |
|         | Overheating and deformation   | Failing to provide normally supporting/ centering functions   | Incorrect lubrication, design or manufacture.                               | Minor or major         |
|         | Wear                          | Affecting supporting/ centering functions   | Unsuitable bearing surface and lubrication condition.                       | Minor                  |

|                                   |   |  |   |                              |
|-----------------------------------|---|--|---|------------------------------|
| Shaft                             | Breakage  | Loss of transmission function  | Excessive loading and/or insufficient load capacity or excessive vibration.                     | Catastrophic                 |
|                                   | Excessive vibration                                       | Leading to breakage resulting in loss of transmission function                       | Unsuitable design, manufacture, assembly, dynamic balancing and operation conditions.           | Major or catastrophic        |
|                                   | Spline excessive wear, spalling and breakage              | Affecting or total loss of transmission function                                     | Unsuitable design, manufacture, assembly and operation conditions.                              | Minor, major or catastrophic |
| Coupling                          | Breakage  | Affecting or total loss of transmission function                                     | Unsuitable design and manufacture.  | Major or catastrophic        |
|                                   | Delamination or bolt looseness for flexible film coupling | Affecting transmission function and may leading to severer damages.                  | Unsuitable design, manufacture, assembly and operation conditions.                              | Major                        |
| Clutch                            | Breakage  | Loss of transmission function  | Incorrect assembling operation, end load concentration, excessive loading and/or vibration      | Major or catastrophic        |
|                                   | Spalling  | Enlarging vibration, leading to breakage resulting in loss of transmission function. | Excessive loading and/or vibration  | Minor or major               |
| Casing                            | Breakage  | Loss of supporting and reacting loads function.                                      | Excessive loading, insufficient static or fatigue strength, uneven distribution of the strength | Catastrophic                 |
|                                   | Excessive deformation                                     | Affecting the supporting and reacting loads function of the casing.                  | Excessive loading, insufficient stiffness, uneven stiffness distribution                        | Major                        |
| Lubrication system and components | Failing to accomplish the expected performances           | Affecting or total loss of lubrication and cooling functions.                        | Unsuitable design and/or manufacture of the lubrication system.                                 | Major                        |
|                                   | Element physical crack                                    | Affecting or total loss of lubrication and cooling functions.                        | Unsuitable design and/or manufacture of the lubrication components.                             | Major                        |
|                                   | Oil leakage   | Affecting the normal operation of the gearbox.                                       | Operation conditions.   | Major                        |
|                                   | False warning   |  |   | Minor or major               |

## Gear Failure

The failures of transmission system gears are of three main types: tooth surface damage, tooth breakage and rim and web vibration fatigue breakage.

**Tooth Surface Damage.** The pitting and spalling are the main types of the transmission system gear tooth surface failure, which are due to the heavy local contact stress exceeding the fatigue limit. The pitting on the loaded surface of a main gearbox (MGB hereafter) accessory gear is shown in Fig. 1. The pitting is initial and in the middle of the profile under the pitch circle.

Failure analysis reveals the reason for the failure. The surface hardness of the teeth is not sufficient and the minimum case hardening depth is too small due to the improper stock removal resulting in strength weakening. Besides, the contact pattern of the gear shows double line contact along profile resulting in high contact stress. With improvement of the technological process the problem was solved.

The deterioration of pitting will result in spalling. In Fig. 2 a MGB spiral bevel pinion after bench endurance test is shown. On the loaded side of all the teeth spalling could be seen. The area of the maximum spalling is about  $5 \times 2$  mm. The spalling is contact fatigue damage and due to the poor pattern showing diagonal contact and loading concentration.



Fig. 1 Pattern and pitting area of accessory gear

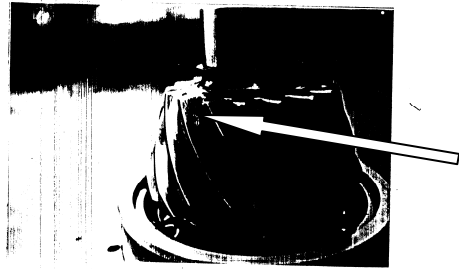


Fig. 2 Spalling of MGB spiral bevel pinion

Load concentration also may occur on the doubled cylindrical gear or rigidly installed sun gear of planetary gear train. The surface spalling of a sun gear after bench test is as shown in Fig.3. The boundary of the spalling is in accordance with the edge of mating. Micro cracks due to high contact stress could be seen above the spalling source (Fig.4). For this failure, teeth spiral line modification is an effective corrective action.



Fig. 3 Spalling of sun gear tooth



Fig. 4 Micro crack above spalling source

The scratch and scoring are other types of gear tooth surface failure and related to the excessive local loading or poor lubrication and do not clearly related to the running time. In Fig. 5 a scratched MGB collective stage pinion is shown after bench test. The scratches occur in the middle of the teeth width on both pinion and gear and in the profile direction. The unsuitable contact pattern is the main cause for the scratch.

**Tooth Breakage.** In transmission system most breakage failures is fatigue breakage due to the excessive loading or insufficient teeth load capability. However, in some cases vibration load is the cause of breakage. In Fig. 6, a broken tooth of gear is shown. On a tooth about  $1/4$  circle apart there is a spalling in the middle of profile. This is the typical characteristic of pitch diameter vibration [1].



Fig.5 Scratch of a MGB collective stage pinion



Fig.6 Breakage of gear tooth

**Vibration Fatigue Breakage of Gear Rim and Web.** For high speed bevel gear, the vibration vertical to the web and of shell shape may occur. The vibration transmits in two opposite direction producing forward and backward travel waves. The vibration may result in the gear breakage [2, 3] as shown in Fig. 7.

### Bearing Failure

**Spalling.** The causes for the bearings spalling are different according to the bearing types and operational conditions.

In general the planet gear spherical bearing design should meet the following two requirements:

- The tangential line at the roller and outer raceway contact point should intersect the bearing center line and roller axis at one point to ensure the pure rolling of the rollers.
- The resultant forces on the roller must be balanced to eliminate the turning moment and to ensure the even distribution of the load on the inner race.

A planet gear spherical bearing spalled in test on the inner race or rollers. As calculated the contact point of the roller with the inner race is 0.54mm from the roller middle and the displacement of the contact point is  $\pm 6.7\text{mm}$  when the roller maximum diameter position tolerance is  $\pm 0.05\text{mm}$ . Since the displacement is too great, the movement of the roller is not steady and the resultant forces were not balanced. This resulted in the load concentration and fatigue spalling. Therefore the manufacture accuracy of roller maximum diameter position and inner race height need to be improved and the position of inner and outer race contact point needs to be strictly controlled [5].

The spalling of an accessory drive gear angular contact ball bearing outer race during MGB bench test is as shown in Fig.8. Its inner race and balls also spalled. The failure is due to the unsuitable axial clearance of the bearing resulting in the outer race inclining, contact angle error increasing and bearing load concentration.

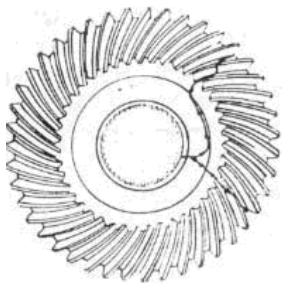


Fig.7 Gear pitch diameter vibration breakage



Fig.8 Spalling of angular contact ball bearing outer race (The rolling and grinding pattern is clearly near the outer side edge)

The stiffness of the cantilevered supported gear is relatively lower and easy to deflect resulting in bearing load concentration. The spalling of a roller bearing outer race of a cantilever supported pinion during bench test is as shown in Fig. 9. The spalling locates at the side of the race corresponding to the gear deformation. For this, the support stiffness should be increased.

The spalling of a bearing roller during bench test is as shown in Fig. 10. The spalling initiated from the  $\mu\text{m}$  initial spalling in circumferential strips on rollers. The low roughness of the inner raceway ( $Ra0.28\mu\text{m}\sim 0.47$ ) created local oil film rupture and metal-metal interactions which generate local overstress resulting in surface  $\mu\text{m}$  initial spalling.



Fig. 9 Spalling of a roller bearing outer race



Fig. 10 Spalling of a input gear bearing roller

**Overheating and Deformation.** Insufficient lubrication, such as insufficient oil tube area, insufficient oil jet flow and obstructed oil scavenge, may result in the bearing failure like color change of the raceway or rolling element and raceway deformation and, even heavier, rolling element spalling or scoring.

For example, due to design defect the oil supply to a tail gearbox bearing was insufficient resulting in overheating and scoring. The splash trough for the bearing was improved, the oil quantity was increased and the problem was solved.

**Wear.** The raceway wear could be of three types: scoring wear, fatigue wear and abrasive wear. The scoring wear is caused by slid rubbing with excessive clearance at high speed and low loading. The fatigue wear is a early type of spalling and due to low roughness or long time operation at acceleration or deceleration states which create  $\mu\text{m}$  initial circumferential spalling strips at the raceway. The abrasive wear occurs when the oil is contaminated or metal chips enter the raceway.

After endurance bench test the contact surface between the cage and rollers of a MGB input pinion taped roller bearing was worn. The failure is due to the cage shape and dimension exceeding the allowed tolerances and not uniform rollers effective length resulting in local contact between rollers and cage.

## Shaft Failure

**Shaft Breakage and Vibration Failure.** The criticality of the shaft breakage is significant and must be avoided.

Besides, the excessive vibration of a shaft will deteriorate its operation condition and also needs to be eliminated. During a transmission system ground running the tail boom vibration was significant. According to the spectrum analysis the vibration mainly comes from the tail drive shaft rotation frequency. The balancing method and tools were improved, the balancing condition was controlled to simulate the operation state as close as possible and the problem was solved.

The supercritical tail drive shaft and, between the shaft and gearbox, the floating involute spline without axial restriction has often been used. A study highlights [4] that for spline connected rotor support system self-exciting vibration will appear if operating at supercritical state. The vibration will significantly affect the shaft life. In design the actions to restrain the self-exciting vibration should be taken, e.g. damping near the spline.

**Spline Failure.** Excessive wear and spalling are main failure modes of the transmission system floating spline. The enough contact strength and hardness of the teeth surface should be ensured. For example a internal spline of 0.5mm module was initially tempering treated (outer spline is casehardened). During operating due to the relative inclination and stress concentration the internal spline was worn out gradually. Therefore the internal spline was nitrided, the spline lubrication and centering was improved and the problem was solved.

## Coupling Failure

Couplings commonly used in the transmission system include flexible film coupling, diaphragm coupling (Bendix coupling), other flexible coupling and spline coupling, etc.

Flexible film coupling composed of films bonded together by the fasteners with the shaft flange. The main failure modes of the coupling are film breakage, twisting, delamination and bolt looseness (Fig.11, 12).

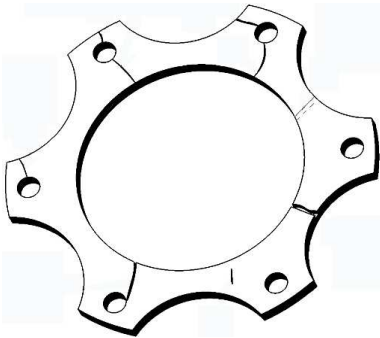


Fig.11 Type of flexible film breakage



Fig.12 Example for twisting and delamination of flexible film coupling



Fig.13 Diaphragm coupling breakage in the high cycle fatigue test

The main failure mode of the diaphragm coupling is transient and fatigue breakage. In order to avoid the failure the diaphragm profile should be optimized, the minimum thickness of the diaphragm should be determined correctly, the material of the coupling should be selected properly (generally, martensite aged steel or high strength Titanium alloy are used), proper heat treatment and surface process should be adopted and appropriate accuracy should be assured.

The coupling shown in Fig.13 broke early in high cycle fatigue test. The crack originates from the turning trace at the thinnest area of the inner profile (the maximum stress position) where the microscopic structure is rough and residual tensional stress exists. Therefore the technological process was improved to eliminate the residual stress and turning trace and to refine the material grain. With these improvement the coupling passed the high cycle fatigue test.

## Clutch Failure

There are two types of overruning clutch now widely used in the transmission system: roller clutch and sprag clutch.

**Wear and Spalling of Contact Surface.** The main causes for the surface wear and spalling is insufficient hardness and strength of the surface. Torsional vibration in service may also introduce the failures.

Apart from deep casehardening (up to 1.5mm~2mm), roller or sprag surfaces often are covered with a wear-resisting layer which is formed with physical or chemical gas phase deposition. The technological parameters of the deposition should be controlled strictly. Otherwise layer spalling may take place.

**Breakage of Roller or Sprag.** The failure may be transient or fatigue breakage. An example is shown in Fig.15.

Incorrect installation or operation may incur transient breakage. Fatigue breakage is mainly related to end stress concentration and overloading. Torsional vibration may increase contact loading to enhance the possibility of breakage. End modification (sloping) may reduce the end load concentration and avoid the breakage.



Fig. 14 Wear of sprag surface layer



Fig. 15 Breakage of sprag

**Cage Damage.** The failure of clutch cage is wear, deformation and breakage mainly. For instance, the ribs of a MGB roller clutch cage broke during starting (Fig.16). The breakage is due to the position error of the cage holes exceeding the limit affecting the simultaneous engagement and disengagement of the rollers. The clutch shaft is worn abnormally resulting in the rollers inclining and oscillating in the cage holes. Thus significant alternative stress appeared in the ribs resulting in fatigue breakage.

**Spring Failure.** The clutch spring operates under high alternative stress. As shown in Fig.17, the spring locates in the slots of the sprags and contacts the sprag slot edge at over-torque or overrunning conditions. Under torsional and radial vibration the inclining angle of the sprag will increase and varies alternatively. Thus the spring will contacts the inner and outer edges of the sprag slots heavily resulting in wear and fatigue breakage. It is recommended to shot peen and standing treat the spring to enhance its fatigue strength.

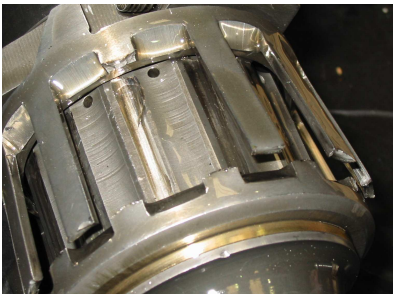


Fig.16 Cage rib breakage condition

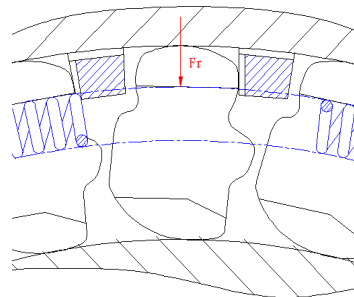


Fig.17-1 Contact between spring and sprag slot at normal condition

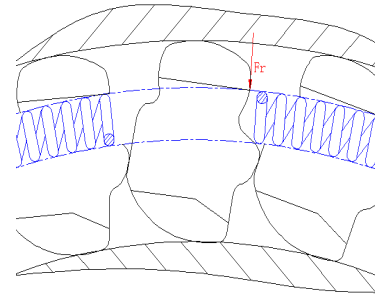


Fig.17-2 Contact between spring and sprag slot at over-torque

### Case Failure

The cases failures are often related to its structural design and metallurgical quality. In Fig.18 the fracture of a MGB case is shown which occurred in fatigue test earlier than expected. As shown in Fig.19, the gas hole and shrinkage defects of the casting deteriorate the fatigue capacity of the case causing the cracks to take place.

The case breakage is catastrophic and must be avoided. The main actions are as follows.

- Comprehensive analysis of the cases load and load distribution under each condition at each area.
- Correct design of cases lugs, ribs, corners, fillets and holes to ensure even distribution of the stresses and avoid weak area.
- Improving casting and forging technique to ensure the metallurgical quality and mechanical properties.